

Changes to the manuscript: "Validation of Aura-OMI QA4ECV NO₂ Climate Data Records with ground-based DOAS networks: role of measurement and comparison uncertainties"

S. Compernelle, T. Verhoelst, et al.

April 30, 2020

Abstract

Note: we refer here to pages and line numbers of the marked-up manuscript version (obtained using latexdiff).

Answers to reviewer 1 and corresponding changes

Reviewer 1: *The manuscript by Compernelle et al. presents an important validation work for a satellite-based NO₂ climate data records. The validation process is accurate and comprehensive. The findings, especially the ex-ante uncertainty vs. RMSD budget, in this work are important for end users. The manuscript should be published after addressing the following minor comments.*

Author reply 1: We thank reviewer 1 for his positive comments and helpful remarks. We give a point-by-point answer below.

Reviewer 1: *Page 10, lines 1 to 8. Any comments on the difference caused by AOD inputs (i.e., QA4ECV uses AERONET, whereas bePRO uses OE results)? What if bePRO uses AERONET AOD?*

Authors reply 2: One obvious limitation of using the AERONET AOD with bePRO NO₂ is a loss of data: for part of the bePRO NO₂ data no co-located AERONET AOD is available. This was also a limitation for the QA4ECV MAX-DOAS NO₂ + AERONET AOD combination (see the dashed purple line in Fig. S9 and following). Also, as opposed to the bePRO NO₂/bePRO AOD, co-located bePRO NO₂/AERONET AOD pairs have a temporal collocation mismatch and (where instruments are at different locations) spatial collocation mismatch. Therefore, conclusions based on bePRO NO₂/AERONET AOD combination are in generally less clear than for bePRO NO₂/bePRO AOD.

Manuscript changes:

Page 9, line 12. Regarding bePRO, added "measurements at the same temporal sampling as the NO₂ measurements."

Page 10, line 7. New text: A limitation when investigating AOD dependencies in satellite-MAX-DOAS comparisons using AERONET AOD with QA4ECV MAX-DOAS tropospheric NO₂ VCD data (as compared to using bePRO AOD with bePRO NO₂ data) is that it implies a subsetting: for part of the QA4ECV MAX-DOAS NO₂ data no co-located AERONET AOD is available. Also, as opposed to the bePRO NO₂/bePRO AOD combination, co-located QA4ECV MAX-DOAS NO₂/AERONET AOD data pairs have a temporal co-location mismatch and (where instruments are at different locations) a spatial co-location mismatch. A test was performed (results not shown) using the bePRO NO₂/AERONET AOD combination. It was generally found that the results are less clear than for the bePRO NO₂/bePRO AOD combination.

Reviewer 1: *Page 17, Figure 5. The model adjusted SAOZ AM and PM data have a larger discrepancy in winter at OHP (Fig. 5 right panel, green and cyan dash lines). This effect is not observed at Kerguelen, i.e., its July data. Is this due to the heavy local tropospheric NO₂ signal at OHP (in winter)? Any comments?*

Authors reply 3: Weve added a paragraph on this, but it remains an open question. The tropospheric column is in principle the one above the station for both sunrise and sunset observations (as it is below the scattering altitude), so it would require a diurnal cycle in the tropospheric column at the station to cause this discrepancy. This could be investigated with MAX-DOAS data, but that is beyond the scope of the current analysis.

Manuscript changes: Page 18, line 8. New paragraph. At OHP, the wintertime agreement between sunrise and sunset after photochemical adjustment is not as good. Contamination by tropospheric pollution is expected to be similar for both sunrise and sunset measurements, as it contributes to the airmass below the scattering altitude, i.e. the column above the station, as opposed to the large and offset area of sensitivity in the stratosphere. Differences between sunrise and sunset contamination could still be caused by a diurnal cycle in the tropospheric column, but an analysis of that diurnal cycle (e.g. from MAX-DOAS data) is beyond the scope of this work.

Reviewer 1: *Page 20, Figure 7. It is very difficult to see if there is or isnt any seasonal variation. The symbols are jammed. One needs to find better methods to show this, e.g., sub-panels by seasons.*

Authors reply 4: We chose an entirely different visualization in the new version of the manuscript, which is hopefully clearer, and actually contains more information.

Manuscript changes: Page 17, Figure 6. Here is now a mosaic plot included (x:Day of Year, y: latitude, z: median difference)

Reviewer 1: *Page 24, Figure 8. Taking the fact the size of superpixels*

from OMI and TROPOMI are similar, why Uccle and Thessaloniki show very large changes in the smoothing difference error (OMI vs. TROPOMI). Is this indicate these sites have more fine-scale variation than others? Note that for Mainz, the smoothing difference error in Fig. 8a and 8b are not very different.

Authors reply 5: There are two major differences between the Fig. 8a and Fig. 8b approach: (i) the different size of the central pixel, which is way bigger for OMI. As the reviewer suggests therefore, one expects more sensitivity to fine-scale variation in Fig. 8b. (ii) the different temporal range (starting from 2004 for OMI and from 2018 for TROPOMI) will capture differently evolution in NO₂ concentration patterns (caused by e.g., new emission policies over time). We added a sentence citing the above two differences in approach as probable reasons for differences between Fig. 8a and 8b.

Manuscript changes: Page 23, line 6. New text. Differences between the OMI and TROPOMI-based calculations are likely caused by (i) the much larger central pixel of OMI compared to TROPOMI, leading to a lower sensitivity to fine-scale variations in Fig. 8a, and (ii) evolution in e.g., NO₂ concentration patterns, captured differently by the different temporal ranges used in Fig. 8a and b.

Reviewer 1: *Figure 8. Any comments on the positive mean difference for Xianghe and Cabauw in Fig 8b, at JFM? This figure is fascinating and revelled many important aspects of these two generations of satellite data products. Although this is a bit out of the scope for this paper, I would still suggest the author give more comments on their difference.*

Authors reply 6: As opposed to many of the other MAX-DOAS sensors, these two sites are not located at urban centers, although pollution centers are in the neighbourhood. Therefore, the positive mean differences at JFM captured by TROPOMI could well be due to NO₂ fields captured at the border of the TROPOMI superpixel. This is in agreement with very recent work of Pinardi et al. (2020) on the horizontal smoothing effect. The estimated horizontal dilution factors in Fig. S3 of Pinardi et al. (2020) are positive for Cabauw and Xianghe, indicating that NO₂ is higher in the periphery than at the MAX-DOAS location. Based on the above, we added an explanation in the text as an example of the higher sensitivity to fine-scale variation of the TROPOMI-based calculation. (See the previous remark on the same Figure).

New Reference: Pinardi et al. (2020) Pinardi, G.; Van Roozendaal, M.; Hendrick, F.; Theys, N.; Abuhasan, N.; Bais, A.; Boersma, F.; Cede, A.; Chong, J.; Donner, S.; Drosoglou, T.; Frie, U.; Granville, J.; Herman, J. R.; Eskes, H.; Holla, R.; Hovila, J.; Irie, H.; Kanaya, Y.; Karagkiozidis, D.; Kouremeti, N.; Lambert, J.-C.; Ma, J.; Peters, E.; Piters, A.; Postlyakov, O.; Richter, A.; Remmers, J.; Takashima, H.; Tiefengraber, M.; Valks, P.; Vlemmix, T.; Wagner, T. and Wittrock, F. Validation of tropospheric NO₂ column measurements of GOME-2A and OMI using MAX-DOAS and direct sun network observations, Atmospheric Measurement Techniques Discussions, 2020, 2020, 1-55 10.5194/amt-2020-76

Manuscript changes: Page 23, line 8. New text. A case in point are the positive mean differences in JFM and OND captured in the TROPOMI-based calculation but not in the OMI-based calculation. Both MAX-DOAS sensors are not located at urban centers, although pollution centers are in the neighbourhood. Therefore, the positive mean differences at JFM and OND captured by TROPOMI is likely due to NO₂ fields in the periphery of the TROPOMI superpixel. This is in agreement with very recent work of Pinardi et al. (2020) on the horizontal smoothing effect. The estimated 'horizontal dilution factors' in Fig. S3 of Pinardi et al. (2020) are positive for Cabauw and Xianghe, indicating that NO₂ is higher in the periphery than at the MAX-DOAS location.

Reviewer 1: *Page 31, lines 28-29. For the Xianghe site, why smoothing can increase the seasonal variance this much (baseline vs. GB smoothed, var (seasonal) increased by about a factor of two)? Can the author confirm this is simply due to the non-harmonized a priori? Why GB harmonized has less seasonal variance than GB harm + smoothed. The figure leaves the impression that the averaging kernel smoothing caused this increase of seasonal variance, no matter one harmonizes a priori or not. Please provide some comments and explanations.*

Authors reply 7: The increase in seasonal variance is caused by the interplay of the seasonal variation of the MAX-DOAS vertical profile and of the satellite vertical averaging kernel. Specifically, it is found for the Xianghe case that in wintertime averaging kernels have higher values close to the surface while MAX-DOAS NO₂ profiles can also be peaked at the surface. The combination causes increased MAX-DOAS columns upon vertical smoothing. This is seen e.g., in the comparison of GOME-2 AC SAF GDP 4.8 NO₂ product with MAX-DOAS at Xianghe (see Fig. 7.14 of AC-SAF 2018 report and Figs. S3 and S5 of Liu et al. (2019)) and Figs. S3 and S5 of Liu (2019)). While the a priori harmonization seems to mitigate this effect, it does not resolve it. It should be a focus of future research if improved MAX-DOAS a priori profiles and/or improved satellite averaging kernels can improve the situation. Based on the above, we provide an explanation in the text.

New references: EUMETSAT AC SAF operations report 1/2018, SAF/AC/FMI/OPS/RP/001, https://acsaf.org/docs/or/AC_SAF_Operations_Report_1-2018.pdf

Liu et al. (2019) Liu, S.; Valks, P.; Pinardi, G.; De Smedt, I.; Yu, H.; Beirle, S. and Richter, A. An improved total and tropospheric NO₂ column retrieval for GOME-2 Atmospheric Measurement Techniques, 2, 2019, 12, 1029-1057 10.5194/amt-12-1029-2019

Manuscript changes: Page 31, line 1. New text. The increase in seasonal variance is caused by the interplay of the seasonal variation of the MAX-DOAS vertical profile and of the satellite vertical averaging kernel. Specifically, it is found for the Xianghe case that in wintertime averaging kernels have higher values close to the surface while MAX-DOAS NO₂ profiles can also be peaked at the surface. The combination causes increased MAX-DOAS columns upon

vertical smoothing. This is also seen e.g., in the comparison of GOME-2 AC SAF GDP 4.8 NO₂ product with MAX-DOAS at Xianghe (see Fig. 7.14 and 7.15 of Hovila et al. (2018) and Figs. S3 and S5 of Liu et al. (2019)). While the a priori harmonization seems to mitigate this effect, it does not resolve it. It should be a focus of future research if improved MAX-DOAS a priori profiles and/or improved satellite averaging kernels can improve the situation.

Reviewer 1: *Technical corrections:*

Page 3, line 8. Define OMI here. Done.

Page 3, line 9. Define DOAS here. Done.

fig. 4. Use consistent abbreviations for stratospheric and tropospheric, i.e., strat or strato, trop or tropo. The abbreviations in Fig. 4 have been replaced by stratospheric and tropospheric.

Page 8, line 26. Modify by Irie et al. (e.g., 2011, Fig. 17) to by e.g., Fig. 17 in Irie et al. 2011. Corrected.

Page 10, line 2. AOD has been defined twice in this line, remove the 2nd one. Corrected.

Page 11, line 21. Change MAXDOAS to MAX-DOAS. Corrected.

Page 15, Figure 3. Please define MXD in the caption. Inserted (MXD) after MAX- DOAS data.

Page 38, line 7. Change n/a-n/a to proper page numbers. There are several other n/a-n/a in the references. Corrected.

Answers to reviewer 2 and corresponding changes

Reviewer 2: *General Comments.* The manuscript entitled *Validation of Aura-OMI QA₄ECV NO₂ Climate Data Records with ground-based DOAS networks: role of measurement and comparison uncertainties* by Compernelle et al. describes the results of a validation exercise, comparing satellite-borne QA₄ECV tropospheric and stratospheric NO₂ partial VCDs with ground-based observations from a large number of stations. The paper is very well written and represents a significant contribution to the validation of satellite observations. Data products, validation methodology and data screening are described in detail. Error sources and potential reasons for discrepancies between ground-based and satellite-borne observations are discussed thoroughly. As far as I can judge as a non-native English speaker, there are hardly any grammatical or syntactical errors. I recommend the publication after addressing some minor issues as listed below. In particular, I would appreciate if the processing of the ground-based data sets and the differences between QA₄ECV and bePRO data products would be discussed in some more detail.

Authors reply 8: We are grateful to reviewer 2 for this positive feedback! We agree that more detail on the ground-based data sets would be useful for the reader. We give a point-by-point answer below.

Reviewer 2: *Specific Comments Section 2.2.2:* I feel that the MAX-DOAS

retrieval algorithms should be described in more detail. It should be stated more clearly that the QA4ECV and the bePRO algorithms are distinctly different, with QA4ECV retrieving NO₂ VCDs directly by dividing the dSCD from a single elevation angle by the differential AMF, while bePRO VCDs are determined by integrating a vertical NO₂ profile retrieved by an OEM algorithm based on measurements from several elevation angles. There are recent studies on the performance of bePRO in comparison with other profile retrieval algorithms (Friess et al., *Atmos. Meas. Tech.*, 2019, <https://doi.org/10.5194/amt-12-2155-2019>; Tirpitz et al., *Atmos. Meas. Tech. Discuss*, <https://doi.org/10.5194/amt-2019-456>) which should be cited here. I would furthermore appreciate if it would be discussed to what extent the problems with the stability of the bePRO NO₂ vertical profile retrieval identified within these studies affects the quality of the data used here for OMI validation.

Authors reply 9: We acknowledge that more details could have been included. We include now more details on QA4ECV MAX-DOAS especially from the reference Hendrick et al. (2016) (see also our answer further below regarding the vertical grid) and on bePRO, especially from the reference Hendrick et al. (2014). We added a short text highlighting the difference between both approaches.

Furthermore, we add both suggested references. However, it is difficult to judge in how far the bePRO stability problems are important as, as stated by Friess et al. "The synthetic data used for the study are not necessarily representative of real measurements, especially in terms of dSCDs errors, and sensitivity tests performed by increasing the dSCDs errors but also previous publications (e.g. Hendrick et al., 2014; Vlemmix et al., 2015b) have shown that bePRO performs generally well with real measurement data, also in terms of convergence." Therefore, we rather limit ourselves to the statement that in future validation work, consideration of other retrieval algorithms, well-performing in the intercomparison exercises of Friess et al. and Tirpitz et al., would be of high interest.

Manuscript changes:

Page 8, line 23. New paragraph. There is a clear distinction between the QA4ECV MAX-DOAS and bePRO retrieval algorithms. In the QA4ECV MAX-DOAS algorithm, the VCD is obtained by dividing a differential SCD by a differential AMF at a single elevation angle (see section 1.3 of Hendrick et al. (2016)). In the bePRO approach (Clemer et al., 2010; Hendrick et al., 2014; Vlemmix et al., 2015) a VCD is obtained by integrating a vertical NO₂ profile retrieved by an OEM using measurements at several elevation angles.

Page 9, line 8. New paragraph. We note that the bePRO profile retrieval algorithm has recently been compared to several other retrieval algorithms (Friess et al. (2019), Tirpitz et al. (2020)). In future validation work, consideration of other retrieval algorithms, that perform well in the intercomparison exercises of Friess et al. (2019), Tirpitz et al. (2020) would be of high interest.

Reviewer 2: P7, L10: Please provide a reference (or an URL) for the

description of the NDACC standard procedure.

Authors reply 10: The following url was added to the manuscript: http://ndacc-uvvis-wg.aeronomie.be/tools/NDACC_UVVIS-WG_NO2settings_v4.pdf

Reviewer 2: *P8, L31: Given that QA4ECV MAX-DOAS tropospheric NO₂ is determined by dividing the tropospheric SCD by the tropospheric AMF, I don't understand how a vertical grid can be involved here.*

Authors reply 11: Details of the QA4ECV MAX-DOAS approach are available in Hendrick et al. (2016). In short, NO₂ AMF is produced using the bePRO/LIDORT radiative transfer suite (Clmer et al., 2010; Spurr, 2008). The tool uses, among else, the following input: a set of NO₂ vertical profile shapes, vertical averaging kernels LUTs, geometry parameters (solar angles, viewing angles etc.), aerosol AOD vertical profile shapes, etc. Column AVK LUTs have been calculated based on the Eskes and Boersma (2003)s approach, using the bePRO/LIDORT RTM initialized with similar parameter values as for the AMF LUTs calculation. Interpolated AMFs, but also corresponding profile shapes and column averaging kernels, quantities defined on a vertical grid, are generated by the tool. We add more details of the QA4ECV MAX-DOAS approach in the text, especially on the origin of the MAX-DOAS a priori profiles and averaging kernels.

Manuscript changes: Page 8, line 6. New text. "The NO₂ AMF LUT are produced using the bePRO/LIDORT ..." The NO₂ AMF LUT are produced using the bePRO/LIDORT radiative transfer suite (Clemer et al.,2010; Spurr, 2008). This tool uses, among else, the following input: a set of NO₂ vertical profile shapes, vertical averaging kernels LUTs, geometry parameters (like solar angles and viewing angles), aerosol AOD vertical profile shapes, etc. Column AVK LUTs have been calculated based on the Eskes and Boersma (2003) approach, using the bePRO/LIDORT radiative transfer model initialized with similar parameter values as for the AMF LUTs calculation. Interpolated AMFs, but also corresponding vertical profile shapes and column averaging kernels, are generated by the tool. More detail is provided in Hendrick et al., (2016).

New reference: Spurr, R.: Light Scattering Reviews, vol. 3, chap. LIDORT and VLIDORT: Linearized pseudo-spherical scalar and vector discrete ordinate radiative transfer models for use in remote sensing retrieval problems, Springer, Berlin, Heidelberg, 2008.

Reviewer 2: *P12, L6: Explain what you mean with the term observation operator.*

Authors reply 12: It is already defined in the following sentence, but for better readability we rephrased that sentence.

Manuscript changes: Page 12, line 6. New text. This observation operator is a 2-D polygon that results from the parametrization of the actual extent of the air mass to which the ZSL-DOAS measurement is sensitive.

Reviewer 2: P12, L7: Which ray tracing code did you use here?

Authors reply 13: UVspec/DISORT. This was added to the text.

Manuscript changes: Page 12, line 8. New text. Its horizontal dimensions were derived using the UVSPEC/DISORT ray tracing code (Mayer and Kylling, 2005).

Reviewer 2: Last paragraph of Section 3.3 and Figure 7: It is not clear to me in which way the bias-correction for the annual mean difference has been performed - please explain in more detail.

Authors reply 14: As we chose an entirely different visualization of the seasonal features in the new version of the manuscript (as requested by the other referee), this bias correction is no longer required (and thus not discussed).

Reviewer 2: P23, L6: By how much has the satellite a priori profile been shifted?

Authors reply 15: This depends of course on the location. We add now a range of values in the text.

p. 22, line 3. New text. The ground levels are shifted by, on average, 0.03 km (Cabauw, De Bilt) to 0.4 km (Athens, Bujumbura).

Reviewer 2:

Technical Comments

P21, L4: characterized with \rightarrow characterized by Corrected.

P21, L22: Insert being before tropospheric VCD Inserted.

P22, L25: Add right parenthesis: (see Eq. (1)) Corrected.

P23, L12 and L30: Add space between number and unit Corrected.

P31, L1: does \rightarrow do Corrected.

Other changes

Note: we refer here to pages and line numbers of the marked-up manuscript version (obtained using latexdiff).

p. 6, line 15. Update on total uncertainty.

p. 15. Lines 25 and following. As Figure 6 uses now a different visualization approach, the corresponding text has changed as well.

Validation of Aura-OMI QA4ECV NO₂ Climate Data Records with ground-based DOAS networks: role of measurement and comparison uncertainties

Steven Compernelle¹, Tijn Verhoelst¹, Gaia Pinardi¹, José Granville¹, Daan Hubert¹, Arno Keppens¹, Sander Niemeijer², Bruno Rino², Alkis Bais³, Steffen Beirle⁴, Folkert Boersma^{5,8}, John P. Burrows⁶, Isabelle De Smedt¹, Henk Eskes⁵, Florence Goutail⁷, François Hendrick¹, Alba Lorente⁸, Andrea Pazmino⁷, Ankie PETERS⁵, Enno Peters⁶, Jean-Pierre Pommereau⁷, Julia Remmers⁴, Andreas Richter⁶, Jos van Geffen⁵, Michel Van Roozendaal¹, Thomas Wagner⁴, and Jean-Christopher Lambert¹

¹Royal Belgian Institute for Space Aeronomy (BIRA-IASB), Uccle, Belgium

²Es&t Corporation, Delft, The Netherlands

³Aristotle University of Thessaloniki, Laboratory of Atmospheric Physics (AUTH), Thessaloniki, Greece

⁴Max Planck Institute for Chemistry (MPIC), Mainz, Germany

⁵Royal Netherlands Meteorological Institute (KNMI), De Bilt, The Netherlands

⁶Institute of Environmental Physics, University of Bremen (IUP-B), Bremen, Germany

⁷Laboratoire Atmosphères, Milieux, Observations Spatiales, CNRS, Guyancourt, France

⁸Wageningen University, Meteorology and Air Quality Group, Wageningen, the Netherlands

Correspondence: steven.compernelle@aeronomie.be

Abstract. The QA4ECV version 1.1 stratospheric and tropospheric NO₂ vertical column density (VCD) climate data records (CDR) from the satellite sensor OMI are validated, using NDACC zenith scattered light DOAS (ZSL-DOAS) and Multi Axis-DOAS (MAX-DOAS) data as a reference. The QA4ECV OMI stratospheric VCD have a small bias of $\sim 0.2 \text{ Pmolec cm}^{-2}$ (5-10%) and a dispersion of 0.2 to 1 Pmolec cm^{-2} with respect to the ZSL-DOAS measurements. QA4ECV tropospheric VCD observations from OMI are restricted to near-cloud-free scenes, leading to a negative sampling bias (with respect to the unrestricted scene ensemble) of a few Pmolec cm^{-2} up to $-10 \text{ Pmolec cm}^{-2}$ (-40%) in one extreme high-pollution case. QA4ECV OMI tropospheric VCD has a negative bias with respect to the MAX-DOAS data (-1 to $-4 \text{ Pmolec cm}^{-2}$), a feature also found for the OMI OMNO2 standard data product. The tropospheric VCD discrepancies between satellite and ground-based data exceed by far the combined measurement uncertainties. Depending on the site, part of the discrepancy can be attributed to a combination of comparison errors (notably horizontal smoothing difference error), measurement/retrieval errors related to clouds and aerosols, and to the difference in vertical smoothing and a priori profile assumptions.

1 Introduction

Nitrogen oxides ($\text{NO}_x = \text{NO}_2 + \text{NO}$) play a significant role in the atmosphere, since they catalyse tropospheric ozone formation through a suite of chemical reactions, impact the oxidizing capacity of the atmosphere and thus influence the atmospheric burdens of major pollutants like methane and carbon monoxide (Seinfeld and Pandis, 1997). In addition, they are responsible

for secondary aerosol formation (Sillman et al., 1990). Fossil fuel combustion is the dominant source to the global NO_x emission budget (~50%), followed by natural emissions from soils, lightning and open vegetation fires (Delmas et al., 1997). High ozone, aerosol and NO_x have adverse effects on human health (Hoek et al., 2013; World Health Organization, 2013), and recommended limits from the EU and the World Health Organization are often exceeded especially in densely populated and industrialized regions (European Environment Agency, 2018). The emissions of NO_x have been therefore the main target of abatement strategies throughout the globe (e.g., the Protocol of Gothenburg, 1999). The effects of NO_x emissions on climate are complex and not fully understood so far. On the one hand, the emissions of NO_x result in the increase of ozone and thus to a net warming (since ozone is a greenhouse gas). On the other hand, they lead to a decrease of methane abundances at longer time scales, and therefore to a cooling effect (Myhre et al., 2013). Due to their indirect impact on radiative forcing and potential role on climate (Shindell et al., 2009), NO_x are identified as an Essential Climate Variable (ECV) precursor by the Global Climate Observing System (GCOS) (GCOS, 2016). NO_x are also present in the stratosphere (Noxon, 1979), where they contribute to the catalytic destruction of ozone (Crutzen, 1970).

Observations from satellite nadir-viewing sensors are essential for mapping the global multi-year picture of the NO_x distribution and trend. However, the quality of these datasets needs to be carefully assessed, using ground-based measurements at different sites (see e.g., Petritoli et al., 2004; Pinardi et al., 2014; Heue et al., 2005; Brinksma et al., 2008; Celarier et al., 2008, for validations on GOME, GOME-2, SCIAMACHY and OMI data). A limitation often encountered is that uncertainties in satellite and/or ground-based data are not adequately characterized, and the ground-based datasets are generally not harmonized across networks.

The EU Seventh Framework Programme (FP7) QA4ECV (Quality Assurance for Essential Climate Variables) project (www.qa4ecv.eu) demonstrated how reliable and traceable quality information can be provided for satellite and ground-based measurements of climate and air quality parameters. We highlight here three of its achievements. (i) The development of a quality assurance framework for climate data records (CDRs) (Nightingale et al., 2018), covering aspects as product traceability, uncertainty description, validation and documentation, following international standards (QA4EO; Joint Committee for Guides in Metrology, 2008, 2012). Among its components are a generic validation protocol (Compernelle et al. (2018), building further on Keppens et al. (2015)), a compilation of recommended terminology for CDR quality assessment (Compernelle and Lambert, 2017; Compernelle et al., 2018) and a validation server (Compernelle et al., 2016; Rino et al., 2017), the latter being prototype for the operational validation servers for S5P-MPC (Sentinel-5p Mission Performance Center) and CAMS (Copernicus Atmosphere Monitoring Service). (ii) The establishment of multi-decadal CDRs for 6 ECVs along the guidelines of the quality assurance framework. Among them are the QA4ECV NO₂ (Lorente et al., 2017; Zara et al., 2018; Boersma et al., 2018) and HCHO (De Smedt et al., 2018) version 1.1 satellite products, available for several sensors. (iii) The development of a NO₂ and HCHO long-term ground-based data set for 10 MAX-DOAS instruments, harmonized in measurement protocol, data format and with extensive uncertainty characterization (Hendrick et al., 2016; Richter et al., 2016).

A general across-community issue in the geophysical validation of satellite data sets with respect to ground-based reference measurements are the additional uncertainties that appear when comparing data sets characterized ~~with~~ by different temporal/spatial/vertical sampling and smoothing properties (Loew et al., 2017). This is especially critical in the case of short-lived

tropospheric gases (Richter et al., 2013b). This issue was the focus of the EU H2020 project GAIA-CLIM (Gap Analysis for Integrated Atmospheric ECV CLimate Monitoring (Verhoelst et al., 2015; Verhoelst and Lambert, 2016).

In this work we report a comprehensive validation of the QA4ECV NO₂ version 1.1 data product on the OMI ([Ozone Monitoring Instrument](#)) sensor, using as a reference the ground-based measurements acquired by networks of DOAS ([Differential Optical Absorption Spectroscopy](#)) UV-visible instruments developed in the context of the Network for the Detection of Atmospheric Composition Change (NDACC). Zenith-scattered light DOAS (ZSL-DOAS) data obtained routinely as part of NDACC monitoring activities is used to validate the stratospheric vertical column density (VCD), while Multi-axis DOAS (MAX-DOAS) data, either from NDACC or further harmonized within the QA4ECV project is used to validate the tropospheric VCD. We focus on how well the ex-ante¹ uncertainties and comparison errors can explain the observed discrepancies, making use of the framework and methodology developed within the projects QA4ECV and GAIA-CLIM.

In section 2 the satellite and reference data sets are described. Section 3.1 provides details about the validation methodology. In section 3.2 we outline how the quality screening of QA4ECV OMI NO₂, notably the exclusion of cloudy scenes, leads to underestimated early afternoon tropospheric NO₂ VCDs. Section 3.3 presents the comparison of QA4ECV OMI stratospheric NO₂ VCD with ZSL-DOAS. In section 3.4 the satellite tropospheric VCD is compared with measurements from 10 MAX-DOAS instruments. The differences are analysed in relation to the uncertainties and comparison errors. Potential causes of the discrepancies (e.g., horizontal smoothing difference error, low-lying clouds or aerosols, profile shape uncertainty, etc.) and attempts for resolving the discrepancies are discussed. Finally, the conclusions are formulated in section 4.

¹An ex-ante quantity does not rely on a statistical comparison with external data (von Clarmann, 2006). This is to be contrasted with ex-post quantities like the mean difference of satellite data vs. reference data.

2 Description of the data sets

2.1 Satellite data

2.1.1 QA4ECV OMI NO₂

The QA4ECV NO₂ OMI version 1.1 data product is retrieved from level-1 UV-Vis spectral measurements (OMI-Aura_L1-
5 OML1BRVG radiance files) from the Dutch-Finnish UV-Vis nadir viewing spectrometer OMI (Ozone Monitoring Instrument) on NASA's EOS-Aura polar satellite. The nominal footprint of the OMI ground pixels is 24×13 km² (across × along track) at nadir to 165×13 km² at the edges of the 2600 km swath, and the ascending node local time is 13:42 hrs. For more details on the instrument, see Levelt et al. (2006). The data product provides a level-2 (L2) tropospheric, stratospheric, and total NO₂ VCD.

10 The QA4ECV algorithm includes the following steps: (i) the retrieval of the total slant column density (SCD) N_s using Differential Optical Absorption Spectroscopy (DOAS), (ii) estimation of the stratospheric SCD $N_{s,\text{strat}}$ from data assimilation using the chemistry transport model (CTM) TM5, after which (iii) the tropospheric contribution is obtained by subtraction, and (iv) the calculation of tropospheric air mass factors (AMFs) M_{trop} converting the SCD to a VCD $N_{v,\text{trop}}$ (See Table 1). The retrieval equation is as follows

$$15 \quad N_{v,\text{trop}} = \frac{N_s - N_{s,\text{strat}}}{M_{\text{trop}}} \quad (1)$$

More information can be found in the QA4ECV NO₂ Product Specification Document (Boersma et al., 2017) and in Zara et al. (2018); Boersma et al. (2018). A preliminary evaluation of the data indicated that QA4ECV NO₂ values are 5-20% lower than the earlier version DOMINO v2 of the OMI NO₂ data product over polluted regions, and agree slightly better with MAX-
20 DOAS NO₂ VCD measurements in Tai'an (China) and De Bilt (The Netherlands) than the DOMINO v2 VCDs (Lorente et al., 2017; Lorente Delgado, 2019).

The data product files contain a comprehensive amount of metadata. Per pixel the satellite data product provides a total *ex-ante* uncertainty on the retrieved tropospheric VCD, as well as a breakdown of the uncertainty u_{SAT} into an *ex-ante* uncertainty budget, with the following uncertainty source components: uncertainty in total SCD u_{SAT,N_s} , stratospheric SCD $u_{\text{SAT},N_{s,\text{strat}}}$, and tropospheric AMF $u_{\text{SAT},M_{\text{trop}}}$, which contains contributions from uncertainties in surface albedo u_{SAT,A_s} , cloud fraction (CF) $u_{\text{SAT},f_{cl}}$, cloud pressure $u_{\text{SAT},p_{cl}}$ and a priori profile shape u_{SAT,S_a} , and an albedo-CF cross-term (with $c_{A_s,f_{cl}}$ the error correlation coefficient between both properties) (Boersma et al., 2018, section 6).

$$25 \quad \begin{aligned} u_{\text{SAT}}^2 &= u_{\text{SAT},N_s}^2 + u_{\text{SAT},N_{s,\text{strat}}}^2 + u_{\text{SAT},M_{\text{trop}}}^2 \\ u_{\text{SAT},M_{\text{trop}}}^2 &= u_{\text{SAT},A_s}^2 + u_{\text{SAT},f_{cl}}^2 + u_{\text{SAT},p_{cl}}^2 + u_{\text{SAT},S_a}^2 + 2c_{A_s,f_{cl}} u_{\text{SAT},A_s} u_{\text{SAT},f_{cl}} \end{aligned} \quad (2)$$

Furthermore, the satellite data files provide several relevant instrument parameters, influence quantities (e.g., cloud fraction, surface albedo, terrain height, ...), intermediate quantities (SCD, AMF, stratospheric SCD, ...), and the column averaging kernel \mathbf{a}_{SAT} , which relates the retrieved VCD to the true profile. The a priori NO₂ profiles (simulated with TM5) are not stored

in the data files. In the case a user has to adapt a (measured or modelled) profile \mathbf{x}_h at high vertical resolution to the vertical sensitivity of the satellite, he can apply (eq. (11) of Eskes and Boersma, 2003),

$$\mathbf{a}_{\text{SAT}} \cdot \mathbf{x}_h = \mathbf{x}_{h,\text{sm}} \quad (3)$$

where the a priori profile $\mathbf{x}_{\text{SAT},a}$ is not explicit. The dependence of the retrieval on $\mathbf{x}_{\text{SAT},a}$ is already implicit via the averaging
5 kernel \mathbf{a}_{SAT} .

However, the reference data in the current work are column retrievals or profile retrievals with a limited vertical resolution, and are based on an a priori profile that is different from the satellite retrieval. Before smoothing, satellite and reference retrievals should be adjusted such that they use the same a priori profile (Rodgers and Connor, 2003), therefore knowledge of the satellite a priori profile is relevant. These can be derived from the TM5-MP data files (Huijnen et al., 2010; Williams
10 et al., 2017), available upon request (see Boersma et al., 2017, for contact details), by spatially interpolating the profiles to the location of the satellite ground pixel.

In this work, we considered data from 2004 up to and including 2016 for the tropospheric VCD and up to and including 2017 for the stratospheric VCD.

2.1.2 OMI STREAM stratospheric NO₂

15 The STRatospheric Estimation Algorithm from Mainz (STREAM) (Beirle et al., 2016) was included as an alternative stratospheric estimation scheme in the QA4ECV NO₂ data files. In STREAM, the estimate of stratospheric columns is based on satellite observations with negligible tropospheric contribution, i.e. generally over regions with low tropospheric NO₂ levels, and for satellite pixels with high clouds, where the tropospheric column is shielded. The stratospheric field is then smoothed and interpolated globally, assuming that the spatial pattern of stratospheric NO₂ does not feature strong gradients.

20 2.1.3 NASA OMNO2 data product

Although not the main focus of this work, we do include as benchmark comparisons of an alternative retrieval product, the NASA's OMI NO₂ data - OMNO2 version 3.1 (Bucsela et al., 2016; Krotkov et al., 2017) -, with QA4ECV MAX-DOAS. Like QA4ECV OMI NO₂, it is also based on the DOAS approach, but nearly all retrieval steps are different between the QA4ECV and NASA OMI NO₂ algorithms (Table 1). A detailed comparison between the QA4ECV and NASA fitting approaches
25 showed small differences between NO₂ SCDs (Zara et al., 2018), so differences between the spectral fitting approaches explain only a small part of the differences in the tropospheric VCDs. The stratospheric correction approach differs between the two algorithms. Although the QA4ECV and NASA stratospheric SCDs have not been compared directly, previous evaluations suggest that differences between the approaches typically lead to small but spatially widespread differences of up to $0.5\text{-}1.0 \times 10^{15}$ molec cm⁻² in tropospheric VCDs. This leaves differences between the tropospheric AMF calculations, and especially
30 the prior information used in their calculations, as the most likely explanation of the lower NASA than QA4ECV NO₂ VCDs (e.g., Goldberg et al., 2017).

Table 1. OMI satellite data products considered in this work.

Data product	Spectral fitting	Stratospheric correction	Tropospheric AMF
OMI QA4ECV v1.1	Zara et al. (2018)	Data assimilation in TM5-MP (Boersma et al., 2018)	Surface albedo from Kleipool et al. (2008) 5-yr climatology at $0.5^\circ \times 0.5^\circ$; clouds from OMI O ₂ -O ₂ algorithm (OMCLDO2 data product, Veeffkind et al., 2016); a priori NO ₂ profiles from daily TM5-MP at $1^\circ \times 1^\circ$
OMI STREAM ^a		Weighted (observations with negligible trop contrib (clean regions, cloudy pixels)) convolution (Beirle et al., 2016)	
OMNO2 v3.1	Marchenko et al. (2015)	Three-step (interpolation, filtering, smoothing) strat field reconstr to fill in the trop contam scenes (Bucsela et al., 2013)	Surface albedo from Kleipool et al. (2008) 5-yr climatology at $0.5^\circ \times 0.5^\circ$; clouds from OMI O ₂ -O ₂ algorithm (OMCLDO2 data product), a priori profiles from monthly GMI at $1^\circ \times 1.25^\circ$ (Strahan et al., 2013)

a. OMI STREAM stratospheric VCD is contained in the OMI QA4ECV v1.1 data files.

2.2 Ground-based data

2.2.1 Zenith-scattered-light DOAS

The ZSL-DOAS data are part of the Network for the Detection of Atmospheric Composition Change (NDACC) (De Mazière et al., 2018, see also <http://www.ndaccdemo.org/>), a major contributor to WMO's Global Atmospheric Watch. A significant part of the multi-decadal ZSL-DOAS data is provided by the subnetwork Système d'Analyse par Observation Zénithale (SAOZ; see Pommereau and Goutail, 1988) from LATMOS, using SAOZ instrumentation in automated data acquisition mode and with fast data delivery.

Zenith-sky measurements are performed during twilight at sunrise and sunset. Due to this measurement geometry with a long optical path in the stratosphere, the measured column is about 14 times more sensitive to stratospheric NO₂ than to tropospheric NO₂ (Solomon et al., 1987). Moreover, it allows usable measurements during cloudy conditions as well. Processing followed the NDACC Standard Operation Procedure (http://ndacc-uvvis-wg.aeronomie.be/tools/NDACC_UVVIS-WG_NO2settings_v4.pdf), as implemented for instance in the LATMOS_v3 SAOZ processing. From slant column intercomparisons, Vandaele et al. (2005) deduce an uncertainty of about 4-7%, but this excludes the uncertainty on the AMF required to convert the slant to vertical columns. Ionov et al. (2008) estimate a total uncertainty on the vertical columns of 21%, but this is probably an overestimation for the most recent processing, as Bognar et al. (2019) now suggest a 13% total uncertainty. A visualisation of

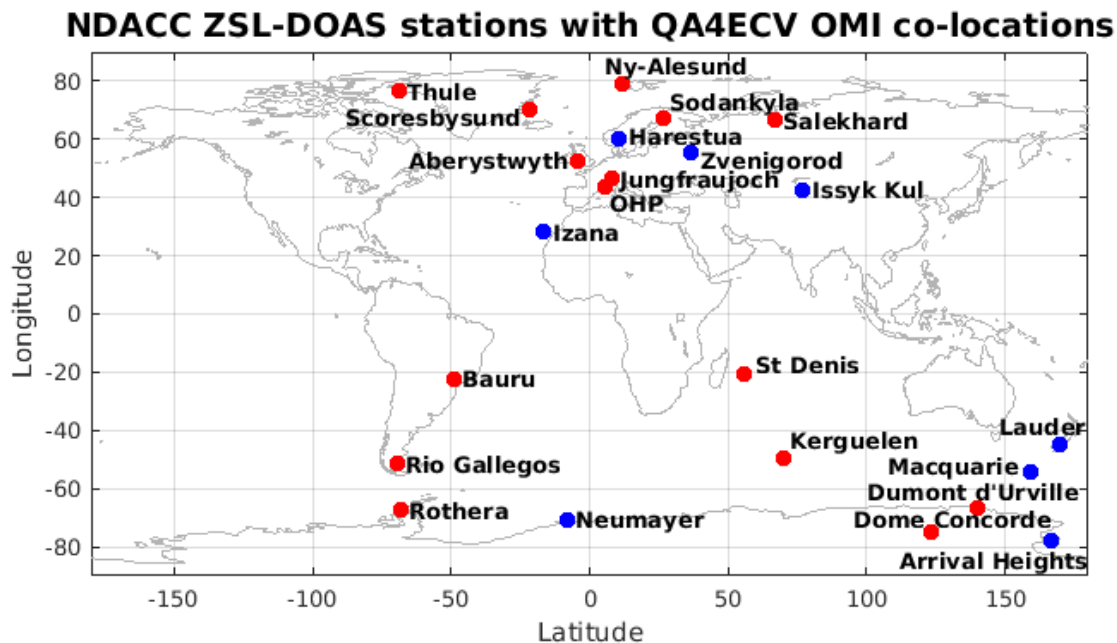


Figure 1. Global distribution of the ZSL-DOAS instruments used here. Red markers indicate SAOZ instruments, blue markers other NDACC ZSL-DOAS instruments.

the geographical distribution of the instruments is provided in Fig. 1. More details about the particular co-location scheme, taking into account the large horizontal smoothing of these measurements, and the photochemical adjustment required to convert twilight measurements to satellite overpass times, are provided in Sect. 3.1.

2.2.2 Multi axis-DOAS

5 The tropospheric NO_2 VCD data used as a reference are a long-term record of MAX-DOAS (Multi AXis-DOAS) measurements from 10 instruments, reprocessed by different teams for the project QA4ECV (see Table 2). MAX-DOAS measure scattered sunlight under different viewing elevations from the horizon to the zenith (Platt and Stutz, 2008). The observed light travels a long path (length dependent on the elevation angle) in the lower troposphere, while the stratospheric contribution is removed by a reference zenith measurement. Two different processings of MAX-DOAS data were used for the current validation study, QA4ECV MAX-DOAS and bePRO (Belgian Profiling) MAX-DOAS (Cl mer et al., 2010), the latter being part of NDACC.

Thanks to an extensive harmonisation effort within the QA4ECV project, reference QA4ECV MAX-DOAS data sets were produced by the different teams for all 10 instruments. Those are available at http://uv-vis.aeronomie.be/groundbased/QA4ECV_MAXDOAS/index.php. This effort was based on a four-step approach (see http://uv-vis.aeronomie.be/groundbased/QA4ECV_MAXDOAS/QA4ECV_MAXDOAS_readme_website.pdf; Hendrick et al., 2016; Richter et al., 2016; Peters et al., 2017), including (i) the establishment of recommendations for DOAS analysis settings from an intercomparison of NO_2 slant

column densities retrieved from common spectra; (ii) the development of NO₂ AMF look-up tables (LUTs) for harmonising the conversion of SCDs into VCDs; (iii) the establishment of a first harmonised error budget; (iv) the generation of MAX-DOAS data files in the Generic Earth Observation Metadata Standard (GEOMS) as common format. It is worth noting that since in this QA4ECV approach, only SCDs measured at a relatively high elevation angle (typically 30°) are used to minimize the impact of aerosols and a priori profile shape on the retrieval, the horizontal location of the centre of the effectively probed air mass is close to the instrument location (typically only 1 km difference). The NO₂ AMF LUT are produced using the bePRO/LIDORT radiative transfer suite (Clémer et al., 2010; Spurr, 2008). This tool uses, among else, the following input: a set of NO₂ vertical profile shapes, vertical averaging kernels LUTs, geometry parameters (like solar angles and viewing angles), aerosol AOD vertical profile shapes, etc. Column AVK LUTs have been calculated based on the Eskes and Boersma (2003) approach, using the bePRO/LIDORT radiative transfer model initialized with similar parameter values as for the AMF LUTs calculation. Interpolated AMFs, but also corresponding vertical profile shapes and column averaging kernels, are generated by the tool. More detail is provided in Hendrick et al. (2016).

The second processing, bePRO MAX-DOAS (Clémer et al., 2010; Hendrick et al., 2014; Vlemmix et al., 2015), is available for three BIRA-IASB instruments (at Bujumbura, Uccle and Xianghe). This approach, based on the optimal estimation method (OEM; see Rodgers, 2000), provides profile measurements, albeit with a limited degree of freedom for signal in the vertical dimension, typically ~2 (Bujumbura, Uccle) or ~3 (Xianghe). The horizontal extension of the air masses probed by profile retrieval MAX-DOAS is within about 5 to 15 km distance from the instrument in the viewing direction (Richter et al., 2013a). The extension depends on the atmospheric visibility (smaller extension for lower visibility) and altitude of the NO₂ layer (smaller extension with decreasing profile height). This is in line with typical distances estimated by ~~Irie et al. (e.g., 2011, Fig. 17)~~ e.g., Fig. 17 in Irie et al. (2011). The horizontally projected area of the MAX-DOAS-probed air mass is estimated to be in the order of 0.01 to 0.2 km² for QA4ECV MAX-DOAS and ~1 km² for bePRO MAX-DOAS, assuming a 1° field-of-view and a simple geometrical approximation.

There is a clear distinction between the QA4ECV MAX-DOAS and bePRO retrieval algorithms. In the QA4ECV MAX-DOAS algorithm, the VCD is obtained by dividing a differential SCD by a differential AMF at a single elevation angle (see section 1.3 of Hendrick et al. (2016)). In the bePRO approach (Clémer et al., 2010; Hendrick et al., 2014; Vlemmix et al., 2015) a VCD is obtained by integrating a vertical NO₂ profile retrieved by an OEM using measurements at several elevation angles.

MAX-DOAS probe the lower troposphere, with the highest sensitivity (described by the column averaging kernel) close to the surface, typically in the lowest 1.5 km of the atmosphere. Nevertheless, the vertical grid extends to ~10 km for QA4ECV MAX-DOAS and ~3 km for bePRO MAX-DOAS.

The MAX-DOAS sites span a wide range of NO₂ levels, from relatively low at OHP and Bujumbura (mean tropospheric MAX-DOAS VCD around OMI overpass time ~3 Pmolec cm⁻²) to strongly polluted at Xianghe (mean MAX-DOAS value ~24 Pmolec cm⁻²) (see Fig. 3c, black boxplots), while the other sites are moderately polluted (mean value between 5.6 and 11 Pmolec cm⁻²).

The MAX-DOAS tropospheric VCD is provided with an *ex-ante* uncertainty in the GEOMS data files. Unfortunately the employed uncertainty estimation approach is not harmonised among all data providers. Therefore, we set for QA4ECV MAX-

Table 2. Overview of contributing sources for the QA4ECV MAX-DOAS reference data set.

Station	Location	Start+end time	Class	Contributor ^a
Bremen (DE)	53.10°N, 8.85°E	02/2005-12/2016	Urban	IUP-UB
De Bilt (NL) ^c	52.10°N, 5.18°E	03/2011-11/2017	Sub-urban	KNMI
Cabauw (NL) ^{c,d}	51.97°N, 4.93°E			
Uccle (BE) ^{b,d}	50.80°N, 4.36°E	04/2011-06/2015	Urban	BIRA-IASB
Mainz (DE) ^d	49.99°N, 8.23°E	06/2013-12/2015	Urban	MPG
Observatoire Haute Provence (FR) ^d	43.94°N, 5.71°E	02/2005-12/2016	Rural / Background	BIRA-IASB
Thessaloniki (GR) ^d	40.63°N, 22.96°E	01/2011-05/2017	Urban	AUTH
Xianghe (CHN) ^{b,d}	39.75°N, 116.96°E	04/2010-01/2017	Sub-urban	BIRA-IASB
Athens (GR) ^d	38.05°N, 23.86°E	09/2012-10/2016	Urban	IUP-UB
Nairobi (KEN)	1.23°S, 36.82°E	01/2004-11/2014	Rural / Urban	IUP-UB
Bujumbura (BU) ^{b,d}	3.38°S, 29.38°E	01/2014-12/2016	Sub-urban	BIRA-IASB

^a Contributing teams: Aristotle University of Thessaloniki (AUTH), Royal Belgian Institute of Space Aeronomy (BIRA-IASB), Institute of Environmental Physics at University of Bremen (IUP-UB), Max Planck Institute (MPG), Royal Netherlands Meteorological Institute (KNMI). ^b For this sensor also bePRO MAX-DOAS data, providing profile data, is available. ^c The same instrument was operated at two different locations, De Bilt and Cabauw, which are at approximately 30 km distance. ^d An AERONET instrument, measuring aerosol optical depth, is located at this site or at close distance.

DOAS instead the total uncertainty at 22.2% of the retrieved VCD, following the QA4ECV deliverable D3.9 recommendation (Richter et al., 2016). Following sensitivity tests, aerosol effects (20%) and NO₂ a priori profile shape (8%) were identified as the main contributors to the MAX-DOAS uncertainty, while uncorrelated instrument noise is only 2%. However, we do not follow D3.9 (Richter et al., 2016) in its recommended division of the uncertainty into random error and systematic error uncertainty contributions² and consider only a total uncertainty. Regarding bePRO MAX-DOAS, we consider 12% total uncertainty for Uccle and Xianghe (following Hendrick et al., 2014), and 21% for Bujumbura (following Gielen et al., 2017). We finally note that for clean sites, an absolute scale uncertainty estimate might be more appropriate.

[We note that the bePRO profile retrieval algorithm has recently been compared to several other retrieval algorithms \(Frieß et al., 2019; Tirpitz et al., 2020\) would be of high interest.](#)

As the accuracy of satellite or ground-based remote sensing can be affected by the presence of aerosol, tracking aerosol optical depth (AOD) is useful. The bePRO MAX-DOAS provides aerosol optical depth (~~AOD~~ measurements measurements at

²In D3.9, the systematic error uncertainty is set at 3%, arising from absorption cross-section related systematic error uncertainty on the SCD, while the random error uncertainty is set at 22%, arising from uncertainty on the AMF. However, the assumption that e.g., an error in a priori profile shape would translate to a random error on the retrieved column is not evident in our opinion. In a later analysis (Hendrick et al., 2018), a comparison of QA4ECV MAX-DOAS with more advanced MAX-DOAS profiling methods was performed. This highlighted systematic differences between -12% and +7%, considerably larger than the D3.9-recommended systematic error uncertainty of 3%. This suggests that a larger part of the total uncertainty should be assigned as due to systematic error. Therefore in this work we only consider a total uncertainty of 22.2%, derived from sum in quadrature of the recommended systematic and random components.

[the same temporal sampling as the NO₂ measurements](#). The QA4ECV MAX-DOAS provides an AOD climatology (Hendrick et al., 2016) based on AERONET (AERONET Aerosol Robotic Network) data (Giles et al., 2019); however, we found that the precision of this climatological data set was inadequate for the current work, especially for urban sites. Instead, we considered AOD directly from AERONET (Giles et al., 2019) (<http://aeronet.gsfc.nasa.gov>), whose measurements are based on Cimel
5 Electronique Sun–sky radiometers. Level 2.0 AOD at wavelength 440 nm was chosen, which is within the QA4ECV MAX-DOAS retrieval window of 425 - 490 nm. Note that the AERONET data is already cloud filtered.

[A limitation when investigating AOD dependencies in satellite-MAX-DOAS comparisons using AERONET AOD with QA4ECV MAX-DOAS tropospheric NO₂ VCD data \(as compared to using bePRO AOD with bePRO NO₂ data\) is that it implies a subsetting: for part of the QA4ECV MAX-DOAS NO₂ data no co-located AERONET AOD is available. Also, as
10 \[opposed to the bePRO NO₂/bePRO AOD combination, co-located QA4ECV MAX-DOAS NO₂/AERONET AOD data pairs have a temporal co-location mismatch and \\(where instruments are at different locations\\) a spatial co-location mismatch. A test was performed \\(results not shown\\) using the bePRO NO₂/AERONET AOD combination. It was generally found that the results are less clear than for the bePRO NO₂/bePRO AOD combination.\]\(#\)](#)

3 Validation

15 3.1 Validation methodology

The generic validation protocol is similar to that outlined by Keppens et al. (2015), and tailored within the QA4ECV project for the ECVs NO₂, HCHO and CO (Compernelle et al., 2018). Terms and definitions applicable to the quality assurance of ECV data products have been agreed upon within QA4ECV (Compernelle et al., 2018); the full set can be found at Compernelle and Lambert (2017). The discussion and analysis on comparison error follows the terminology and framework detailed within
20 the GAIA-CLIM project (Verhoelst et al., 2015; Verhoelst and Lambert, 2016).

In the following sections, we detail the baseline validation methodology.

3.1.1 Screening criteria

Filters to the satellite data product are applied following the recommendations in the QA4ECV NO₂ product specification document (PSD) (Boersma et al., 2017), and to minimize comparison error with MAX-DOAS.

25 Following the QA4ECV NO₂ product specification document (PSD) (Boersma et al., 2017), satellite data is kept for tropospheric NO₂ validation if the following conditions are met:

- (1) no raised errorflag,
- (2) satellite solar zenith angle (SZA) < 80°,
- (3) the so-called 'snow-ice flag' indicating either 'snow free land', or 'ice free ocean' or a sea-ice coverage below 10%

- (4) the ratio of tropospheric AMF over geometric AMF, $\frac{M_{\text{trop}}}{M_{\text{geo}}}$, must be higher than 0.2, to avoid scenes with very low tropospheric AMF (typically occurring when the TM5 model predicts a large amount of NO_2 close to the surface in combination with aerosols or clouds effectively screening this NO_2 from detection) and
- (5) effective cloud fraction (CF) < 0.2. This last filter is comparable to the PSD recommendation of cloud radiance fraction (CRF) < 0.5, and was chosen because effective cloud fraction is a more general property than CRF. Note that the effective cloud properties cloud fraction and cloud height are sensitive to both aerosol and cloud (Boersma et al., 2004). It should be mentioned that cloudy pixel retrievals - although subject to larger errors compared to clear-sky pixels - can still be used (e.g., in data assimilation), provided the averaging kernel is taken into account (Schaub et al., 2006).
- (6) Not mentioned in the PSD, but applied by Boersma et al. (2018), is a filter to limit the impact of aerosol haze and low clouds. In the latter work, this was accomplished by excluding ground pixels with a high retrieved cloud pressure, i.e. $p_c > 850$ hPa. Unfortunately, this filter can remove a substantial portion of the data, therefore a less strict filter was searched for in the current work. A low cloud can lead to a high uncertainty in the retrieved tropospheric NO_2 value when it is uncertain if it is located above the trace gas (mainly a screening effect and therefore a low AMF) or is at similar height (partial screening effect, partial surface albedo effect, and therefore a higher AMF). This is registered in the uncertainty component due to cloud pressure u_{SAT, p_c} available within the data product. Data analysis reveals that for several sites (Xianghe, Uccle, De Bilt, Bremen, Athens), a relatively small number of ground pixels are responsible for an important contribution to the root-mean-square (RMS) of the ex-ante satellite uncertainty, via the cloud pressure component u_{SAT, p_c} . Most of these high-uncertainty ground pixels have a low retrieved effective cloud pressure (Fig. S1 in supplement), indicative of aerosol haze or low-lying cloud. The aforementioned cloud pressure filter used by Boersma et al. (2018) would effectively remove these suspicious ground pixels, but also many other pixels with a low u_{SAT, p_c} . Therefore, we chose instead to apply as filter (6) a one-sided sigma-clipping on u_{SAT, p_c} : data where $u_{\text{SAT}, p_c, i} > \text{mean}(u_{\text{SAT}, p_c, i}) + 3 \times \text{SD}(u_{\text{SAT}, p_c, i})$ are removed. This sigma-clipping removes a smaller percentage of the data, while still achieving its goal of limiting u_{SAT, p_c} and u_{SAT} . After this filtering step, u_{SAT, p_c} is only a minor contributor to the OMI uncertainty budget.
- (7) Finally, satellite ground pixels with a footprint > 950 km^2 , corresponding to the 5 outermost rows at each swath edge of the OMI orbit, are removed to limit the horizontal smoothing difference error with the ~~MAXDOAS~~ MAX-DOAS data. Filter (7) is not a filter on satellite data quality, but rather a limit on the scope of the validation.

Regarding stratospheric NO_2 validation, only filters (1)-(3) are applied. Hence both cloudy and non-cloudy scenes are used.

Regarding the OMNO2 data product, we followed the recommendation of Bucsela et al. (2016) by only including ground pixels for which the least-significant bit of the variable VcdQualityFlags is zero (indicating good data). Furthermore, the effective cloud fraction must be < 0.2 and the pixel area < 950 km^2 .

No screening was applied to the ground-based reference data sets. In particular, filtering on the MAX-DOAS cloud flag is not applied as baseline as it is not available for all data sets. It should be noted that clouds can impact the quality of MAX-DOAS retrievals (see e.g., radiative transfer simulations of Ma et al., 2013; Jin et al., 2016).

3.1.2 Co-location criteria and processing

Stratospheric column

The airmass to which a ZSL-DOAS measurement is sensitive spans over many hundreds of kilometers towards the rising or setting Sun (e.g. Solomon et al., 1987). The co-location scheme employed here takes this into account by averaging all OMI ground pixels of a temporally co-located orbit (maximum allowed time difference of 12 hours) which have their center within the ZSL-DOAS observation operator. ~~This~~ This observation operator is a 2-D polygon that results from the parametrization of the actual extent of the airmass to which the ZSL-DOAS measurement is sensitive. Its horizontal dimensions were derived using ~~a~~ the UVSPEC/DISORT ray tracing code (Mayer and Kylling, 2005), mapping the 90% interpercentile of the stratospheric vertical column to a projection on the ground and then parametrized as a function of the solar zenith and azimuth angles during the twilight measurement, where the SZA during a nominal single measurement sequence is assumed to range from 87° to 91° (at the location of the station). Note that the station location is not part of the area of actual measurement sensitivity. The average OMI stratospheric column over this observation operator can then be compared to the column measured by the ZSL-DOAS instrument. An illustration of a single such co-location is presented in Fig. 2. Note that at polar sites, the above mentioned SZA range may not be covered entirely. For more details, we refer to Lambert et al. (1996) and Verhoelst et al. (2015).

To account for effects of the photochemical diurnal cycle of stratospheric NO₂, the ZSL-DOAS measurements, obtained twice daily at twilight at each station, are adjusted to the OMI overpass time using a model-based factor. The latter is extracted from LUTs calculated with the PSCBOX 1D stacked-box photochemical model (Errera and Fonteyn, 2001; Hendrick et al., 2004) initiated by daily atmospheric composition and meteorological fields from the SLIMCAT chemistry-transport model (Chipperfield, 1999). The amplitude of the adjustment depends strongly on the effective SZA assigned to the ZSL-DOAS measurements. It is taken here to be ~~89.5°~~ 89.5°. The uncertainty related to this adjustment is of the order of 10% or 1 to 2 10¹⁴ molec cm⁻².

Tropospheric column

Regarding the tropospheric column validation, satellite data is kept if the satellite ground pixel covers the MAX-DOAS instrument location, and if a MAX-DOAS measurement is within a 1-hour interval centered at the satellite measurement time. The average of all MAX-DOAS measurements within this 1-hour interval is taken. The typical number of MAX-DOAS measurements taken within this time interval was 2-4 for most sites. This procedure was applied to both QA4ECV OMI NO₂ and the OMNO2 comparisons.

3.2 Impact of quality screening

Quality screening is a necessary step before a satellite data product can be used, but it can be a limit to the data product's scope. Fig. 3a presents the remaining fractions of satellite overpass data at the MAX-DOAS sites at each of the 7 successive filter steps described in section 3.1.1. Note that the sites Cabauw and De Bilt are not included, as the results are very close to that of Uccle.

Observation Operator co-location OMI - SAOZ at OHP, Sunrise on 01-10-2010

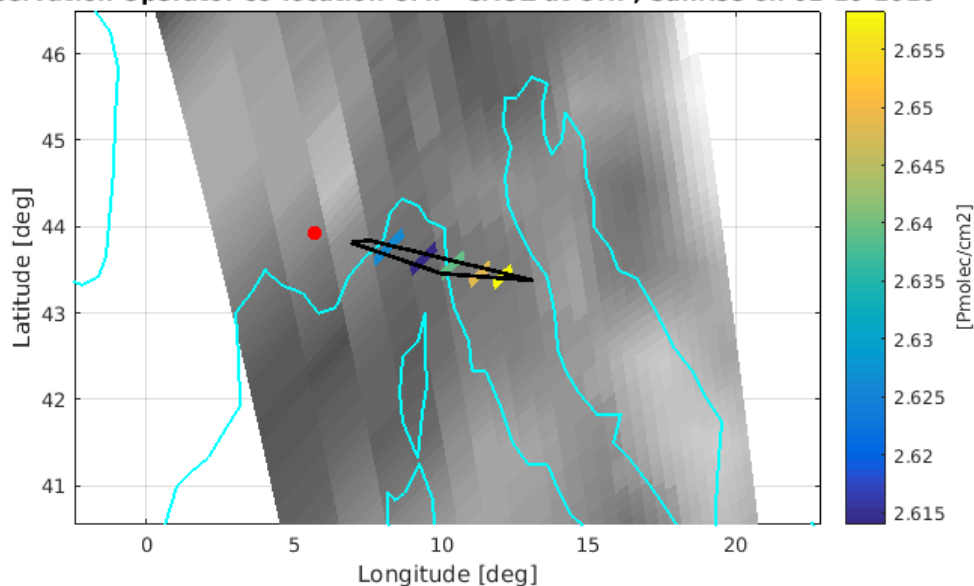


Figure 2. Illustration of a single co-location between OMI and a sunrise ZSL-DOAS measurement using the dedicated observation operator. The red dot marks the location of the ground instrument, the cyan lines the coast lines of this part of the Mediterranean. The grey-scale background contains the full orbit data, the coloured pixels are those that have their center within the observation operator (black polygon), i.e. those that are averaged to obtain a satellite measurement comparable to that of the ZSL-DOAS instrument.

The error flag (1) removes ~10-30% of the data, filters on SZA and snow-ice flag (2, 3) have a relatively small impact, the filter on AMF ratio (4) has a large impact on the sites Bremen, Mainz, Cabauw, De Bilt, Uccle and Xianghe (35-40% of data removed), and finally the filter on CF (5) has an important screening impact on all sites (see Fig. 3), removing up to 60% of the data at the site of Bujumbura. As an alternative to the CF filter, we tested also the $CRF < 0.5$; for most sites the CRF and CF filter have a near identical impact, but for Bujumbura and Nairobi the CRF filter is more restrictive (results not shown). In combination, the PSD-recommended quality filters (filters (1) to (5)) remove between 56% (Athens) and 90% (Bremen) of the data.

Filter (6), the filter on the uncertainty component due to cloud pressure u_{SAT, p_c} , removes at most 5% of data, at the site of Xianghe, while the alternative filter on cloud pressure would have removed 15% of data (Fig. S1). The filter on ground pixel size (7) removes 3-16% additional data.

The screening can have a strong seasonal effect; for example, the winter months are strongly underrepresented for the West-European urban sites (Fig. 3b). Fig. 3c presents, per MAX-DOAS site, box plots of co-located MAX-DOAS tropospheric NO_2 measurements before (black) and after (blue) screening. Both mean and median value decrease by the filtering step. We conclude that the quality screening tends to reject scenes with a high tropospheric NO_2 VCD, i.e., the restriction to quality-screened scenes leads to a negative sampling bias with respect to the ensemble of all scenes. In absolute scale, the

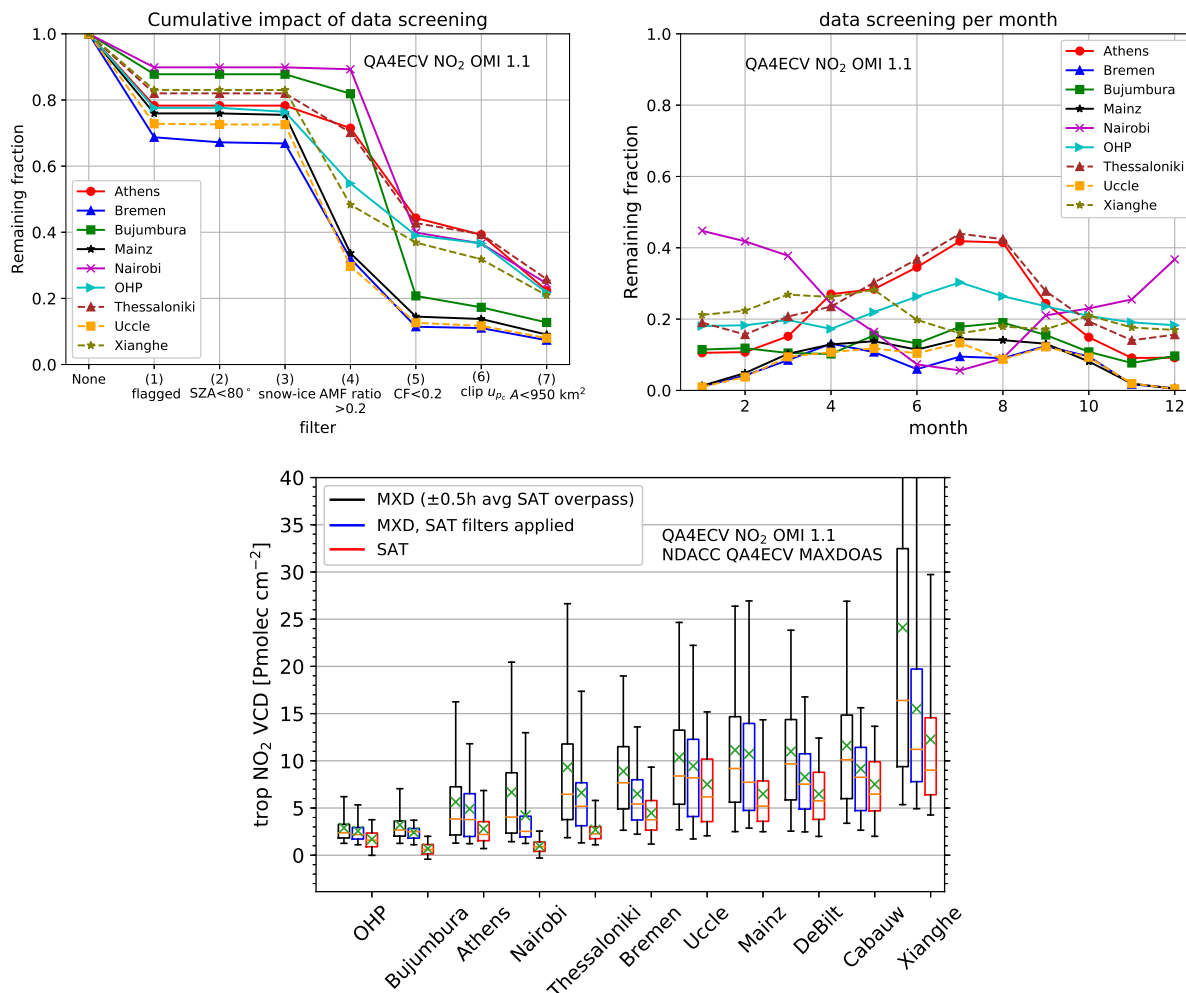


Figure 3. a) Starting from satellite data with ground pixel covering the MAXDOAS MAX-DOAS site, the remaining data fraction after applying each of the 7 filter criteria is presented. The criteria are explained in section 3.1.1. The sites Cabauw and De Bilt are not included here, as the fractions are very close to that of Uccle. b) Remaining fraction per month, after applying all filters. c) Per site, boxplots of QA4ECV MAX-DOAS data (MXD) co-located with QA4ECV OMI, before applying the filters (black), after applying the filters (blue), and of QA4ECV OMI co-located with MAX-DOAS and after applying the filters (SAT). The sites are sorted according to the median MAX-DOAS value before filtering. Boxplot legend: box edges: 1st and 3th quartiles; orange line: median; green cross: mean; whiskers: 5th and 95th percentiles.

screening effect is the strongest at the site Xianghe, leading to a reduction in yearly mean tropospheric NO_2 from 24 to 15 Pmolec cm^{-2} (40% decrease). At Nairobi, Thessaloniki, Bremen, De Bilt and Cabauw, the tropospheric VCD is reduced by several Pmolec cm^{-2} . The cloud filter is a main contributor to this sampling bias. This is in accordance with the results of Ma et al. (2013), where higher tropospheric NO_2 was measured by MAX-DOAS in Beijing in cloudy conditions compared to clear-sky conditions. Indeed, cloudy conditions lead to less photochemical loss of tropospheric NO_2 , as explained by with model results (Boersma et al., 2016). In comparisons of OMI tropospheric NO_2 with independent data, care should be taken that the independent data is also sampled for clear-sky conditions (Boersma et al., 2016). A systematic influence of clouds on the MAX-DOAS retrievals might contribute to the observed sampling bias effect.

It can be argued that the AMF ratio filter (filter (4)) is too restrictive. In section S2 results are presented for the less restrictive $\frac{\text{AMF}_{\text{trop}}}{\text{AMF}_{\text{geo}}} \geq 0.05$. The remaining data fraction is slightly increased at the sites Bremen, Mainz, Uccle, De Bilt and Cabauw (from ~8% to ~10%) and the winter months are better represented (see Fig. S2). The negative sampling bias at De Bilt and Bremen is reduced and removed at Mainz. As will be shown in section 3.4.6, this adapted filtering generally has no negative impact on the satellite vs MAX-DOAS comparisons.

3.3 Comparison of OMI stratospheric NO_2 - NO_2 with ZSL-DOAS

Figure 4 contains time series of stratospheric NO_2 - NO_2 columns, from both satellite (QA4ECV product) and ground-based instruments, at two illustrative ground sites: Kerguelen in the Southern Indian Ocean, which is representative for very clean background conditions, and the Observatoire de Haute Provence in France, which is affected by significant tropospheric pollution in local winter, often exceeding the wintertime stratospheric column. The graphs show the well-known seasonal cycle in stratospheric NO_2 - NO_2 , which is captured similarly by satellite and ZSL-DOAS instrument. Already evident from perusal of the results at OHP, is that the stratospheric comparison is hardly affected by the peaks in tropospheric pollution, e.g. in winter 2005-2006, indicating a good separation between troposphere and stratosphere in the QA4ECV OMI retrievals.

To better reveal differences in representation of the seasonal cycle, Fig. 5 contains a mapping of the full time series at these two stations to a single "average" year, with a 1-month smoothing function applied. While the seasonal cycle is in general well represented, with accurate levels in local summer, the QA4ECV OMI stratospheric NO_2 - NO_2 column does appear to be systematically a little lower than the ground-based value in local winter, at these two sites. This is however not a network-wide feature, as illustrated in Fig. 6, which shows for every station, ordered by latitude, the median difference for each day of the year, where the median is taken over the entire 14-year time series.

From this figure, it is clear that the agreement is poorer at high latitudes, owing to more difficult measurement conditions (such as a high SZA) and at times a highly variable atmosphere (e.g. vortex dynamics), which amplify errors due to imperfect co-location. At more moderate latitudes, some seasonal features can be observed, but their sign varies from station to station, e.g., for Lauder and Kerguelen. A potential source of seasonal errors lies in the use of NO_2 cross sections at a fixed temperature. The QA4ECV NO_2 retrieval includes a 2nd order a posteriori temperature correction to adjust for the difference in absorption cross section between the assumed 220K and the true effective temperature (Zara et al., 2017). The ZSL-DOAS data however were not temperature corrected and Hendrick et al. (2012) estimate the impact to range between a 2.4% overestimation in

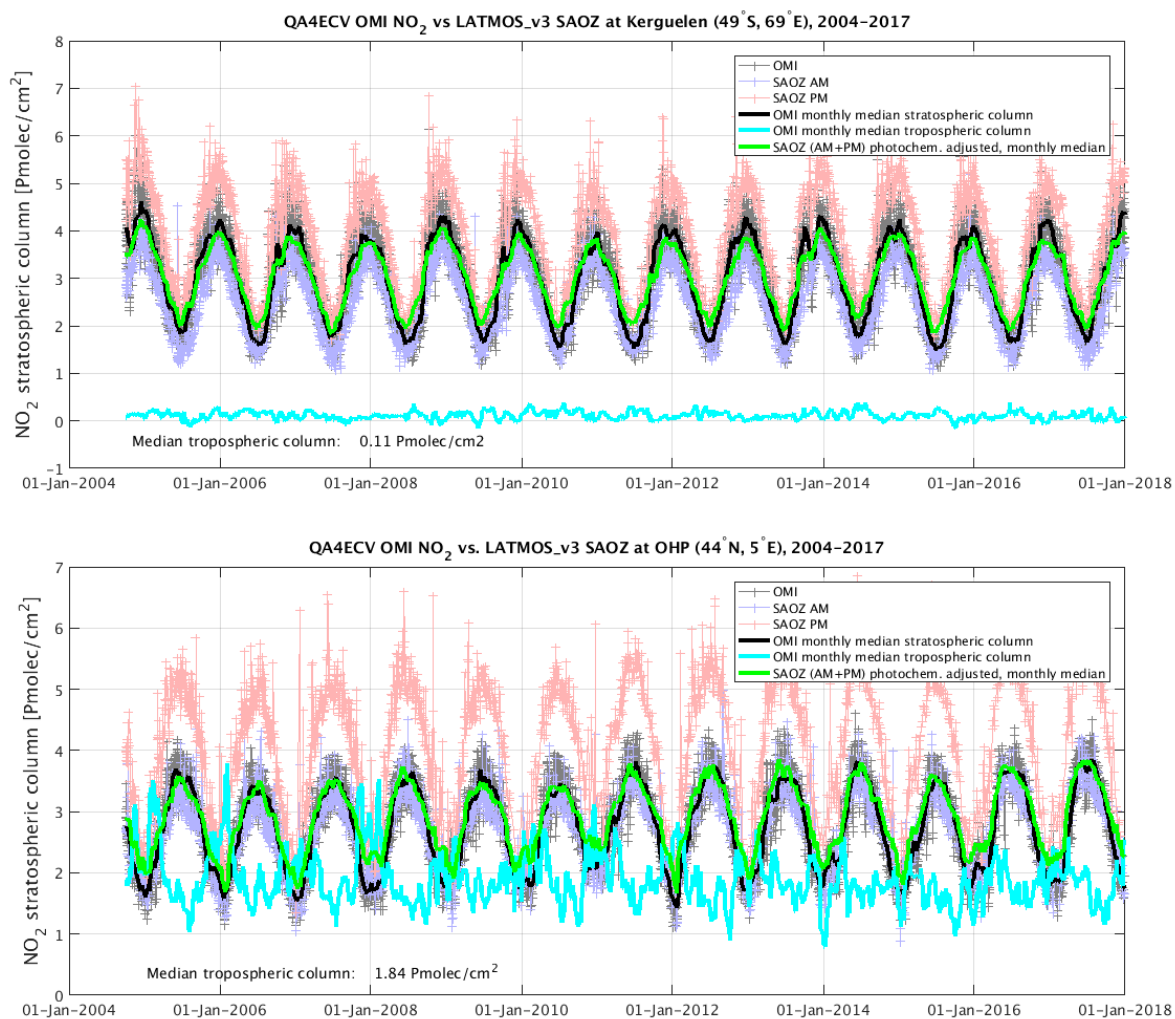


Figure 4. *Upper panel:* Time series of OMI and SAOZ stratospheric NO₂-NO₂ above the NDACC station of Kerguelen in the Indian Ocean, typical for clean background conditions. *Lower panel:* Similar to the upper panel but for the Observatoire de Haute Provence, which shows more significant tropospheric columns in winter due to [anthropogenic](#) pollution.

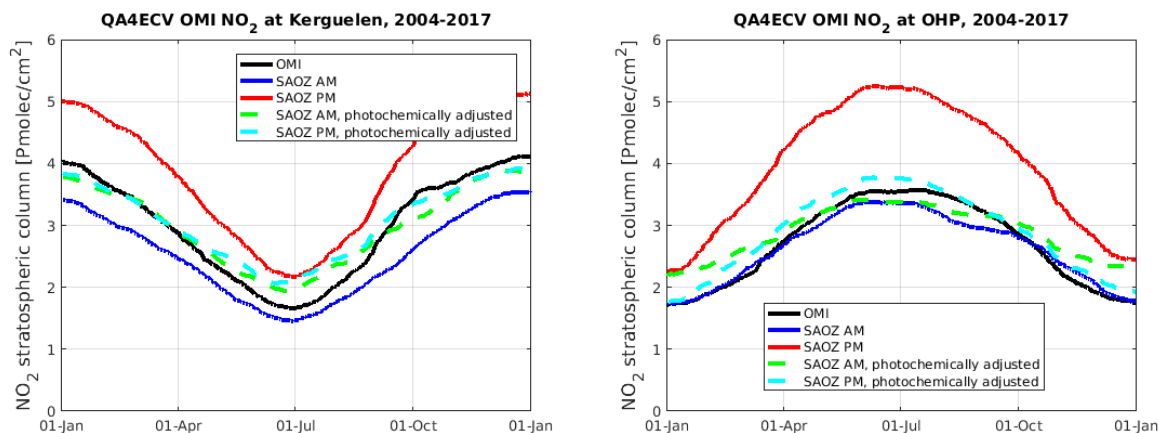


Figure 5. Climatological, i.e., all years mapped to a single year and with a 1-month smoothing function applied, comparison between QA4ECV OMI stratospheric NO_2 - NO_2 and the ZSL-DAOS instruments at Kerguelen and OHP, revealing overall good agreement.

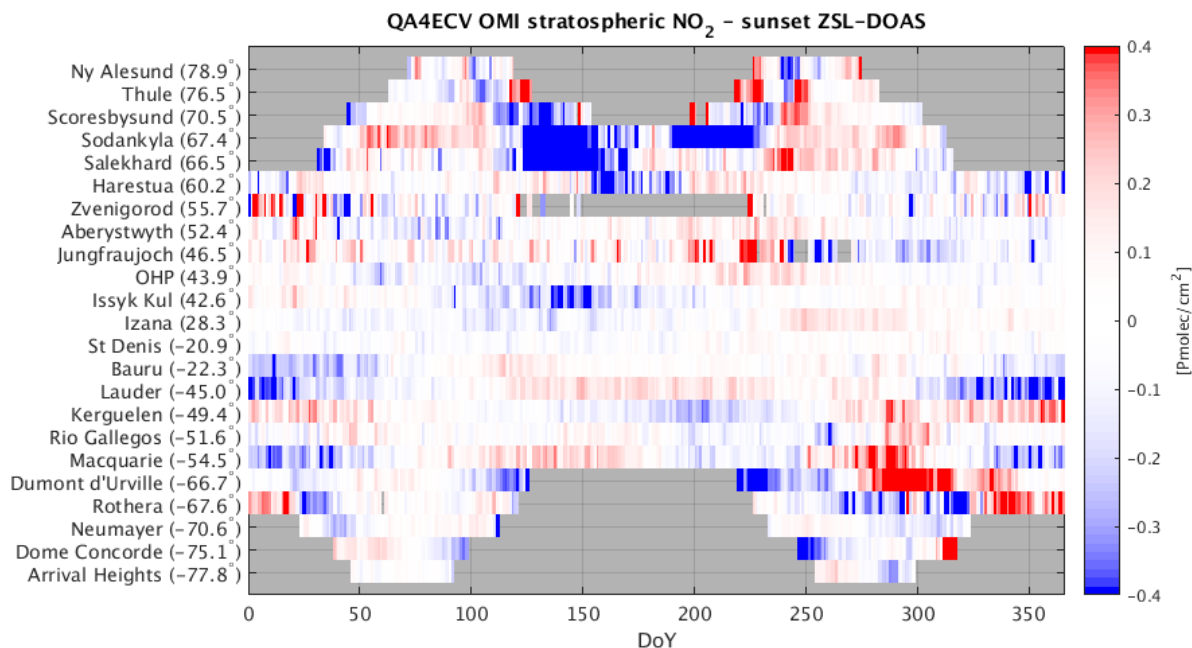


Figure 6. Median difference, per station (ordered by latitude) and per day of the year, over the entire 14-year record, between QA4ECV OMI stratospheric NO_2 and the co-located, photochemically adjusted, sunset ZSL-DOAS measurements.

local winter ~~and to~~ a 3.6% underestimation in local summer for ZSL-DOAS measurements at Jungfraujoch. In other words, the amplitude of the seasonal cycle should be about 6% larger than now reported by the ZSL-DOAS. ~~This could explain a significant~~ at mid latitudes, for an assumed effective stratospheric temperature of 220K. This effect could therefore explain part of the discrepancy between satellite and ground seasonal cycle at ~~these two sites~~ sites such as Kerguelen, but requires confirmation with a proper ZSL-DOAS temperature correction. Development work on this is ongoing (Hendrick, priv. comm.) but beyond the scope of the current paper. The excellent agreement between sunrise and sunset ZSL-DOAS measurements after mapping to the OMI overpass time at Kerguelen suggests the photochemical adjustment to work well, but it does not exclude the presence of biases that are common to sunrise and sunset measurements. At OHP, the wintertime agreement between sunrise and sunset after photochemical adjustment is not as good. Contamination by tropospheric pollution is expected to be similar for both sunrise and sunset measurements, as it contributes to the airmass below the scattering altitude, i.e. the column above the station, as opposed to the large and offset area of sensitivity in the stratosphere. Differences between sunrise and sunset contamination could still be caused by a diurnal cycle in the tropospheric column, but an analysis of that diurnal cycle (e.g. from MAX-DOAS data) is beyond the scope of this work.

Fig. 7 presents the network-wide results in terms of bias and comparison spread per station as a function of latitude. On average, QA4ECV OMI stratospheric NO₂ seems to have a minor negative bias (-0.2 Pmolec/cm²) w.r.t. the ground-based network, ~~related mostly to differences in local winter as described above~~. In view of the station-to-station scatter of the order of 0.3 Pmolec/cm² and the uncertainties on the ground-based data, this is hardly significant and it is roughly in line with validation results for other data sets of OMI stratospheric NO₂ (e.g. Celarier et al., 2008; Dirksen et al., 2011). Interestingly, the STREAM stratospheric NO₂ product, also included in the data files but based on a very different approach (Beirle et al., 2016), does not present this negative bias (see lower panel in Fig. 7). This deserves further exploration but that is outside the scope of the current paper. The comparison spread at a single station varies from 0.2 Pmolec/cm² to 0.5 Pmolec/cm², corresponding to about 10% of the stratospheric column. Raw comparisons at Zvenigorod, Russia, yielded a higher comparison spread (1.2 Pmolec/cm²) due to very large pollution events in the Moscow area affecting the ZSL-DOAS measurements, but for Fig. 7 these were excluded by filtering out co-located pairs with an OMI tropospheric column larger than 3 Pmolec/cm².

~~Returning to the issue of a potential stratospheric temperature (and hence seasonal) dependence in the differences, Fig.?? contains a pole-to-pole graph of the bias between QA4ECV OMI stratospheric NO₂ and sunset ZSL-DOAS, separated by season. No clear seasonal signature can be observed here across all latitudes, at least not one that is significant w.r.t the station-to-station scatter or w.r.t. the standard deviation of the difference within a season (the error bars on the graph). Meridian dependence of the mean and standard deviation (error bars) of the differences between QA4ECV OMI stratospheric NO₂ column data and sunset ZSL-DOAS reference data, bias-corrected for the annual mean difference, represented at individual stations from the Antarctic to the Arctic and separated by season.~~

3.4 Comparison of OMI tropospheric NO₂ with MAX-DOAS

A key issue in the geophysical validation of satellite data sets with respect to sub-orbital reference measurements are the additional uncertainties that appear when comparing different perceptions of the inhomogeneous and variable atmosphere, that

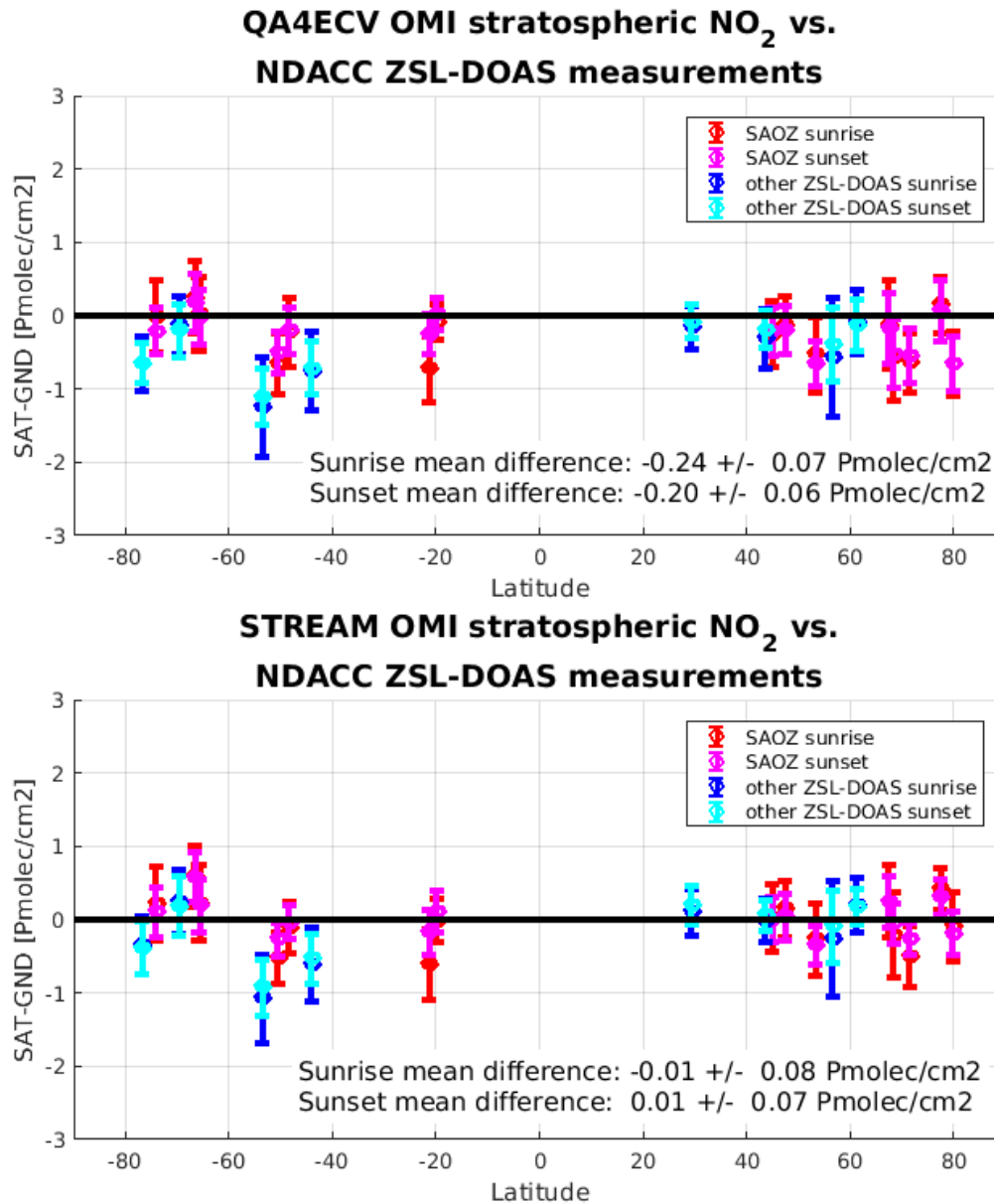


Figure 7. Meridian dependence of the mean (the circular markers) and standard deviation ($\pm 1\sigma$ error bars) of the individual differences between QA4ECV (upper panel) and STREAM (lower panel) OMI stratospheric NO₂ column data and ZSL-DOAS reference data, represented at individual stations from the Antarctic to the Arctic. The values in the legend correspond to the mean and standard error of all mean (per station) differences.

is, when comparing data sets characterized with-by different sampling and smoothing properties, both in space and time, a main topic of the European project GAIA-CLIM (Verhoelst et al., 2015; Verhoelst and Lambert, 2016). Potential comparison error sources for satellite vs MAX-DOAS are discussed in sections 3.4.1 to 3.4.5, following the framework and terminology of Verhoelst et al. (2015); Verhoelst and Lambert (2016). The impact of horizontal smoothing difference error on the bias is presented in a qualitative way in Figs. 8 and S5-S8.

Comparison results of QA4ECV OMI with MAX-DOAS are provided in section 3.4.6. Overall bias and dispersion are provided in boxplots of the differences per site (Fig. 9); here also comparisons of the NASA OMI data product OMNO2 with MAX-DOAS are shown. The seasonality of the bias for each site is shown in Figs. 10 and 11. Fig. 12 presents the overall discrepancy between QA4ECV OMI and MAX-DOAS as given by the mean-squared deviation (MSD), split into bias, seasonally cyclic and residual components. This figure also presents the consistency of the RMSD with the combined ex-ante uncertainty. The impact of adapting screening criteria on bias and dispersion is shown in Fig. S9-S13. A priori profile harmonization and vertical smoothing is presented in Fig. 13 for the bePRO sites Uccle and Xianghe. The discussion of these figures is point-by-point given in section 3.4.6. Table 3 gives an overview of the error source attributions.

3.4.1 Comparison error sources: overview

Part of the discrepancies between the OMI and the MAX-DOAS data sets are due to comparison errors. Starting from the general comparison equation (Verhoelst et al., 2015; Verhoelst and Lambert, 2016), the difference between satellite and reference measured values can be approximated in this specific case as

$$N_{v,\text{trop},\text{SAT}} - N_{v,\text{trop},\text{REF}} = e_{\text{total}} = -e_{\text{REF}} + e_{\text{SAT}} + e_{S_r} + e_{\Delta_r} + e_{\Delta_t} + e_{\Delta_z} \quad (4)$$

with $N_{v,\text{trop},\text{SAT}}$ and $N_{v,\text{trop},\text{REF}}$ being tropospheric VCD values measured by satellite and reference ground-based sensors respectively, $e_{\text{SAT}}, e_{\text{REF}}$ the errors in both measurements, e_{S_r} the horizontal smoothing difference error (as the horizontal projection of the probed air mass of satellite and ground-based measurement is different), and $e_{\Delta_r}, e_{\Delta_t}, e_{\Delta_z}$ the horizontal, temporal and vertical sampling difference error (as satellite and ground-based measurement are not taken at exactly the same space and time).

3.4.2 Temporal sampling difference error

The temporal sampling difference error, and MAX-DOAS uncorrelated random error, are already mitigated by averaging the MAX-DOAS measurements within a 1.0 h interval. We found that using larger time intervals can lead to an increase in the bias, likely because of photochemical evolution and transport of the NO_2 molecule, but at this small time window the temporal sampling difference error has a random character³. The residual uncertainty can be estimated by taking the uncertainty of the mean of the MAX-DOAS values within each time interval. Subtracting in quadrature this component from the RMSD, the $N_{v,\text{trop},\text{SAT}} - N_{v,\text{trop},\text{REF}}$ discrepancies at the different sites would be reduced by less than $0.1 \text{ Pmolec cm}^{-2}$ for the sites OHP, Bujumbura, Athens and Nairobi, and by 0.1 to at most $0.5 \text{ Pmolec cm}^{-2}$ for the other sites. Temporal sampling difference

³This is checked by comparing MAX-DOAS measurements before and after the satellite overpass time, for the different overpasses.

error and MAX-DOAS uncorrelated random error can therefore be considered as insignificant contributions to the $N_{v,\text{trop},\text{SAT}}$ - $N_{v,\text{trop},\text{REF}}$ discrepancies, and are not discussed further here. In agreement with this, Wang et al. (2017) found that the impact of temporal sampling difference error on satellite vs. MAX-DOAS tropospheric NO_2 VCD comparisons was negligible.

3.4.3 Horizontal sampling difference error

- 5 Tropospheric NO_2 has a large spatial variability, especially at polluted sites, therefore random and systematic features in the true NO_2 field at the scale of the distance between MAX-DOAS location and co-located satellite ground pixel (typically a few to a few tens of km, ~ 10 -14 km on average) can be expected. However, one must realize that (i) there is no directional preference in the co-locations, therefore directional features are averaged out in the comparison, and (ii) the satellite measurements are strongly spatially smoothed.
- 10 To estimate the impact of horizontal sampling difference error, we compare two sets of QA4ECV OMI NO_2 tropospheric VCDs. Regarding the first set ($N_{v,\text{trop},\text{SAT1}}$), it is required that its ground pixel covers the MAX-DOAS site and its pixel center is within 5 km from the site. The second set ($N_{v,\text{trop},\text{SAT2}}$) has its ground pixel second-nearest to the site, within the same overpass. SAT_1 pixels are on average at 3-4 km from the site and SAT_2 pixels at 11-12 km, while the distance between SAT_1 and SAT_2 pixels is typically 13.6 km, i.e., comparable to the mean distances encountered in the OMI vs. MAX-DOAS comparisons. Note
- 15 that the discrepancy between $N_{v,\text{trop},\text{SAT1}}$ and $N_{v,\text{trop},\text{SAT2}}$ is due to both horizontal sampling difference error and to random noise error.

Details of the analysis are in section S3 of the supplemental material. The main conclusions are as follows.

- The bias caused by horizontal sampling difference error reaches at most ~ -0.6 Pmolec cm^{-2} (at Athens, Bremen and Mainz), and is therefore only a very minor contributor to the observed bias between OMI and MAX-DOAS (discussed later in section 3.4.6).
- The dispersion of $N_{v,\text{trop},\text{SAT2}} - N_{v,\text{trop},\text{SAT1}}$ can in principle be due to variation in total slant column, in AMF or in stratospheric slant column (see Eq. (1)). It is shown in the supplement that it is largely due to variation of the slant column. It follows that uncorrelated random noise error mainly originates from the slant column, not from AMF or stratospheric column (since these do not vary much between neighbouring pixels). This then justifies the use of the ex-ante uncertainty component due to SCD uncertainty, u_{SAT,N_s} , as an estimate of the total random error uncertainty. Note that u_{SAT,N_s} was scaled such that it only accounts for random error of the slant column (Zara et al., 2018), not for systematic error.
- At the sites Bujumbura and Nairobi, $u_{\text{SAT1},N_s}^2 + u_{\text{SAT2},N_s}^2$ exceeds the variance of the difference, indicating that u_{SAT,N_s} is sometimes overestimated.
- The standard deviation caused by horizontal sampling difference error (obtained by subtracting in quadrature the dispersion due to random noise) is minor compared to the discrepancies encountered in the OMI vs. MAX-DOAS comparisons.

3.4.4 Vertical sampling difference error

Two sources of vertical sampling difference error can be identified. First, the surface altitude of the ground-based MAX-DOAS sensor, and the mean surface altitude of the OMI ground pixel, are not exactly the same. To estimate a correction, we applied a VMR-conserving vertical shift of the satellite a priori profile, described by Zhou et al. (2009). The ground levels are shifted by, on average, 0.03 km (Cabauw, De Bilt) to 0.4 km (Athens, Bujumbura). This hardly changed $N_{v,\text{trop,SAT}} - N_{v,\text{trop,REF}}$ (bias changes of $0.3 \text{ Pmolec cm}^{-2}$ or less). This VMR-conserving approach probably underestimates the discrepancy at the sites Athens and Bujumbura which have a complicated orography. The MAX-DOAS instrument at Athens is located on one of the hills surrounding the city at 527 m altitude, while the mean surface altitude of the co-located satellite pixels is $\sim 200\text{m}$. The MAX-DOAS measurement therefore misses the lowest part of the tropospheric column; correcting for this would increase the already negative bias. The MAX-DOAS instrument at Bujumbura is at 860 m altitude, at the edge of the city which is located in a valley surrounded by ~~2000-3000m~~ 2000-3000 m high mountains (Gielen et al., 2017); this causes the mean surface altitude of the co-located satellite pixels ($\sim 1.2 \text{ km}$) to be higher than the MAX-DOAS instrument.

A second source of vertical sampling difference error is the fact that the MAX-DOAS only measures the lower tropospheric NO_2 VCD, while the satellite measures the full tropospheric VCD. This is, in principle, a source of positive bias in $N_{v,\text{trop,SAT}} - N_{v,\text{trop,REF}}$ and therefore cannot explain the observed negative bias in the comparison. A proper quantification of this bias source depends critically on the assumed vertical profile shape and is out of scope of the current work.

3.4.5 Horizontal smoothing difference error

Ideally, subpixel variation of the tropospheric VCD would be estimated using a high resolution model with grid cell area comparable to the MAX-DOAS horizontally projected area of the probed air mass. Instead, we employ here two semi-quantitative approaches to estimate the bias from horizontal smoothing difference error.

In the first approach, the horizontal smoothing effect is estimated from the QA4ECV OMI NO_2 data itself. 'Superpixel' OMI tropospheric VCDs are constructed by averaging OMI VCDs of individual pixels of relatively small size ($\leq 500 \text{ km}^2$) within a 20 km radius centered at the MAX-DOAS site. Per overpass, such a superpixel VCD is compared with the individual ground pixel VCD covering the MAX-DOAS site. With this procedure, a superpixel consists on average of 3 individual ground pixels. The mean difference per season, over the years 2004-2016, is presented in Fig. 8. The second approach is similar, but uses S5p TROPOMI NO_2 data (May 2018 to May 2019, RPRO (reprocessed) + OFFL (offline) data with processor version 01.02.00-01.02.02), and the superpixel tropospheric VCD is constructed by averaging, per overpass, VCDs of individual pixels that are within a latitude, longitude box of $\Delta\text{lat} = 0.14^\circ$, $\Delta\text{lon} = 0.7^\circ$ centered at the MAX-DOAS site. TROPOMI has a similar overpass time as OMI (early afternoon) and a considerably finer resolution ($3.5 \times 7 \text{ km}^2$ at nadir). The area of this superpixel corresponds to $\sim 700\text{-}900 \text{ km}^2$, i.e., about the size of a bigger OMI pixel, and contains typically 20 TROPOMI ground pixels.

The OMI-based approach has as advantage that the time range is appropriate but it is limited by the large ground pixel size. Regarding the finer-resolution TROPOMI data, one should keep in mind that its ground pixel size is still large compared

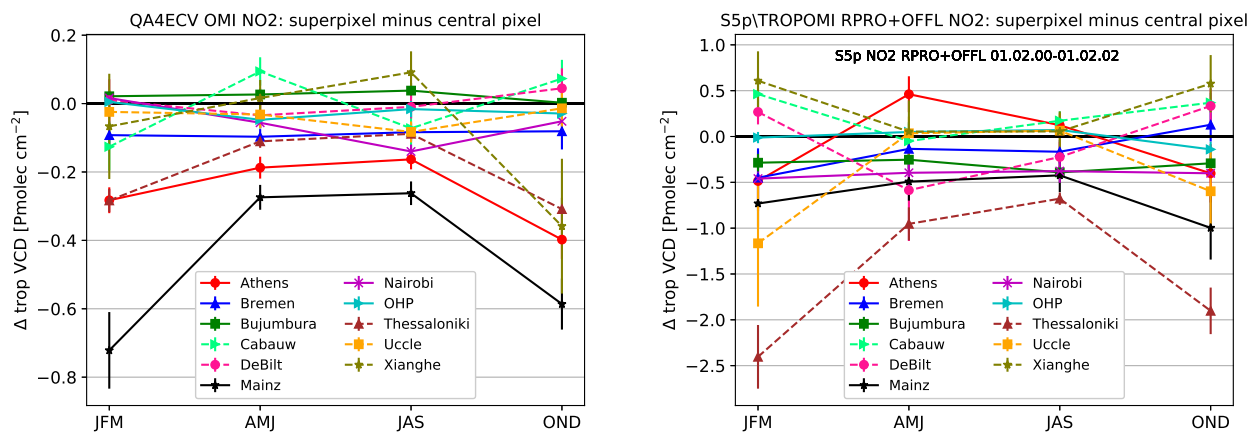


Figure 8. a: Mean difference, per season, between QA4ECV OMI superpixel (ground pixels averaged within 20 km of the central site) and the central OMI ground pixel, using data in the time range 2004-2016. b: Similar as (a), but using TROPOMI NO₂ data (time range 04/2018-05/2019, and the superpixel is defined within a latitude, longitude box of $\Delta\text{lat} = 0.14^\circ$, $\Delta\text{lon} = 0.7^\circ$ centered at the MAX-DOAS site.

to the horizontally projected area of probed air mass of the MAX-DOAS⁴, hence the contribution of horizontal smoothing difference error to bias and comparison might still be underestimated. Another limitation is that the considered TROPOMI time range does not overlap with the considered time range of OMI. Both approaches suggest a negative bias contribution due to horizontal smoothing difference error at the sites Mainz and Thessaloniki and no such bias contribution at OHP, while for other sites the results are mixed (bias is varying over the seasons, and/or different results between the OMI and TROPOMI-based calculations). Differences between the OMI and TROPOMI-based calculations are likely caused by (i) the much larger central pixel of OMI compared to TROPOMI, leading to a lower sensitivity to fine-scale variations in Fig. 8a, and (ii) evolution in e.g., NO₂ concentration patterns, captured differently by the different temporal ranges used in Fig. 8a and b. A case in point are the positive mean differences in JFM and OND captured in the TROPOMI-based calculation but not in the OMI-based calculation. Both MAX-DOAS sensors are not located at urban centers, although pollution centers are in the neighbourhood. Therefore, the positive mean differences at JFM and OND captured by TROPOMI is likely due to NO₂ fields in the periphery of the TROPOMI superpixel. This is in agreement with very recent work of Pinardi et al. (2020) on the horizontal smoothing effect. The estimated 'horizontal dilution factors' in Fig. S3 of Pinardi et al. (2020) are positive for Cabauw and Xianghe, indicating that NO₂ is higher in the periphery than at the MAX-DOAS location.

⁴The horizontal distance of the QA4ECV MAX-DOAS measurements is small compared to a TROPOMI pixel in both the viewing and the perpendicular direction. Regarding bePRO MAX-DOAS, while having a small field-of-view, its probed distance in the viewing direction (~10 km) is of similar or slightly larger magnitude as the cross-section of a TROPOMI ground-pixel.

A tropospheric NO₂ monthly field with sub-pixel variability is derived from the QA4ECV OMI NO₂ data, using a variant of the temporal averaging approach of Wenig et al. (2008)⁵, and visualised in Fig. S5-S8, for months with a minimal (left column) and maximal (right column) OMI vs. MAX-DOAS bias (as derived from Figs. 10-Figs. 11). Fields are constructed for each month, by averaging over the years 2004-2016. The resulting field is horizontally smoothed; the variability is an underestimate of the true horizontal NO₂ variability. Sub-pixel enhanced tropospheric NO₂ approximately centered at the MAX-DOAS site can be identified in high-bias months at Nairobi, Thessaloniki and Mainz, while for the sites OHP, Bujumbura, Uccle, De Bilt/Cabauw and Xianghe this is clearly not the case. At Athens the pollution peak centre is at some 10 km from the sensor, and for Bremen no clear peak is identified.

The contribution of horizontal smoothing difference error to the (OMI - MAX-DOAS) bias at Mainz is consistent with the results of Drosoglou et al. (2017), who achieved a significant bias reduction by adjusting the OMI data with factors derived from air quality simulations at a high spatial resolution of 2 km.

Similar maps were constructed by Ma et al. (e.g., 2013); Chen et al. (e.g., 2009) to estimate the impact of the horizontal smoothing effect on satellite vs. DOAS comparisons.

3.4.6 Comparison results

Bias and dispersion. Fig. 9 (black boxplots) presents, per MAX-DOAS site, boxplots of the difference of QA4ECV OMI with co-located QA4ECV MAX-DOAS. At all sites, the bias of QA4ECV OMI with respect to QA4ECV MAX-DOAS is negative. In absolute scale, it is the smallest at the lower-pollution sites OHP and Bujumbura (mean difference -0.9 and -1.7 Pmolec cm⁻² respectively), and largest at the sites Thessaloniki and Mainz (mean difference of ~-4 Pmolec cm⁻²). In relative scale, the bias is smallest (median relative difference between -15 to -20%) at the sites Uccle, Cabauw, De Bilt and Xianghe and largest (median relative difference ~-70%) at Bujumbura and Nairobi. The difference dispersion, expressed as interquartile range (IQR) is smallest at the sites Bujumbura, OHP and Nairobi (~1-2 Pmolec cm⁻²) and largest at the sites Mainz and Xianghe (~5-6 Pmolec cm⁻²). As discussed in sections 3.4.2 to 3.4.5, among the different comparison error components only horizontal smoothing difference error is expected to induce an important negative bias, and this only for some sites (e.g., Thessaloniki, Mainz), while for other sites (e.g., OHP, Xianghe) this is not expected. This means that the bias is at least in some cases due to error in the satellite and/or MAX-DOAS measurement, and not due to comparison error.

We present in the same figure boxplots of the tropospheric NO₂ VCD difference between OMNO2 data with QA4ECV MAX-DOAS measurements (blue boxplots). The bias of OMNO2 vs. QA4ECV MAX-DOAS is comparable to that of QA4ECV OMI NO₂ vs. QA4ECV MAX-DOAS, although slightly more negative at all sites except Cabauw. If one considers only the subset of OMNO2 pixels where QA4ECV OMI has an accepted pixel, the OMNO2 bias becomes closer to that of QA4ECV OMI for most sites. Although bePRO MAX-DOAS has in principle a better correction for aerosols and vertical profile effects compared to QA4ECV MAX-DOAS, the bias of QA4ECV OMI with respect to bePRO MAX-DOAS (Fig. 9, green boxes, only for the sites Bujumbura, Uccle and Xianghe) is comparable to that of QA4ECV OMI vs. QA4ECV MAX-DOAS.

⁵Here, Per 0.02×0.02 grid cell the arithmetic average of covering satellite ground pixels is taken, rather than a weighted average as done by Wenig et al. (2008). Only ground pixels with area $< 950\text{km}^2$ are considered.

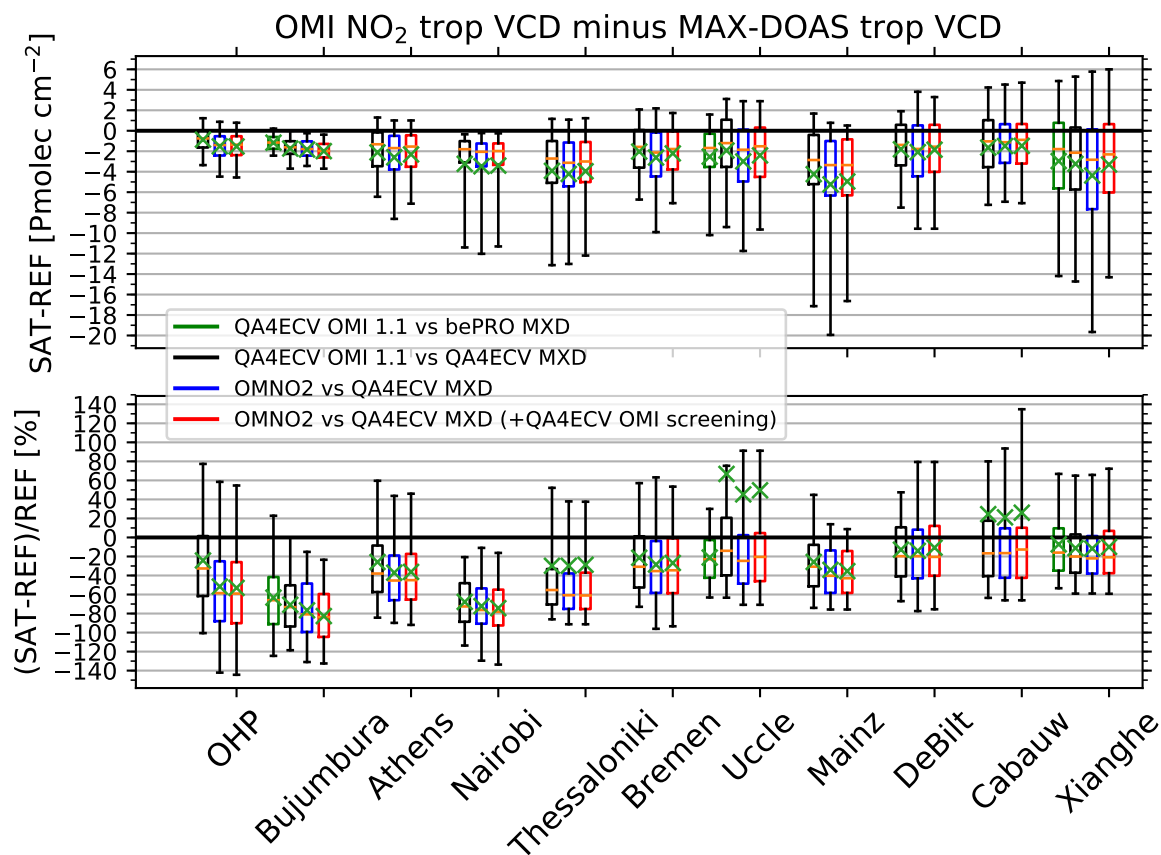


Figure 9. Per site, boxplots of QA4ECV OMI NO₂ vs. QA4ECV MAX-DOAS (black boxes), QA4ECV OMI NO₂ vs. bePRO MAX-DOAS (green boxes, only for 3 sites), OMNO2 vs. QA4ECV MAX-DOAS (blue) and OMNO2 vs. QA4ECV MAX-DOAS, for the subset of OMNO2 pixels where QA4ECV OMI has an accepted pixel (red boxes). The top plot displays boxplots of SAT-REF tropospheric VCD differences, the bottom plot of (SAT-REF)/REF. The same boxplot conventions as in Fig. 3 are applied. Outlying mean relative differences (green crosses) can occur when low REF values are present.

We conclude that in most cases, mutual differences between the tropospheric NO₂ VCD of the two OMI satellite data products on one hand, and between both MAX-DOAS processings on the other hand, are small compared to the differences between the satellite OMI data products and the MAX-DOAS measurements. The main exception is at the site OHP, where the median difference and relative difference of OMNO₂ vs. QA4ECV MAX-DOAS (-1.4 Pmolec cm⁻², -60%) is considerably
5 more negative than that of QA4ECV OMI vs. QA4ECV MAX-DOAS (-0.8 Pmolec cm⁻², -30%). The observation of higher MAX-DOAS tropospheric VCD compared to satellite is a common finding in the literature (e.g., Ma et al., 2013; Kanaya et al., 2014; Chan et al., 2015; Jin et al., 2016; Drosoglou et al., 2017, 2018). The negative bias is therefore not specific to a particular satellite or MAX-DOAS data product.

Seasonal cycle of the bias. Fig. 10 and 11 present for each site a seasonal plot (i.e., all data mapped to 1 year) of QA4ECV
10 OMI tropospheric NO₂ VCD, of QA4ECV MAX-DOAS, and of the difference. Also indicated are rolling monthly mean and median, and outliers identified by iterative 4- σ clipping.

A seasonal cycle in the bias, with a larger underestimation in seasons with high NO₂, is a recurring feature (Fig. 10). This is the case at the more polluted sites e.g., Xianghe, Mainz, Thessaloniki, in winter months, and is in agreement with several literature results (Ma et al., 2013; Kanaya et al., 2014; Jin et al., 2016). Note however that we find also in the relatively
15 clean site OHP a seasonal cycle in the bias. A very strong seasonal cycle in bias (10-fold increase) is present at Nairobi, where the MAX-DOAS sensor measures a strongly elevated NO₂, peaking in July and August, which is not or hardly picked up by the satellite. Likely this is a spatially local phenomenon; this would be consistent with the locally enhanced NO₂ in Fig. S5. This site is characterized by local traffic. The enhanced NO₂ concentrations in July and August (as measured by MAX-DOAS) are possibly related to meteorology. This season is characterized by low precipitations, low wind speeds (see
20 <https://weather-and-climate.com/average-monthly-Rainfall-Temperature-Sunshine,Nairobi,Kenya>), and a high cloud cover (as indicated by QA4ECV OMI cloud fraction measurements) limiting NO₂ photolysis, therefore a build-up of locally emitted NO₂ is a possible explanation. The fact that OMI hardly measures this elevated NO₂ can be due to the local character of the emissions.

Overall discrepancy and consistency with ex-ante uncertainty. The discrepancy, as measured by the root-mean squared
25 difference (RMSD) between satellite and MAX-DOAS, exceeds for all sites the combined ex-ante uncertainty⁶ (see Fig. 12, for the squared quantities). Clearly, comparison error contributes significantly to the RMSD, and/or there are underestimated/unrecognized errors in the satellite or reference data.

The mean squared difference in Fig. 12 is split into 3 additive components: (i) squared mean difference (bias component), (ii) variance of the rolling monthly mean difference (seasonal cycle component) and (iii) variance of the residual difference.
30 The first two components can be attributed to systematic error, the third component to random error and any uncharacterized systematic error. The leading component can be different per site (e.g., bias component at Bujumbura, seasonal component at Nairobi, residual at Mainz and Xianghe).

⁶Although root-mean squared error (RMSE) and uncertainty are not exactly equivalent, they should be roughly comparable if all error sources are well characterized. If all error is purely random, the RMSE equals the standard deviation of errors, of which the uncertainty is an ex-ante estimate. If the error is fully systematic and constant, RMSE equals the absolute value of the bias, which is expected to be smaller than twice the uncertainty with 95% probability.

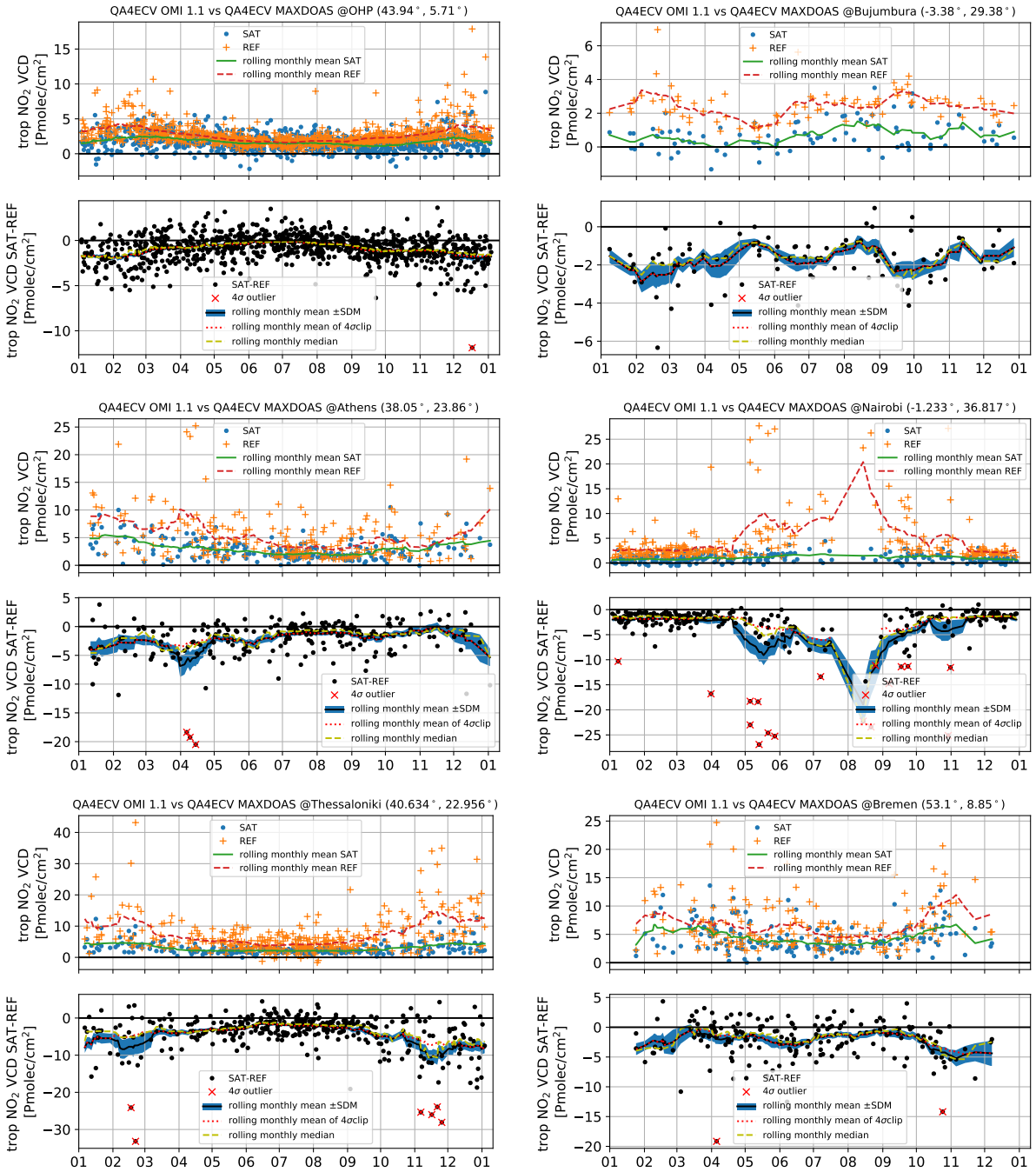


Figure 10. Seasonal cycle plots for the sites OHP, Bujumbura, Athens, Nairobi, Thessaloniki and Bremen. Top panel: tropospheric VCD of QA4ECV OMI NO₂ and QA4ECV MAX-DOAS, and rolling monthly mean and median of both. Bottom panel: differences between QA4ECV OMI NO₂ and QA4ECV MAX-DOAS, outliers indicated by 4- σ clipping, and rolling monthly mean and median of the difference.

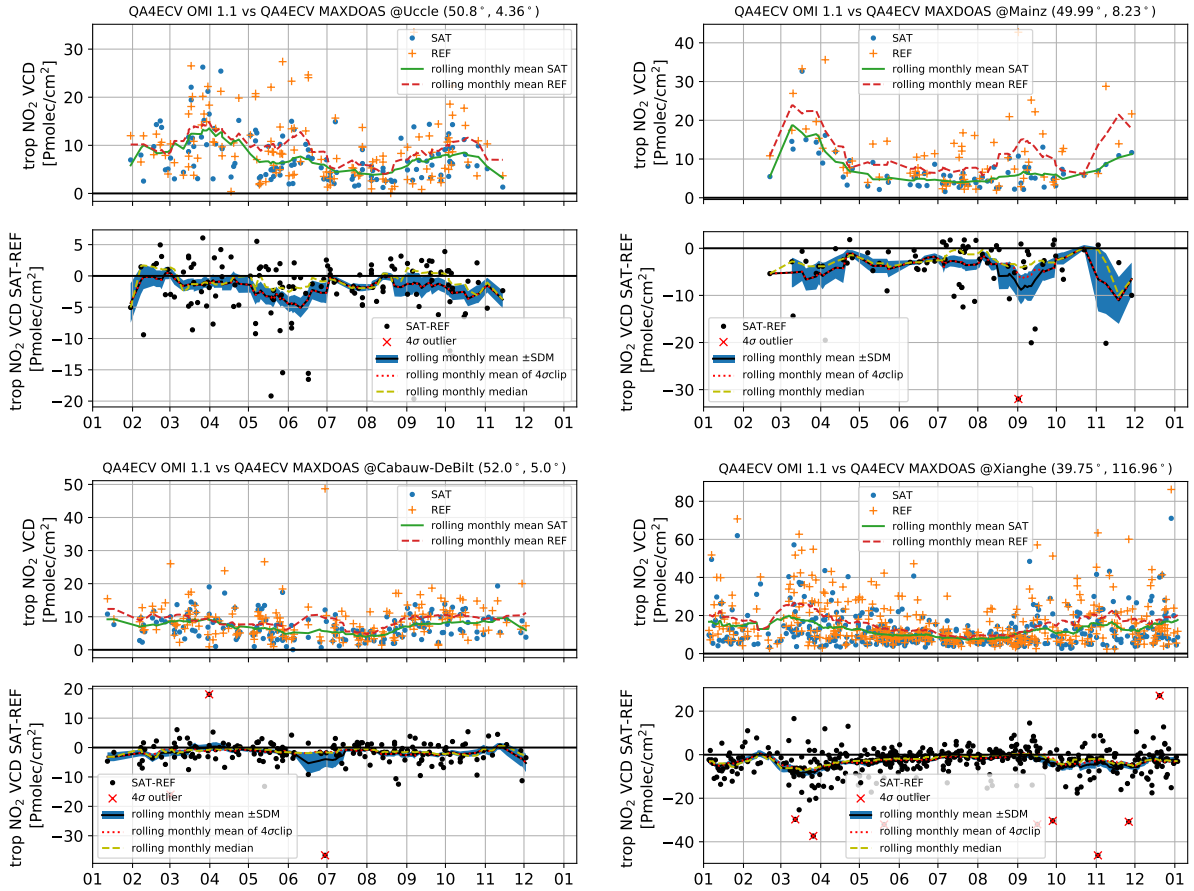


Figure 11. As in Fig. 10 but for the sites Uccle, Mainz, Cabauw/De Bilt and Xianghe.

The satellite and reference data products do not provide the information to split the squared uncertainty according to the random or systematic nature of the error source. Instead, the squared uncertainty in Fig. 12 is separated into additive components according to origin: (i) uncertainty in the MAX-DOAS measurement u_{GB} , (ii) uncertainty in the satellite measurement due to error in SCD (expected to be mainly random in nature) u_{SAT,N_s} , (iii) stratospheric SCD $u_{SAT,N_s, strat}$, and (iv) uncertainty in satellite measurement due to error in tropospheric AMF $u_{SAT,M_{trop}}$. For the sites with the lowest NO_2 levels (OHP and Bujumbura), uncertainty in SCD is the main contributor, while for the other sites the MAX-DOAS uncertainty becomes the leading component.

By analysing and intercomparing the tropospheric AMF calculation methods between different retrieval groups, Lorente et al. (2017) concluded that the uncertainty due to differences in retrieval methodology (i.e., methodological uncertainty, termed structural uncertainty by Lorente et al. (2017)) is 32% in unpolluted and 42% in polluted conditions, mostly due to different choices in the ancillary data surface albedo, a priori profile and cloud parameters by different groups. In Fig. 12,

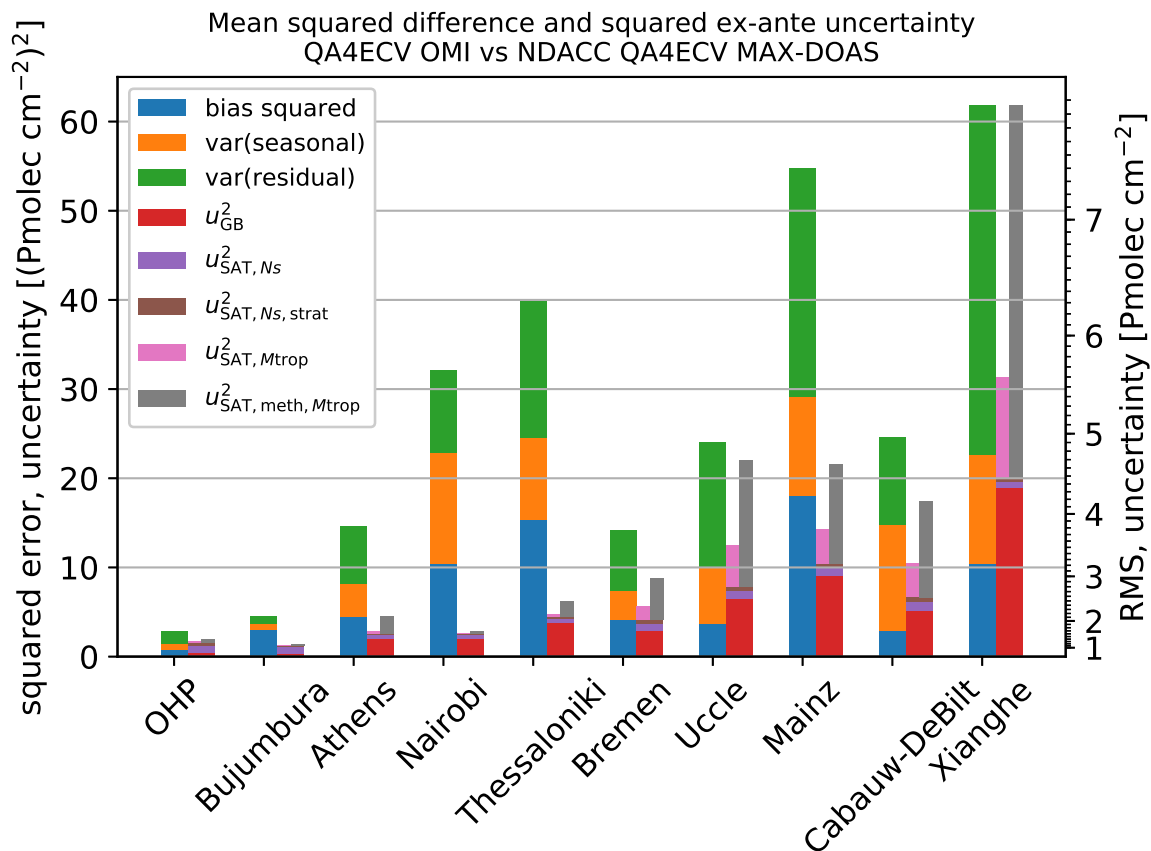


Figure 12. Per site two stacked bar plots are provided. The left bar shows the mean squared difference of QA4ECV OMI NO₂ vs. QA4ECV MAX-DOAS, split into 3 components: (i) square of the mean difference; (ii) variance of the rolling monthly mean difference; (iii) variance of the residual difference. The right bar shows the combined ex-ante uncertainties of QA4ECV OMI NO₂ - QA4ECV MAX-DOAS, split into 4 components: (i) MAX-DOAS squared uncertainty; (ii) QA4ECV OMI squared uncertainty contribution from the total SCD; (iii) from the stratospheric SCD; (iv) QA4ECV OMI squared uncertainty contribution from the tropospheric AMF. Also shown is the AMF-component of methodological uncertainty, derived by intercomparing retrieval methodologies by Lorente et al. (2017, called structural uncertainty in this work). The right y-axis provides a square-root scaling of the corresponding RMS.

this AMF-component of methodological uncertainty, $u_{\text{SAT, meth}, M_{\text{trop}}}$, is presented as alternative to the ex-ante $u_{\text{SAT}, M_{\text{trop}}}$ obtained by uncertainty propagation, where we classified OHP and Bujumbura as non-polluted sites and the others as polluted. In all cases, the methodological uncertainty exceeds the ex-ante uncertainty $u_{\text{SAT}, M_{\text{trop}}}$. At 4 sites, using this methodological uncertainty the discrepancy between OMI and MAX-DOAS can be explained for the most part (Uccle, Cabauw/De Bilt) or even completely (Xianghe), but not at the other sites.

Modifying screening criteria. Applying a more strict screening protocol can, at least in principle, mitigate discrepancies in bias and dispersion, at the expense of data loss. In the case at hand, results are mixed for the different sites (see Fig. S9-S13); stricter criteria ~~does~~ do not resolve bias or dispersion for all sites. For the sites Uccle, Mainz, Cabauw and Xianghe strong reductions in bias and/or dispersion ($\sim 0.5\text{-}2 \text{ Pmolec cm}^{-2}$) can be achieved by filtering more strictly on the effective cloud properties cloud fraction, cloud pressure, the uncertainty component due to cloud pressure $u_{\text{SAT}, p_{\text{cl}}}$, on the MAX-DOAS cloud flag (removing scenes with thick or broken clouds) or on AOD. This suggests that part of the discrepancy is caused by clouds and/or aerosol. More minor reductions in bias and/or dispersion are achieved for the sites Bujumbura, Nairobi, Athens, Bremen and De Bilt.

Screening more strictly on ground pixel area leads to improvements in bias for Mainz and Thessaloniki, confirming (see section 3.4.5) that horizontal smoothing difference error is a component of the bias. Improvements in dispersion are found for Mainz, Thessaloniki, Uccle and Xianghe.

Using a stricter filtering on effective cloud properties, the RMSD can be made consistent with the ex-ante uncertainty for the sites Uccle and Cabauw-De Bilt (results not shown). For Mainz, this can be achieved if furthermore ground pixels larger than 400 km^2 are excluded (keeping only 25% of the data). Finally, we note that at the site OHP, RMSD and uncertainty are consistent in the months from May to and including August (when NO_2 values are low) without the need of stricter filtering.

For most sites, additional screening (within reasonable limits) cannot lower the RMSD sufficiently to match the uncertainty. Likely some uncertainty components in either OMI or MAX-DOAS data are underestimated, or not included.

While we found that stricter screening using the uncertainty component due to cloud pressure, $u_{\text{SAT}, p_{\text{cl}}}$, often leads to better results, the obtained threshold values are quite low. This indicates that $u_{\text{SAT}, p_{\text{cl}}}$ is underestimated in the satellite data product. As expected, relaxing the cloud fraction filter beyond the baseline can lead to an increase in bias and/or dispersion (see e.g., Bujumbura, Nairobi, Uccle in Figs. S9-S13), motivating the $\text{CF} \leq 0.2$ (or almost equivalently $\text{CRF} \leq 0.5$) recommendation. On the other hand, relaxing the AMF ratio filter beyond the baseline has no large impact on the comparison, while further restricting it has sometimes a negative impact (e.g., increase of bias and/or dispersion at Uccle, Xianghe and Cabauw). Therefore, the current baseline recommended lower bound ($\frac{\text{AMF}_{\text{trop}}}{\text{AMF}_{\text{geo}}} \geq 0.2$) can be replaced by a lower value (e.g., 0.1 or 0.05).

Vertical smoothing. The non-uniform vertical sensitivity of the satellite measurement, combined with an approximate a priori profile shape, is a source of error in the satellite measurement. The bePRO MAX-DOAS provides not only column but also profile shape information (albeit with a limited vertical resolution) and therefore allows to assess this error source separately. Fig. 13 shows, for the sites Uccle and Xianghe, the impact of directly applying Eq. (3) on the bePRO MAX-DOAS profile (after vertical alignment using the method of Zhou et al. (2009)) on the mean squared deviation (MSD), and its bias, seasonal cycle and residual components. While direct smoothing of the MAX-DOAS profile improves the MSD

for Uccle, for Xianghe it increases because the seasonal cycle component increases. The increase in seasonal variance is caused by the interplay of the seasonal variation of the MAX-DOAS vertical profile and of the satellite vertical averaging kernel. Specifically, it is found for the Xianghe case that in wintertime averaging kernels have higher values close to the surface while MAX-DOAS NO₂ profiles can also be peaked at the surface. The combination causes increased MAX-DOAS columns upon vertical smoothing. This is also seen e.g., in the comparison of GOME-2 AC SAF GDP 4.8 NO₂ product with MAX-DOAS at Xianghe (see Fig. 7.14 and 7.15 of Hovila et al. (2018) and Figs. S3 and S5 of Liu et al. (2019)). While the a priori harmonization seems to mitigate this effect, it does not resolve it. It should be a focus of future research if improved MAX-DOAS a priori profiles and/or improved satellite averaging kernels can improve the situation.

However, one should take into account that the retrieved bePRO profiles have a low vertical resolution and depend on their own a priori profile shape. As is well known (Eq. (10) of Rodgers and Connor (2003), see also the general profile harmonization overview of Keppens et al. (2019)), a priori profiles of satellite and reference should be harmonized before comparison and smoothing. Here, we aligned the surface levels of the profiles following Zhou et al. (2009) and changed the a priori shape profile of the bePRO data to that of the satellite, while keeping the bePRO a priori VCD size (which is actually obtained from measurement, see Hendrick et al. (2014)) intact. More detail on the applied operations is provided in Section S6. The harmonization operation reduces all components of the MSD (bias, seasonal cycle and residual component) for the Xianghe site. Applying in addition smoothing after the a priori harmonization, the bias component (blue bar in Fig. 13) is almost completely removed, but the other two components increase. Application of the averaging kernel therefore does not lead necessarily to an improvement in all aspects of a comparison; this should be the focus of further research. As the bias component is removed almost completely after harmonization and smoothing at Uccle and Xianghe, one can conclude that -at least at these two sites- the bias is largely due to errors in the a priori profile shape. Using better quality a priori profiles in both satellite and MAX-DOAS data (e.g., from regional scale models) is therefore recommended.

When the averaging kernel is applied, it is recommended to remove the satellite a priori shape component from the uncertainty budget (Boersma et al., 2018). This component was tentatively assigned 10% of the VCD value. This only leads to a modest reduction of the combined uncertainty in Fig. 13 (compare the non-hatched and hatched pink bars) as the dominant contribution to the OMI AMF uncertainty component is related to surface albedo rather than profile shape. E.g., the combined uncertainty at Uccle reduces from 2.8 to 2.7 Pmolec cm⁻². However, the smoothing operation reduces the RMSD at Uccle by about 2 Pmolec cm⁻², strongly suggesting that the current 10% uncertainty assignment is an underestimate.

4 Conclusion

In this work, stratospheric and tropospheric NO₂ VCD of the QA4ECV OMI 1.1 data product are validated, using ground-based NDACC ZSL-DOAS data and MAX-DOAS data, respectively. Two MAX-DOAS processings are used, the NDACC bePRO profile retrieval and the harmonized QA4ECV column retrieval.

Quality screening according to the data product provider recommendations is an essential step before the satellite product can be used. However, a user (e.g., a developer of L3-type temporally averaged data) should be aware that for tropospheric

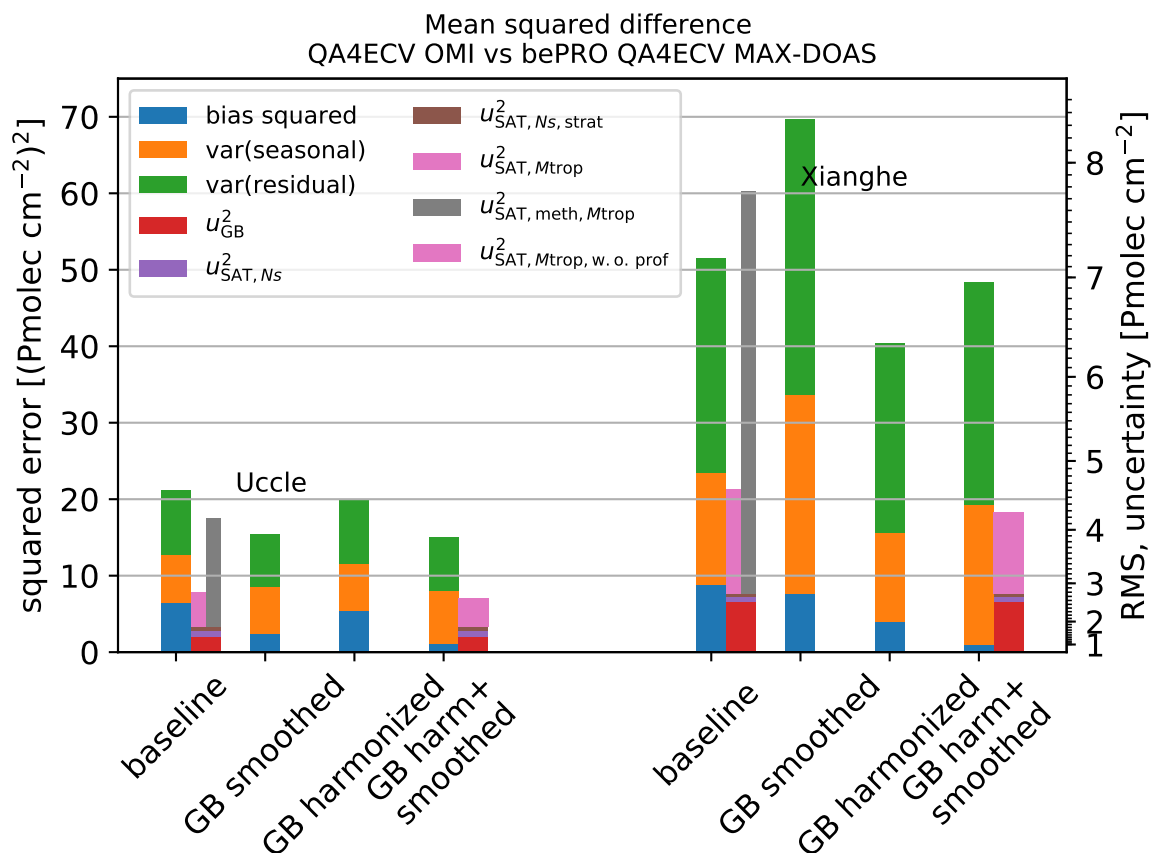


Figure 13. Mean squared deviation of QA4ECV OMI vs. bePRO MAX-DOAS tropospheric VCD at Uccle and Xianghe, split in the components squared mean difference (blue), variance of the rolling monthly mean difference (orange) and variance of the residual difference (green). Per site, from left to right: (i) baseline comparison, (ii) MAX-DOAS profile smoothed by the OMI averaging kernel, (iii) MAX-DOAS a priori replaced with that of the satellite, (iv) First a priori harmonization, then smoothing. Details of the operations are provided in S6. At the baseline (i), also the squared ex-ante uncertainty (divided into components) is provided. The same squared ex-ante uncertainty, minus the satellite profile shape uncertainty contribution, is provided at (iv).

Table 3. Overview of discrepancies and error sources studied in this work. (MXD=MAX-DOAS)

Contribution	Description
full discrepancy e_{total}	Negative bias ranging from $-0.9 \text{ Pmolec cm}^{-2}$ (OHP) to $-4 \text{ Pmolec cm}^{-2}$ (Mainz, Thessaloniki). RMSD ranging from 2 (OHP, Bujumbura) to 8 Pmolec cm^{-2} (Xianghe). RMSD dominated by bias in Bujumbura and Thessaloniki, by seasonal cycle dispersion in Nairobi and by residual dispersion otherwise.
<i>Comparison errors</i>	
temporal sampling diff. error $e_{\Delta t}$	Mitigated by averaging MXD within 1h interval. No systematic component. Impact on dispersion ¹ : $\leq 0.1 \text{ Pmolec cm}^{-2}$ (low pollution) to 0.1 to $0.5 \text{ Pmolec cm}^{-2}$ (high pollution).
horizontal sampling diff. error $e_{\Delta r}$	Mitigated by excluding ground pixels not covering site. Systematic component between zero and $-0.6 \text{ Pmolec cm}^{-2}$. Impact on dispersion ¹ : $\leq 0.1 \text{ Pmolec cm}^{-2}$ (low pollution) to $\leq 0.6 \text{ Pmolec cm}^{-2}$ (high pollution).
vertical sampling diff. error $e_{\Delta z}$, surface level	Alignment of satellite a priori profile to MXD surface level using the method of Zhou changes bias by $\leq 0.3 \text{ Pmolec cm}^{-2}$. Bujumbura: complicated oreography might lead to a higher bias. Athens: MXD on hill is a likely source of positive bias
vertical sampling diff. error $e_{\Delta z}$, top grid level	MAX-DOAS VCD restricted to lower troposphere. Correction estimated from satellite upper tropospheric a priori profile increases the bias.
horizontal smoothing diff. error e_{S_r}	Qualitatively assessed. Contributes to bias in Nairobi, Thessaloniki, Mainz, and does not contribute (significantly) to bias in OHP, Cabauw and Xianghe. For other sites the results are mixed.
<i>Measurement/retrieval errors</i>	
OMI total SCD error $e_{\text{SAT},s}$	Impact of noise term on dispersion ¹ : $\leq 0.1 \text{ Pmolec cm}^{-2}$ (low pollution), negligible (high pollution).
OMI strat. SCD error $e_{\text{SAT},s,\text{strat}}$	Bias in strat VCD of $\sim -0.2 \text{ Pmolec cm}^{-2}$ translates (via $\frac{M_{\text{strat}}}{M_{\text{trop}}}$) to $\sim +0.6 \text{ Pmolec cm}^{-2}$ in trop VCD.
OMI trop. AMF error $e_{\text{SAT},M_{\text{trop}}}$	32% to 42% (Lorente et al., 2017), dominated by choice in a priori profile, cloud parameters and surface albedo. This could explain (most or all) of the discrepancy in Uccle, Cabauw/De Bilt and Xianghe.
error due to cloud or aerosol (OMI or MXD)	Strong reduction in bias and/or dispersion by stricter filtering, for Uccle, Mainz, Cabauw and Xianghe. Simulations (Ma et al., 2013; Jin et al., 2016) indicate cloud or aerosol can cause a factor 2 underestimation for satellite and up to 20% overestimation for MXD.
error due to vertical smoothing	Only assessed with bePRO MXD at Uccle and Xianghe. Applying a priori harmonization and smoothing. Mean difference reduces from -3 to $-1 \text{ Pmolec cm}^{-2}$, and median difference from -2 to 0 Pmolec cm^{-2} . RMSD: small reduction.

¹. 'Impact on dispersion': stated is by how much would the standard deviation of $N_{v,\text{trop},\text{SAT}} - N_{v,\text{trop},\text{REF}}$ reduce if the estimated standard deviation due to this particular error source is subtracted in quadrature.

VCD this leads to a preference of cloud-free scenes and therefore to a negative sampling bias especially at polluted sites (strong reduction in mean VCD from 24 to 15 Pmolec cm⁻² at Xianghe, and reduction by a few Pmolec cm⁻² at Nairobi, Bremen, Thessaloniki and De Bilt/Cabauw). This sampling bias is reduced at De Bilt and Bremen by relaxing the lower bound filter on $\frac{M_{trop}}{M_{geo}}$ from 0.2 to 0.05.

5 The QA4ECV OMI stratospheric NO₂ VCD has a small (mostly wintertime) bias with respect to the ZSL-DOAS measurements of the order of -0.2 ± 0.06 Pmolec cm⁻² (5-10%) and a dispersion of 0.2 to 1 Pmolec cm⁻², with a good representation of the seasonal cycle.

QA4ECV OMI tropospheric NO₂ VCD is negatively biased vs. the MAX-DOAS data. This is not unique to this data product; the same conclusion is reached for NASA's OMI OMNO2 data product, and for several other tropospheric NO₂ data products
10 in the literature. The overall discrepancy exceeds the combined ex-ante uncertainty of satellite and MAX-DOAS data. This is a conclusion opposite to the one of Boersma et al. (2018), where uncertainties seemed overestimated, although that was for a single site in a one-month time period (Tai'an, China, June 2006).

We studied a wide range of potential error sources of the discrepancy in tropospheric VCD between satellite and MAX-DOAS. An overview is provided in Table 3.

15 At several sites the MAX-DOAS instrument is located close (within satellite pixel distance) to an emission source and therefore horizontal smoothing difference error explains (part of) the bias, but there are also a few cases (OHP, Cabauw, Xianghe) where this does not hold. Sampling difference errors were found to be either minor (temporal, horizontal), or to contribute in the opposite direction (vertical).

Measurement/retrieval error in satellite and MAX-DOAS data are other potential sources of discrepancy. Errors in satellite
20 total SCD and stratospheric SCD do not contribute much, leaving errors in satellite tropospheric AMF or MAX-DOAS data as candidate error sources. Part of the discrepancy is caused by errors in either satellite or MAX-DOAS measurement induced by (low) clouds and/or aerosol (e.g., at the sites Mainz, Xianghe). According to radiative transfer simulations (Ma et al., 2013; Jin et al., 2016), these effects impact the satellite tropospheric NO₂ VCD measurements (factor ~2 decrease) more than the MAX-DOAS measurements (overestimation of at most 20%). Also the non-uniform vertical sensitivity of OMI and uncertainty
25 in the a priori profile shape contributes to the discrepancy, as shown here with the QA4ECV OMI vs. bePRO MAX-DOAS comparison. This is in agreement with the work of Lorente et al. (2017): the uncertainty in retrieval method (due to inter-team retrieval setting differences; shorthand methodological uncertainty) in tropospheric AMF is dominated by differences in a priori profile, cloud parameters and surface albedo. Moreover, using this uncertainty estimate for the AMF instead of the ex-ante, one can explain the SAT-REF tropospheric VCD discrepancies for 3 sites (Uccle, Cabauw/De Bilt, Xianghe). For these 3 sites,
30 consistency can also be reached by filtering more strictly on cloud parameters.

Finally, for some of the discrepancies there is no straightforward explanation. A first example is the negative bias at OHP in winter time. Possibly, this is related to a lower tropospheric AMF in winter time, as the planetary boundary layer is more shallow and the SZA is higher. As a result, comparisons become more sensitive to e.g., errors in the profile shape. A second example of unexplained discrepancy is the negative bias at Nairobi, even when focusing on the months December-March when
35 MAX-DOAS measured tropospheric VCD values are relatively low.

The potential impact of horizontal smoothing difference error was analyzed in this work in a rather qualitative way. Analysis using Observing System Simulation Experiments at fine spatial resolution (Verhoelst et al., 2015), or other experimental set-ups (e.g., sensors measuring in multiple azimuth directions (Brinksma et al., 2008; Ortega et al., 2015)), can improve on this.

5 The inter-team harmonization of MAX-DOAS data within the QA4ECV project is an important step forward for satellite validation, although some issues remain e.g., regarding the harmonisation of reported uncertainties. The ESA-funded project FRM4DOAS (<http://frm4doas.aeronomie.be>) should improve on this with the development of a first central processing system for MAX-DOAS measurements built on state-of-the-art retrieval algorithms and corresponding settings.

10 The availability of an ex-ante uncertainty per measurement, and its decomposition in source components, greatly facilitates the validation. However, information on how individual measurement uncertainties should be combined is incomplete in the satellite and MAX-DOAS data files. This limits the ability to check if e.g., the overall bias, the dispersion, or seasonal cycle of the bias each separately are within expectations; in this work we only checked consistency of the overall discrepancy (expressed as RMSD) with the combined total uncertainty. It is recommended that information on the systematic/random nature and error correlation is included in the satellite data product.

15 The ex-ante per-pixel uncertainty in the QA4ECV NO₂ satellite data product is likely underestimated. A solution could be to explicitly account for the methodological uncertainty on AMF; similar as done for the QA4ECV HCHO data product (De Smedt et al., 2018). Alternatively, the uncertainty component due to profile shape in the OMI product could be increased, as tests in this work show that the current 10% assignment is an underestimate. The QA4ECV NO₂ recommended filter on AMF ratio can be made less restrictive (e.g., 0.05 lower bound), reducing data loss and sampling bias without compromising the comparisons with MAX-DOAS. Furthermore, replacement of the coarsely resolved TM5 NO₂ profiles with high-spatial
20 resolution profiles from regional air-quality analyses (e.g., CAMS regional, <http://www.regional.atmosphere.copernicus.eu>) would be very helpful to bridge part of the gap between MAX-DOAS and OMI.

Code and data availability. The QA4ECV OMI NO₂ data is available via <http://www.qa4ecv.eu>, under "ECV data". The OMNO2 data is publicly available from the NASA Goddard Earth Sciences (GES) Data and Information Services Center public website: https://disc.gsfc.nasa.gov/datasets/OMNO2_V003/summary/. The ZSL-DOAS data and bePRO MAX-DOAS as part of the Network for the Detection of
25 Atmospheric Composition Change (NDACC) are publicly available (see <http://www.ndacc.org>). The QA4ECV MAX-DOAS data is available at http://uv-vis.aeronomie.be/groundbased/QA4ECV_MAXDOAS/index.php; it is mandatory to contact instrument principal investigators for any usage of the data. The AERONET AOD data is available at <http://aeronet.gsfc.nasa.gov>. Sentinel-5p NO₂ RPRO (reprocessed) and OFFL (offline) data 01.02.00-01.02.02 can be obtained from the Sentinel-5P Pre-Operations Data Hub (<https://s5phub.copernicus.eu/dhus/#/home>).

30 Part of the validation processing was performed with the data harmonization toolset HARP (©S[&]T, the Netherlands), available at <https://github.com/stcorp/harp> under the BSD 3-Clause "New" or "Revised" License.

Author contributions. SC coordinated the paper and carried out the validation analysis. TV carried out the stratospheric VCD validation analysis. GP contributed insights on the tropospheric VCD validation analysis. DH, AK, J-CL and TV contributed validation expertise. JG, SN and BR created software tools for validation. JG performed general data collection and format harmonisation. FH coordinated the creation of the QA4ECV MAX-DOAS improved data sets. AB, J-PB, FH, AP, JR, AR, MVR, TW are Principal Investigators for the QA4ECV MAX-DOAS measurements. FH and MVR are Principal Investigators for the bePRO MAX-DOAS measurements. FG, AP, and J-PP are Principal Investigators for the SAOZ ZSL-DOAS measurements. FB, HE, AR, IDS, AL, JVG, EP, MVR and TW are the authors of the QA4ECV NO₂ OMI data set. J-CL is the coordinator of this research. All authors reviewed and commented on the manuscript.

Competing interests. The authors declare that they have no conflict of interest.

Acknowledgements. This research was funded by the EU FP7 project Quality Assurance for Essential Climate Variables (QA4ECV, grant no. 5 607405) and the EU H2020 project Gap Analysis for Integrated Atmospheric ECV CLimate Monitoring (GAIA-CLIM, Ares(2014)3708963/Project 640276). In particular the generation of harmonized QA4ECV OMI and MAX-DOAS data sets was funded by the EU FP7 project QA4ECV. Several validation analysis tools were funded by the Belgian Science Policy Office (BELSPO) and ESA through the ProDEx-10 project ACROSAT. We are grateful to Marina Zara (KNMI) for clarifications about the different QA4ECV NO₂ OMI uncertainty fields. Ground-based ZSL-DOAS data and other MAX-DOAS data used in this publication were obtained as part of the Network for the Detection of Atmospheric Composition Change (NDACC) and are publicly available (see <http://www.ndacc.org>). NASA OMNO2 data were obtained through NASA's Earth Observing System Data and Information System (EOSDIS). We are grateful to Nickolay A. Krotkov and Lok Nath Lamsal (NASA/GSFC) for clarifications about the NASA OMNO2 data product. We are also grateful to Trissevgeni Stavrakou (BIRA-IASB) for fruitful discussions on tropospheric NO₂ chemistry. The European Commission is further acknowledged for having supported cross-fertilisation meetings among FP7 (CLIP-C, QA4ECV, ERACLIM-2, EUCLEIA, EUPORIAS, UERRA) and H2020 (GAIA-CLIM, FIDUCEO) climate service related projects. Regarding the AERONET data, we thank the Principal Investigators Rachel Akimana, Vassilis Amiridis, Meinrat Andreae, Alkiviadis Bais, Philippe Goloub, J.S. Bas Henzing, Christian Hermans, Eughne Ndenzako, Pierre Nzohabonayo, Michel Van Roozendael, Ucai Wang, Xiangao Xia, and their staff for establishing and maintaining the 8 AERONET sites used in this investigation. Sentinel-5 Precursor NO₂ data has been used in this work. Sentinel-5 Precursor is a European Space Agency (ESA) mission on behalf of the European Commission (EC). The TROPOMI payload is a joint development by ESA and the Netherlands Space Office (NSO). The Sentinel-5 Precursor ground-segment development has been funded by ESA and with national contributions from The Netherlands, Germany, and Belgium.

References

- Beirle, S., Hörmann, C., Jöckel, P., Liu, S., Penning de Vries, M., Pozzer, A., Sihler, H., Valks, P., and Wagner, T.: The STRatospheric Estimation Algorithm from Mainz (STREAM): estimating stratospheric NO₂ from nadir-viewing satellites by weighted convolution, *Atmos. Meas. Tech.*, 9, 2753–2779, <https://doi.org/10.5194/amt-9-2753-2016>, 2016.
- 5 Boersma, F. et al.: Product Specification Document for the QA4ECV NO₂ ECV precursor product, techreport QA4ECV Deliverable D4.6, KNMI, <http://www.qa4ecv.eu/sites/default/files/D4.6.pdf>, 2017.
- Boersma, K. F., Eskes, H. J., and Brinksma, E. J.: Error analysis for tropospheric NO₂ retrieval from space, *J. Geophys. Res.*, 109, D04311, <https://doi.org/10.1029/2003jd003962>, 2004.
- Boersma, K. F., Vinken, G. C. M., and Eskes, H. J.: Representativeness errors in comparing chemistry transport and chemistry climate models with satellite UV-Vis tropospheric column retrievals, *Geosci. Model Dev.*, 9, 875–898, <https://doi.org/10.5194/gmd-9-875-2016>, 2016.
- 10 Boersma, K. F., Eskes, H. J., Richter, A., De Smedt, I., Lorente, A., Beirle, S., van Geffen, J. H. G. M., Zara, M., Peters, E., Van Roozendael, M., Wagner, T., Maasackers, J. D., van der A, R. J., Nightingale, J., De Rudder, A., Irie, H., Pinardi, G., Lambert, J.-C., and Compernelle, S. C.: Improving algorithms and uncertainty estimates for satellite NO₂ retrievals: results from the quality assurance for the essential climate variables (QA4ECV) project, *Atmos. Meas. Tech.*, 11, 6651–6678, <https://doi.org/10.5194/amt-11-6651-2018>, 2018.
- 15 Bognar, K., Zhao, X., Strong, K., Boone, C., Bourassa, A., Degenstein, D., Drummond, J., Duff, A., Goutail, F., Griffin, D., Jeffery, P., Lutsch, E., Manney, G., McElroy, C., McLinden, C., Millán, L., Pazmino, A., Sioris, C., Walker, K., and Zou, J.: Updated validation of ACE and OSIRIS ozone and NO₂ measurements in the Arctic using ground-based instruments at Eureka, Canada, *Journal of Quantitative Spectroscopy and Radiative Transfer*, 238, 106571, <https://doi.org/https://doi.org/10.1016/j.jqsrt.2019.07.014>, 2019.
- Brinksma, E. J., Pinardi, G., Volten, H., Braak, R., Richter, A., Schönhardt, A., van Roozendael, M., Fayt, C., Hermans, C., Dirksen, R. J., Vlemmix, T., Berkhout, A. J. C., Swart, D. P. J., Oetjen, H., Wittrock, F., Wagner, T., Ibrahim, O. W., de Leeuw, G., Moerman, M., Curier, R. L., Celarier, E. A., Cede, A., Knap, W. H., Veefkind, J. P., Eskes, H. J., Allaart, M., Rothe, R., PETERS, A. J. M., and Levelt, P. F.: The 2005 and 2006 DANDELIONS NO₂ and aerosol intercomparison campaigns, *J. Geophys. Res. Atmos.*, 113, <https://doi.org/10.1029/2007JD008808>, 2008.
- 20 Bucsela, E. J., Krotkov, N. A., Celarier, E. A., Lamsal, L. N., Swartz, W. H., Bhartia, P. K., Boersma, K. F., Veefkind, J. P., Gleason, J. F., and Pickering, K. E.: A new stratospheric and tropospheric NO₂ retrieval algorithm for nadir-viewing satellite instruments: applications to OMI, *Atmos. Meas. Tech.*, 6, 2607–2626, <https://doi.org/10.5194/amt-6-2607-2013>, 2013.
- Bucsela, E. J., Celarier, E. A., Gleason, J. L., Krotkov, N. A., Lamsal, L. N., Marchenko, S. V., and Swartz, W. H.: OMNO2 README Document. Data Product Version 3.0, Tech. rep., NASA /Goddard Space Flight Center, https://acdisc.gesdisc.eosdis.nasa.gov/data/Aura_OMI_Level3/OMNO2d.003/doc/README.OMNO2.pdf, 2016.
- 30 Celarier, E. A., Brinksma, E. J., Gleason, J. F., Veefkind, J. P., Cede, A., Herman, J. R., Ionov, D., Goutail, F., Pommereau, J.-P., Lambert, J.-C., and et al.: Validation of Ozone Monitoring Instrument nitrogen dioxide columns, *J. Geophys. Res.*, 113, D15S15, <https://doi.org/10.1029/2007jd008908>, 2008.
- Chan, K., Hartl, A., Lam, Y., Xie, P., Liu, W., Cheung, H., Lampel, J., Pöhler, D., Li, A., Xu, J., Zhou, H., Ning, Z., and Wenig, M.: Observations of tropospheric NO₂ using ground based MAX-DOAS and OMI measurements during the Shanghai World Expo 2010, *Atmos. Environ.*, 119, 45 – 58, <https://doi.org/doi.org/10.1016/j.atmosenv.2015.08.041>, 2015.
- 35

- Chen, D., Zhou, B., Beirle, S., Chen, L. M., and Wagner, T.: Tropospheric NO₂ column densities deduced from zenith-sky DOAS measurements in Shanghai, China, and their application to satellite validation, *Atmos. Chem. Phys.*, 9, 3641–3662, <https://doi.org/10.5194/acp-9-3641-2009>, 2009.
- Chipperfield, M. P.: Multiannual simulations with a three-dimensional chemical transport model, *J. Geophys. Res.*, 104, 1781–1805, <https://doi.org/10.1029/98jd02597>, 1999.
- Clémer, K., Van Roozendael, M., Fayt, C., Hendrick, F., Hermans, C., Pinardi, G., Spurr, R., Wang, P., and De Mazière, M.: Multiple wavelength retrieval of tropospheric aerosol optical properties from MAXDOAS measurements in Beijing, *Atmos. Meas. Tech.*, 3, 863–878, <https://doi.org/10.5194/amt-3-863-2010>, 2010.
- Compernelle, S. and Lambert, J.-C.: Standard terms and definitions applicable to the quality assurance of Essential Climate Variable data records, Tech. rep., Royal Belgian Institute for Space Aeronomy, <https://doi.org/10.18758/71021041>, <http://www.qa4ecv.eu/lexicon/6>, 2017.
- Compernelle, S., Lambert, J.-C., and Niemeijer, S.: Prototype QA/Validation Service for Atmospheric ECV Precursors : Detailed Processing Model - Version 2, QA4ECV report Deliverable D2.5, Royal Belgian Institute for Space Aeronomy, http://www.qa4ecv.eu/sites/default/files/QA4ECV_BIRA-IASB_D-2-5_AVS-DPMv2_20160623.pdf, 2016.
- 15 Compernelle, S., Lambert, J.-C., Verhoelst, T., Granville, J., Hubert, D., Keppens, A., Niemeijer, S., Rino, B., Pinardi, G., Beirle, S., Boersma, F., Clerbaux, C., Coheur, P., Smedt, I. D., Eskes, H., George, M., Hendrick, F., Lorente, A., Nightingale, J., Peters, E., Richter, A., van Geffen, J., Roozendael, M. V., Wagner, T., and Yu, H.: Quality assessment of QA4ECV climate data records of atmospheric composition: terminology, methodology and application to tropospheric NO₂, HCHO and CO from the GOME-2, IASI and OMI satellites, in: Proceedings for the 2018 EUMETSAT Meteorological Satellite Conference, 17-21 September 2018, Tallinn, Estonia, 2018.
- 20 Crutzen, P.: The influence of nitrogen oxides on the atmospheric ozone content, *Quart. J. Roy. Meteor. Soc.*, 96, 320–325, <https://doi.org/10.1002/qj.49709640815>, 1970.
- De Mazière, M., Thompson, A. M., Kurylo, M. J., Wild, J. D., Bernhard, G., Blumenstock, T., Braathen, G. O., Hannigan, J. W., Lambert, J.-C., Leblanc, T., McGee, T. J., Nedoluha, G., Petropavlovskikh, I., Seckmeyer, G., Simon, P. C., Steinbrecht, W., and Strahan, S. E.: The Network for the Detection of Atmospheric Composition Change (NDACC): history, status and perspectives, *Atmos. Chem. Phys.*, 18, 4935–4964, <https://doi.org/10.5194/acp-18-4935-2018>, 2018.
- 25 De Smedt, I., Theys, N., Yu, H., Danckaert, T., Lerot, C., Compernelle, S., Van Roozendael, M., Richter, A., Hilboll, A., Peters, E., Pedergnana, M., Loyola, D., Beirle, S., Wagner, T., Eskes, H., van Geffen, J., Boersma, K. F., and Veeffkind, P.: Algorithm theoretical baseline for formaldehyde retrievals from S5P TROPOMI and from the QA4ECV project, *Atmos. Meas. Tech.*, 11, 2395–2426, <https://doi.org/10.5194/amt-11-2395-2018>, 2018.
- 30 Delmas, R., Serça, D., and Jambert, C.: Global inventory of NO_x sources, *Nutrient Cycling in Agroecosystems*, 48, 51–60, <https://doi.org/10.1023/A:1009793806086>, 1997.
- Dirksen, R. J., Boersma, K. F., Eskes, H. J., Ionov, D. V., Bucsela, E. J., Levelt, P. F., and Kelder, H. M.: Evaluation of stratospheric NO₂ retrieved from the Ozone Monitoring Instrument: Intercomparison, diurnal cycle, and trending, *J. Geophys. Res.*, 116, D08305, <https://doi.org/10.1029/2010jd014943>, 2011.
- 35 Drosoglou, T., Bais, A. F., Zyrichidou, I., Kouremeti, N., Poupkou, A., Liora, N., Giannaros, C., Koukouli, M. E., Balis, D., and Melas, D.: Comparisons of ground-based tropospheric NO₂ MAX-DOAS measurements to satellite observations with the aid of an air quality model over the Thessaloniki area, Greece, *Atmos. Chem. Phys.*, 17, 5829–5849, <https://doi.org/10.5194/acp-17-5829-2017>, 2017.

- Drosoglou, T., Koukouli, M. E., Kouremeti, N., Bais, A. F., Zyrichidou, I., Balis, D., van der A, R. J., Xu, J., and Li, A.: MAX-DOAS NO₂ observations over Guangzhou, China; ground-based and satellite comparisons, *Atmos. Meas. Tech.*, 11, 2239–2255, <https://doi.org/10.5194/amt-11-2239-2018>, 2018.
- Errera, Q. and Fonteyn, D.: Four-dimensional variational chemical assimilation of CRISTA stratospheric measurements, *J. Geophys. Res.*, 106, 12,253–12,265, 2001.
- Eskes, H. J. and Boersma, K. F.: Averaging kernels for DOAS total-column satellite retrievals, *Atmos. Chem. Phys.*, 3, 1285–1291, <https://doi.org/10.5194/acp-3-1285-2003>, 2003.
- European Environment Agency: Air quality in Europe - 2018 report, Tech. Rep. No 12/2018, European Environment Agency, 2018.
- Frieß, U., Beirle, S., Alvarado Bonilla, L., Bösch, T., Friedrich, M. M., Hendrick, F., Pitters, A., Richter, A., van Roozendaal, M., Rozanov, V. V., Spinei, E., Tirpitz, J.-L., Vlemmix, T., Wagner, T., and Wang, Y.: Intercomparison of MAX-DOAS vertical profile retrieval algorithms: studies using synthetic data, *Atmos Meas Tech*, 12, 2155–2181, <https://doi.org/10.5194/amt-12-2155-2019>, 2019.
- GCOS: The Global Observing System for Climate: Implementation Needs GCOS 2016 Implementation Plan, Tech. Rep. GCOS-200, https://library.wmo.int/opac/doc_num.php?explnum_id=3417, 2016.
- Gielen, C., Hendrick, F., Pinardi, G., De Smedt, I., Fayt, C., Hermans, C., Stavrakou, T., Bauwens, M., Müller, J.-F., Ndenzako, E., Nzonabonayo, P., Akimana, R., Niyonzima, S., Van Roozendaal, M., and De Mazière, M.: Characterisation of Central-African aerosol and trace-gas emissions based on MAX-DOAS measurements and model simulations over Bujumbura, Burundi, *Atmos. Chem. Phys. Discuss.*, 2017, 1–41, <https://doi.org/10.5194/acp-2016-1104>, 2017.
- Giles, D. M., Sinyuk, A., Sorokin, M. G., Schafer, J. S., Smirnov, A., Slutsker, I., Eck, T. F., Holben, B. N., Lewis, J. R., Campbell, J. R., Welton, E. J., Korokin, S. V., and Lyapustin, A. I.: Advancements in the Aerosol Robotic Network (AERONET) Version 3 database – automated near-real-time quality control algorithm with improved cloud screening for Sun photometer aerosol optical depth (AOD) measurements, *Atmos. Meas. Tech.*, 12, 169–209, <https://doi.org/10.5194/amt-12-169-2019>, 2019.
- Goldberg, D. L., Lamsal, L. N., Loughner, C. P., Swartz, W. H., Lu, Z., and Streets, D. G.: A high-resolution and observationally constrained OMI NO₂ satellite retrieval, *Atmos. Chem. Phys.*, 17, 11 403–11 421, <https://doi.org/10.5194/acp-17-11403-2017>, 2017.
- Gothenburg: The 1999 Gothenburg Protocol (part of the Convention on Long-Range Transboundary Air Pollution), <http://www.unece.org/environmental-policy/conventions/air/guidance-documents-and-other-methodological-materials/gothenburg-protocol.html>, 1999.
- Hendrick, F., Barret, B., Van Roozendaal, M., Boesch, H., Butz, A., De Mazière, M., Goutail, F., Hermans, C., Lambert, J.-C., Pfeilsticker, K., and et al.: Retrieval of nitrogen dioxide stratospheric profiles from ground-based zenith-sky UV-visible observations: validation of the technique through correlative comparisons, *Atmos. Chem. Phys.*, 4, 2091–2106, <https://doi.org/10.5194/acp-4-2091-2004>, 2004.
- Hendrick, F., Mahieu, E., Bodeker, G. E., Boersma, K. F., Chipperfield, M. P., De Mazière, M., De Smedt, I., Demoulin, P., Fayt, C., Hermans, C., Kreher, K., Lejeune, B., Pinardi, G., Servais, C., Stübi, R., van der A, R., Vernier, J.-P., and Van Roozendaal, M.: Analysis of stratospheric NO₂ trends above Jungfraujoch using ground-based UV-visible, FTIR, and satellite nadir observations, *Atmos. Chem. Phys.*, 12, 8851–8864, <https://doi.org/10.5194/acp-12-8851-2012>, 2012.
- Hendrick, F., Müller, J.-F., Clémer, K., Wang, P., De Mazière, M., Fayt, C., Gielen, C., Hermans, C., Ma, J. Z., Pinardi, G., and et al.: Four years of ground-based MAX-DOAS observations of HONO and NO₂ in the Beijing area, *Atmos. Chem. Phys.*, 14, 765–781, <https://doi.org/10.5194/acp-14-765-2014>, 2014.
- Hendrick, F., Dils, B., et al.: Historical record of independent reference data for NO₂, HCHO, and CO, techreport QA4ECV Deliverable D3.8, Belgian Institute for Space Astronomy, http://www.qa4ecv.eu/sites/default/files/QA4ECV_D3.8_v1.0_web.pdf, 2016.

- Hendrick, F., Dils, B., Langerock, B., Pinardi, G., Roozendael, M. V., Seyler, A., Peters, F. W. E., Richter, A., PETERS, A., Drosoglou, T., Bais, A., Wagner, T., and Döner, S.: Report on independent validation of atmospheric reference data sets., techreport QA4ECV Deliverable D3.10, Belgian Institute for Space Aeronomy, http://www.qa4ecv.eu/sites/default/files/QA4ECV_D3.10_v2.pdf, 2018.
- Heue, K.-P., Richter, A., Bruns, M., Burrows, J. P., v. Friedeburg, C., Platt, U., Pundt, I., Wang, P., and Wagner, T.: Validation of SCIAMACHY tropospheric NO₂-columns with MAXDOAS measurements, *Atmos. Chem. Phys.*, 5, 1039–1051, <https://doi.org/10.5194/acp-5-1039-2005>, 2005.
- Hoek, G., Krishnan, R. M., Beelen, R., Peters, A., Ostro, B., Brunekreef, B., and Kaufman, J. D.: Long-term air pollution exposure and cardio- respiratory mortality: a review, *Environmental Health*, 12, 43, <https://doi.org/10.1186/1476-069X-12-43>, 2013.
- Hovila, J., Schmidt, A., Valks, P., Tuinder, O., van Versendaal, R., Jönch-Sørensen, H., Koukoulis, M., Garane, K., Delcloc, A., Pinardi, G., Langerock, B., Steinbrecht, W., George, M., Clerbaux, C., Astoreca, R., Hurtmans, D., Coheur, P.-F., and Vicente, C.: EUMETSAT AC SAF Operations report, Issue 1/2018 rev. 2, Reporting period: January –June 2018, Tech. Rep. SAF/AC/FMI/OPS/RP/001, https://acsaf.org/docs/or/AC_SAF_Operations_Report_1-2018.pdf, 2018.
- Huijnen, V., Williams, J., van Weele, M., van Noije, T., Krol, M., Dentener, F., Segers, A., Houweling, S., Peters, W., de Laat, J., Boersma, F., Bergamaschi, P., van Velthoven, P., Le Sager, P., Eskes, H., Alkemade, F., Scheele, R., Nédélec, P., and Pätz, H.-W.: The global chemistry transport model TM5: description and evaluation of the tropospheric chemistry version 3.0, *Geosci. Model Dev.*, 3, 445–473, <https://doi.org/10.5194/gmd-3-445-2010>, 2010.
- Ionov, D. V., Timofeyev, Y. M., Sinyakov, V. P., Semenov, V. K., Goutail, F., Pommereau, J.-P., Bucsele, E. J., Celarier, E. A., and Kroon, M.: Ground-based validation of EOS-Aura OMI NO₂ vertical column data in the midlatitude mountain ranges of Tien Shan (Kyrgyzstan) and Alps (France), *J. Geophys. Res.*, 113, D15S08, <https://doi.org/10.1029/2007jd008659>, 2008.
- Irie, H., Takashima, H., Kanaya, Y., Boersma, K. F., Gast, L., Wittrock, F., Brunner, D., Zhou, Y., and Van Roozendael, M.: Eight-component retrievals from ground-based MAX-DOAS observations, *Atmos. Meas. Tech.*, 4, 1027–1044, <https://doi.org/10.5194/amt-4-1027-2011>, 2011.
- Jin, J., Ma, J., Lin, W., Zhao, H., Shaiganfar, R., Beirle, S., and Wagner, T.: MAX-DOAS measurements and satellite validation of tropospheric NO₂ and SO₂ vertical column densities at a rural site of North China, *Atmos. Environ.*, 133, 12 – 25, <https://doi.org/https://doi.org/10.1016/j.atmosenv.2016.03.031>, 2016.
- Joint Committee for Guides in Metrology: Evaluation of measurement data - Guide to the expression of uncertainty in measurement, Tech. rep., http://www.bipm.org/utis/common/documents/jcgm/JCGM_100_2008_E.pdf, 2008.
- Joint Committee for Guides in Metrology: International Vocabulary of Metrology - Basic and General Concepts and Associated Terms, Tech. rep., http://www.bipm.org/utis/common/documents/jcgm/JCGM_200_2012.pdf, 2012.
- Kanaya, Y., Irie, H., Takashima, H., Iwabuchi, H., Akimoto, H., Sudo, K., Gu, M., Chong, J., Kim, Y. J., Lee, H., Li, A., Si, F., Xu, J., Xie, P.-H., Liu, W.-Q., Dzhola, A., Postlyakov, O., Ivanov, V., Grechko, E., Terpigova, S., and Panchenko, M.: Long-term MAX-DOAS network observations of NO₂ in Russia and Asia (MADRAS) during the period 2007-2012: instrumentation, elucidation of climatology, and comparisons with OMI satellite observations and global model simulations, *Atmos. Chem. Phys.*, 14, 7909–7927, <https://doi.org/10.5194/acp-14-7909-2014>, 2014.
- Keppens, A., Lambert, J.-C., Granville, J., Miles, G., Siddans, R., van Peet, J. C. A., van der A, R. J., Hubert, D., Verhoelst, T., Delcloc, A., Godin-Beekmann, S., Kivi, R., Stübi, R., and Zehner, C.: Round-robin evaluation of nadir ozone profile retrievals: methodology and application to MetOp-A GOME-2, *Atmos. Meas. Tech.*, 8, 2093–2120, <https://doi.org/10.5194/amt-8-2093-2015>, 2015.

- Keppens, A., Compernelle, S., Verhoelst, T., Hubert, D., and Lambert, J.-C.: Harmonization and comparison of vertically resolved atmospheric state observations: methods, effects, and uncertainty budget, *Atmos. Meas. Tech.*, 12, 4379–4391, <https://doi.org/10.5194/amt-12-4379-2019>, 2019.
- Kleipool, Q. L., Dobber, M. R., de Haan, J. F., and Levelt, P. F.: Earth surface reflectance climatology from 3 years of OMI data, *J. Geophys. Res.*, 113, D18 308, <https://doi.org/10.1029/2008jd010290>, 2008.
- Krotkov, N. A., Lamsal, L. N., Celarier, E. A., Swartz, W. H., Marchenko, S. V., Bucsela, E. J., Chan, K. L., Wenig, M., and Zara, M.: The version 3 OMI NO₂ standard product, *Atmos. Meas. Tech.*, 10, 3133–3149, <https://doi.org/10.5194/amt-10-3133-2017>, 2017.
- Lambert, J.-C., Van Roozendael, M., Granville, J., Gérard, P., Simon, P., Claude, H., and Staehelin, J.: Comparison of the GOME ozone and NO₂ total amounts at mid-latitude with ground-based zenith-sky measurements, in: *Atmospheric Ozone, Proceedings of the XVIII Quadrennial Ozone Symposium, L'Aquila, Italy, 12-21 September 1996*, 1996.
- Langerock, B., De Mazière, M., Hendrick, F., Vigouroux, C., Desmet, F., Dils, B., and Niemeijer, S.: Description of algorithms for co-locating and comparing gridded model data with remote-sensing observations, *Geosci. Model Dev.*, 8, 911–921, <https://doi.org/10.5194/gmd-8-911-2015>, 2015.
- Levelt, P. F., van den Oord, G. H. J., Dobber, M. R., Malkki, A., Huib Visser, Johan de Vries, Stammes, P., Lundell, J. O. V., and Saari, H.: The ozone monitoring instrument, *IEEE Trans. Geosci. Remote Sens.*, 44, 1093–1101, <https://doi.org/10.1109/TGRS.2006.872333>, 2006.
- Liu, S., Valks, P., Pinardi, G., De Smedt, I., Yu, H., Beirle, S., and Richter, A.: An improved total and tropospheric NO₂ column retrieval for GOME-2, *Atmos. Meas. Tech.*, 12, 1029–1057, <https://doi.org/10.5194/amt-12-1029-2019>, 2019.
- Loew, A., Bell, W., Brocca, L., Bulgin, C. E., Burdanowitz, J., Calbet, X., Donner, R. V., Ghent, D., Gruber, A., Kaminski, T., Kinzel, J., Klepp, C., Lambert, J.-C., Schaepman-Strub, G., Schröder, M., and Verhoelst, T.: Validation practices for satellite-based Earth observation data across communities, *Rev. Geophys.*, <https://doi.org/10.1002/2017RG000562>, 2017RG000562, 2017.
- Lorente, A., Boersma, K. F., Yu, H., Dörner, S., Hilboll, A., Richter, A., Liu, M., Lamsal, L. N., Barkley, M., Smedt, I. D., Roozendael, M. V., Wang, Y., Wagner, T., Beirle, S., Lin, J.-T., Krotkov, N., Stammes, P., Wang, P., Eskes, H. J., and Krol, M.: Structural uncertainty in air mass factor calculation for NO₂ and HCHO satellite retrievals, *Atmos. Meas. Tech.*, 10, 759–782, <https://doi.org/10.5194/amt-10-759-2017>, 2017.
- Lorente Delgado, A.: From photon paths to pollution plumes: better radiative transfer calculations to monitor NO_x emissions with OMI and TROPOMI, <http://edepot.wur.nl/474563>, 2019.
- Ma, J. Z., Beirle, S., Jin, J. L., Shaiganfar, R., Yan, P., and Wagner, T.: Tropospheric NO₂ vertical column densities over Beijing: results of the first three years of ground-based MAX-DOAS measurements (2008-2011) and satellite validation, *Atmos. Chem. Phys.*, 13, 1547–1567, <https://doi.org/10.5194/acp-13-1547-2013>, 2013.
- Marchenko, S., Krotkov, N. A., Lamsal, L. N., Celarier, E. A., Swartz, W. H., and Bucsela, E. J.: Revising the slant column density retrieval of nitrogen dioxide observed by the Ozone Monitoring Instrument, *J. Geophys. Res. Atmos.*, 120, 5670–5692, <https://doi.org/10.1002/2014JD022913>, 2015.
- Mayer, B. and Kylling, A.: Technical note: The libRadtran software package for radiative transfer calculations - description and examples of use, *Atmospheric Chemistry and Physics*, 5, 1855–1877, <https://doi.org/10.5194/acp-5-1855-2005>, <https://www.atmos-chem-phys.net/5/1855/2005/>, 2005.
- Myhre, G., Shindell, D., Bréon, F.-M., Collins, W., Fuglestedt, J., Huang, J., Koch, D., Lamarque, J.-F., Lee, D., Mendoza, B., Nakajima, T., Robock, A., Stephens, G., Takemura, T., and Zhang, H.: Anthropogenic and Natural Radiative Forcing, in: *Climate Change 2013: The Physical Science Basis. Contribution of Working Group I to the Fifth Assessment Report of the Intergovernmental Panel on Climate*

- Change, edited by Stocker, T., Qin, D., Plattner, G.-K., Tignor, M., Allen, S., Boschung, J., Nauels, A., Xia, Y., Bex, V., and Midgley, P., chap. 8, Cambridge University Press, Cambridge, United Kingdom and New York, NY, USA, 2013.
- Nightingale, J., Boersma, K. F., Muller, J.-P., Compennolle, S., Lambert, J.-C., Blessing, S., Giering, R., Gobron, N., De Smedt, I., Coheur, P., George, M., Schulz, J., and Wood, A.: Quality Assurance Framework Development Based on Six New ECV Data Products to Enhance User Confidence for Climate Applications, *Remote Sensing*, 10, <https://doi.org/10.3390/rs10081254>, 2018.
- Noxon, J. F.: Stratospheric NO₂: 2. Global behavior, *Journal of Geophysical Research: Oceans*, 84, 5067–5076, <https://doi.org/10.1029/JC084iC08p05067>, 1979.
- Ortega, I., Koenig, T., Sinreich, R., Thomson, D., and Volkamer, R.: The CU 2-D-MAX-DOAS instrument – Part 1: Retrieval of 3-D distributions of NO₂ and azimuth-dependent OVOC ratios, *Atmos. Meas. Tech.*, 8, 2371–2395, <https://doi.org/10.5194/amt-8-2371-2015>, 2015.
- Peters, E., Pinardi, G., Seyler, A., Richter, A., Wittrock, F., Bösch, T., Van Roozendaal, M., Hendrick, F., Drosoglou, T., Bais, A. F., Kanaya, Y., Zhao, X., Strong, K., Lampel, J., Volkamer, R., Koenig, T., Ortega, I., Puentedura, O., Navarro-Comas, M., Gómez, L., Yela González, M., Piders, A., Remmers, J., Wang, Y., Wagner, T., Wang, S., Saiz-Lopez, A., García-Nieto, D., Cuevas, C. A., Benavent, N., Querel, R., Johnston, P., Postlyakov, O., Borovski, A., Elokhov, A., Bruchkouski, I., Liu, H., Liu, C., Hong, Q., Rivera, C., Grutter, M., Stremme, W., Khokhar, M. F., Khayyam, J., and Burrows, J. P.: Investigating differences in DOAS retrieval codes using MAD-CAT campaign data, *Atmos. Meas. Tech.*, 10, 955–978, <https://doi.org/10.5194/amt-10-955-2017>, 2017.
- Petritoli, A., Bonasoni, P., Giovanelli, G., Ravegnani, F., Kostadinov, I., Bortoli, D., Weiss, A., Schaub, D., Richter, A., and Fortezza, F.: First comparison between ground-based and satellite-borne measurements of tropospheric nitrogen dioxide in the Po basin, *J. Geophys. Res. Atmos.*, 109, <https://doi.org/10.1029/2004JD004547>, 2004.
- Pinardi, G., Van Roozendaal, M., Lambert, J.-C., Granville, J., Hendrick, F., et al.: GOME-2 total and tropospheric NO₂ validation based on zenith-sky, direct-sun and multi-axis doas network observations, in: EUMETSAT Conference, 2014.
- Pinardi, G., Van Roozendaal, M., Hendrick, F., Theys, N., Abuhassan, N., Bais, A., Boersma, F., Cede, A., Chong, J., Donner, S., Drosoglou, T., Frieß, U., Granville, J., Herman, J. R., Eskes, H., Holla, R., Hovila, J., Irie, H., Kanaya, Y., Karagkiozidis, D., Kouremeti, N., Lambert, J.-C., Ma, J., Peters, E., Piders, A., Postlyakov, O., Richter, A., Remmers, J., Takashima, H., Tiefengraber, M., Valks, P., Vlemmix, T., Wagner, T., and Wittrock, F.: Validation of tropospheric NO₂ column measurements of GOME-2A and OMI using MAX-DOAS and direct sun network observations, *Atmos. Meas. Tech. Discuss.*, 2020, 1–55, <https://doi.org/10.5194/amt-2020-76>, 2020.
- Platt, U. and Stutz, J.: *Differential Optical Absorption Spectroscopy: Principles and Applications*, Springer, <https://doi.org/10.1007/978-3-540-75776-4>, 2008.
- Pommereau, J. and Goutail, F.: O₃ and NO₂ ground-based measurements by visible spectrometry during Arctic winter and spring 1988, *Geophys. Res. Lett.*, 15, 891–894, <https://doi.org/10.1029/GL015i008p00891>, 1988.
- QA4EO: Quality Assurance Framework for Earth Observation - The Guide, Tech. rep., http://qa4eo.org/docs/QA4EO_guide.pdf.
- Richter, A., Godin, S., Gomez, L., Hendrick, F., Hocke, K., Langerock, B., van Roozendaal, M., and Wagner, T.: EC FP7 NORS Technical Note D4.4 - Spatial Representativeness of NORS observations, Tech. rep., Institute of Environmental Physics, University of Bremen, 2013a.
- Richter, A., Weber, M., Burrows, J., Lambert, J.-C., and van Gijsel, A.: Validation strategy for satellite observations of tropospheric reactive gases, *Annals of Geophysics*, 56, <https://doi.org/10.4401/ag-6335>, 2013b.
- Richter, A. et al.: Quality indicators on uncertainties and representativity of atmospheric reference data, techreport QA4ECV Deliverable D3.9, Belgian Institute for Space Aeronomy, <http://www.qa4ecv.eu/sites/default/files/D3.9.pdf>, 2016.

- Rino, B., Niemeijer, S., Compernelle, S., and Lambert, J.-C.: Prototype QA/Validation service for Atmosphere ECVs: Web based prototype, QA4ECV report Deliverable D2.6, s[&]t Corporation, http://www.qa4ecv.eu/sites/default/files/QA4ECV_D-2-6_final.pdf, 2017.
- Rodgers, C. D.: Inverse Methods for Atmospheric Sounding, vol. 2 of *Series on Atmospheric, Oceanic and Planetary Physics*, World Scientific, Singapore, 2000.
- 5 Rodgers, C. D. and Connor, B. J.: Intercomparison of remote sounding instruments, *J. Geophys. Res.*, 108, 4116, <https://doi.org/10.1029/2002JD002299>, 2003.
- Schaub, D., Boersma, K. F., Kaiser, J. W., Weiss, A. K., Folini, D., Eskes, H. J., and Buchmann, B.: Comparison of GOME tropospheric NO₂ columns with NO₂ profiles deduced from ground-based in situ measurements, *Atmos. Chem. Phys.*, 6, 3211–3229, <https://doi.org/10.5194/acp-6-3211-2006>, 2006.
- 10 Seinfeld, J. H. and Pandis, S. N.: *Atmospheric Chemistry and Physics - From air pollution to climate change*, Wiley, John & Sons, first edn., 1997.
- Shindell, D. T., Faluvegi, G., Koch, D. M., Schmidt, G. A., Unger, N., and Bauer, S. E.: Improved Attribution of Climate Forcing to Emissions, *Science*, 326, 716–718, <https://doi.org/10.1126/science.1174760>, 2009.
- Sillman, S., Logan, J. A., and Wofsy, S. C.: The sensitivity of ozone to nitrogen oxides and hydrocarbons in regional ozone episodes, *J. Geophys. Res. Atmos.*, 95, 1837–1851, <https://doi.org/10.1029/JD095iD02p01837>, 1990.
- 15 Solomon, S., Schmeltekopf, A. L., and Sanders, R. W.: On the interpretation of zenith sky absorption measurements, *J. Geophys. Res.*, 92, 8311–8319, <https://doi.org/10.1029/JD092iD07p08311>, 1987.
- Spurr, R.: *Light Scattering Reviews*, vol. 3, chap. LIDORT and VLIDORT: Linearized pseudo-spherical scalar and vector discrete ordinate radiative transfer models for use in remote sensing retrieval problems, Springer, Berlin, Heidelberg, 2008.
- 20 Strahan, S., Douglass, A., and Newman, P.: The contributions of chemistry and transport to low arctic ozone in March 2011 derived from Aura MLS observations, *J. Geophys. Res.*, 118, 1563–1576, <https://doi.org/10.1002/jgrd.50181>, 2013.
- Tirpitz, J.-L., Frieß, U., Hendrick, F., Alberti, C., Allaart, M., Apituley, A., Bais, A., Beirle, S., Berkhout, S., Bogner, K., Bösch, T., Bruchkouski, I., Cede, A., Chan, K. L., den Hoed, M., Donner, S., Drosoglou, T., Fayt, C., Friedrich, M. M., Frumau, A., Gast, L., Gielen, C., Gomez-Martín, L., Hao, N., Hensen, A., Henzing, B., Hermans, C., Jin, J., Kreher, K., Kuhn, J., Lampel, J., Li, A., Liu, C., Liu, H.,
- 25 Ma, J., Merlaud, A., Peters, E., Pinardi, G., Piders, A., Platt, U., Puentedura, O., Richter, A., Schmitt, S., Spinei, E., Stein Zweers, D., Strong, K., Swart, D., Tack, F., Tiefengraber, M., van der Hoff, R., van Roozendaal, M., Vlemmix, T., Vonk, J., Wagner, T., Wang, Y., Wang, Z., Wenig, M., Wiegner, M., Wittrock, F., Xie, P., Xing, C., Xu, J., Yela, M., Zhang, C., and Zhao, X.: Intercomparison of MAX-DOAS vertical profile retrieval algorithms: studies on field data from the CINDI-2 campaign, *Atmos. Meas. Tech. Discuss.*, 2020, 1–49, <https://doi.org/10.5194/amt-2019-456>, 2020.
- 30 Vandaele, A. C., Fayt, C., Hendrick, F., Hermans, C., Humbled, F., Van Roozendaal, M., Gil, M., Navarro, M., Puentedura, O., Yela, M., Braathen, G., Stebel, K., Tørnkvist, K., Johnston, P., Kreher, K., Goutail, F., Mieville, A., Pommereau, J.-P., Khaikine, S., Richter, A., Oetjen, H., Wittrock, F., Bugarski, S., Frieß, U., Pfeilsticker, K., Sinreich, R., Wagner, T., Corlett, G., and Leigh, R.: An intercomparison campaign of ground-based UV-visible measurements of NO₂, BrO, and OClO slant columns: Methods of analysis and results for NO₂, *J. Geophys. Res. Atmos.*, 110, <https://doi.org/10.1029/2004JD005423>, 2005.
- 35 Veefkind, J. P., de Haan, J. F., Sneep, M., and Levelt, P. F.: Improvements to the OMI O2-O2 operational cloud algorithm and comparisons with ground-based radar-lidar observations, *Atmos. Meas. Tech.*, 9, 6035–6049, <https://doi.org/10.5194/amt-9-6035-2016>, 2016.

- Verhoelst, T. and Lambert, J. C.: Generic metrology aspects of an atmospheric composition measurement and of data comparisons. EC Horizon2020 GAIA-CLIM technical Report / Deliverable D3.2, Tech. rep., BIRA-IASB, <http://www.gaia-clim.eu/system/files/publications>, 2016.
- 5 Verhoelst, T., Granville, J., Hendrick, F., Köhler, U., Lerot, C., Pommereau, J.-P., Redondas, A., Van Roozendael, M., and Lambert, J.-C.: Metrology of ground-based satellite validation: co-location mismatch and smoothing issues of total ozone comparisons, *Atmos. Meas. Tech.*, 8, 5039–5062, <https://doi.org/10.5194/amt-8-5039-2015>, 2015.
- Vlemmix, T., Hendrick, F., Pinardi, G., De Smedt, I., Fayt, C., Hermans, C., PETERS, A., Wang, P., Levelt, P., and Van Roozendael, M.: MAX-DOAS observations of aerosols, formaldehyde and nitrogen dioxide in the Beijing area: comparison of two profile retrieval approaches, *Atmos. Meas. Tech.*, 8, 941–963, <https://doi.org/10.5194/amt-8-941-2015>, 2015.
- 10 von Clarmann, T.: Validation of remotely sensed profiles of atmospheric state variables: strategies and terminology, *Atmos. Chem. Phys.*, 6, 4311–4320, <https://doi.org/10.5194/acp-6-4311-2006>, 2006.
- Wang, Y., Beirle, S., Lampel, J., Koukouli, M., De Smedt, I., Theys, N., Li, A., Wu, D., Xie, P., Liu, C., Van Roozendael, M., Stavrou, T., Müller, J.-F., and Wagner, T.: Validation of OMI, GOME-2A and GOME-2B tropospheric NO₂, SO₂ and HCHO products using MAX-DOAS observations from 2011 to 2014 in Wuxi, China: investigation of the effects of priori profiles and aerosols on the satellite products, *Atmos. Chem. Phys.*, 17, 5007–5033, <https://doi.org/10.5194/acp-17-5007-2017>, 2017.
- 15 Wenig, M. O., Cede, A. M., Bucsela, E. J., Celarier, E. A., Boersma, K. F., Veeffkind, J. P., Brinksma, E. J., Gleason, J. F., and Herman, J. R.: Validation of OMI tropospheric NO₂ column densities using direct-Sun mode Brewer measurements at NASA Goddard Space Flight Center, *J. Geophys. Res.*, 113, D16S45, <https://doi.org/10.1029/2007jd008988>, 2008.
- Williams, J. E., Boersma, K. F., Le Sager, P., and Verstraeten, W. W.: The high-resolution version of TM5-MP for optimized satellite retrievals: description and validation, *Geosci. Model Dev.*, 10, 721–750, <https://doi.org/10.5194/gmd-10-721-2017>, 2017.
- World Health Organization: Review of evidence on health aspects of air pollution - REVIHAAP Project, Tech. rep., World Health Organization, Copenhagen, Denmark, <http://www.euro.who.int/>, 2013.
- Zara, M., Boersma, K. F., van Geffen, J., and Eskes, H.: An improved temperature correction for OMI NO₂ slant column densities from the 405–465 nm fitting window - TN-OMIE-KNMI-982, Tech. rep., KNMI, De Bilt, The Netherlands, <https://kfolkertboersma.files.wordpress.com/2019/09/tn-omie-knmi-982.pdf>, 2017.
- 25 Zara, M., Boersma, K. F., De Smedt, I., Richter, A., Peters, E., van Geffen, J. H. G. M., Beirle, S., Wagner, T., Van Roozendael, M., Marchenko, S., Lamsal, L. N., and Eskes, H. J.: Improved slant column density retrieval of nitrogen dioxide and formaldehyde for OMI and GOME-2A from QA4ECV: intercomparison, uncertainty characterisation, and trends, *Atmos. Meas. Tech.*, 11, 4033–4058, <https://doi.org/10.5194/amt-11-4033-2018>, 2018.
- 30 Zhou, Y., Brunner, D., Boersma, K. F., Dirksen, R., and Wang, P.: An improved tropospheric NO₂ retrieval for OMI observations in the vicinity of mountainous terrain, *Atmos. Meas. Tech.*, 2, 401–416, <https://doi.org/10.5194/amt-2-401-2009>, 2009.

Appendix S: Supplement

S1 Pixel screening on low cloud and aerosol

As low clouds and aerosol can induce an error on the column density retrieved by the satellite, a filter on the effective cloud pressure is sometimes employed (Boersma et al., 2018, e.g., only uses pixels with $p_c < 850$ hPa). However, a pixel with a low cloud pressure is not necessarily problematic. In this work, we exclude only pixels where the ex-ante uncertainty due to cloud pressure RMS(u_{SAT, p_c}) is high. Practically, a one-sided 3-sigma-clipping on RMS(u_{SAT, p_c}) is performed. This procedure has a similar effect on RMS(u_{SAT}) and RMS(u_{SAT, p_c}) as a fixed filter on p_c , but has the advantage of removing less pixels. Fig. S1, for the site Xianghe, reveals that most pixels removed by the sigma-clipping approach have indeed a low cloud pressure, but a large portion of pixels with a low cloud pressure are not removed.

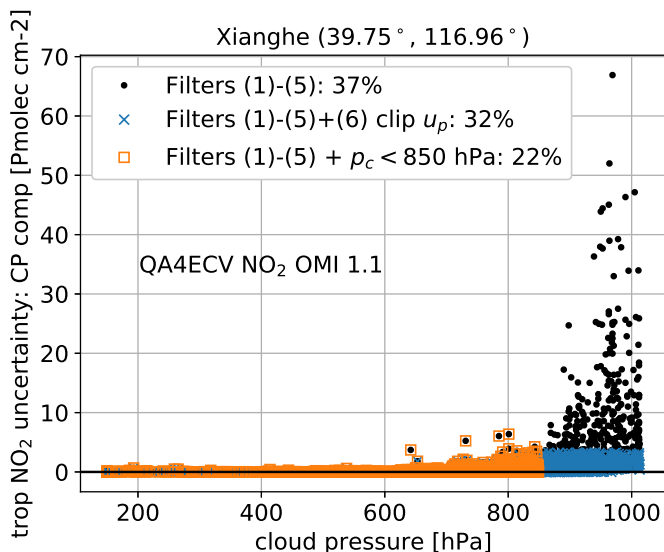


Figure S1. Ex-ante uncertainty due to cloud pressure u_{SAT, p_c} vs. cloud pressure, at the site Xianghe, without and with application of flag (6): remove data with $u_{SAT, p_c, i} > \text{mean}(u_{SAT, p_c, i}) + 3 \times \text{SD}(u_{SAT, p_c, i})$ and the alternative of $p_c < 850$ hPa.

10 S2 Alternative AMF ratio filter

A substantial amount of retrievals are rejected by the lower bound on AMF ratio $\frac{M_{trop}}{M_{geo}} > 0.2$ (see Fig. 3). It can be argued that this recommendation from Boersma et al. (2017) is too restrictive. In Fig. S2 the results with an alternative lower bound, 0.05, are presented. There are now significantly more retrievals that are not rejected by the AMF ratio filter (filter (4)) at the sites Bremen, Mainz, OHP, Uccle, Xianghe and (not shown) De Bilt and Cabauw. However, the net data gain after applying the full screening is more modest as many of these retrievals are still rejected by the filter on cloud fraction (filter (5)). For example, at the sites Bremen, Mainz, Uccle, De Bilt, Cabauw now ~10 % data remains (compared to ~8 % with the baseline filtering). Note that especially at the winter months December and January there is a gain for these sites (less than 1% remaining with the

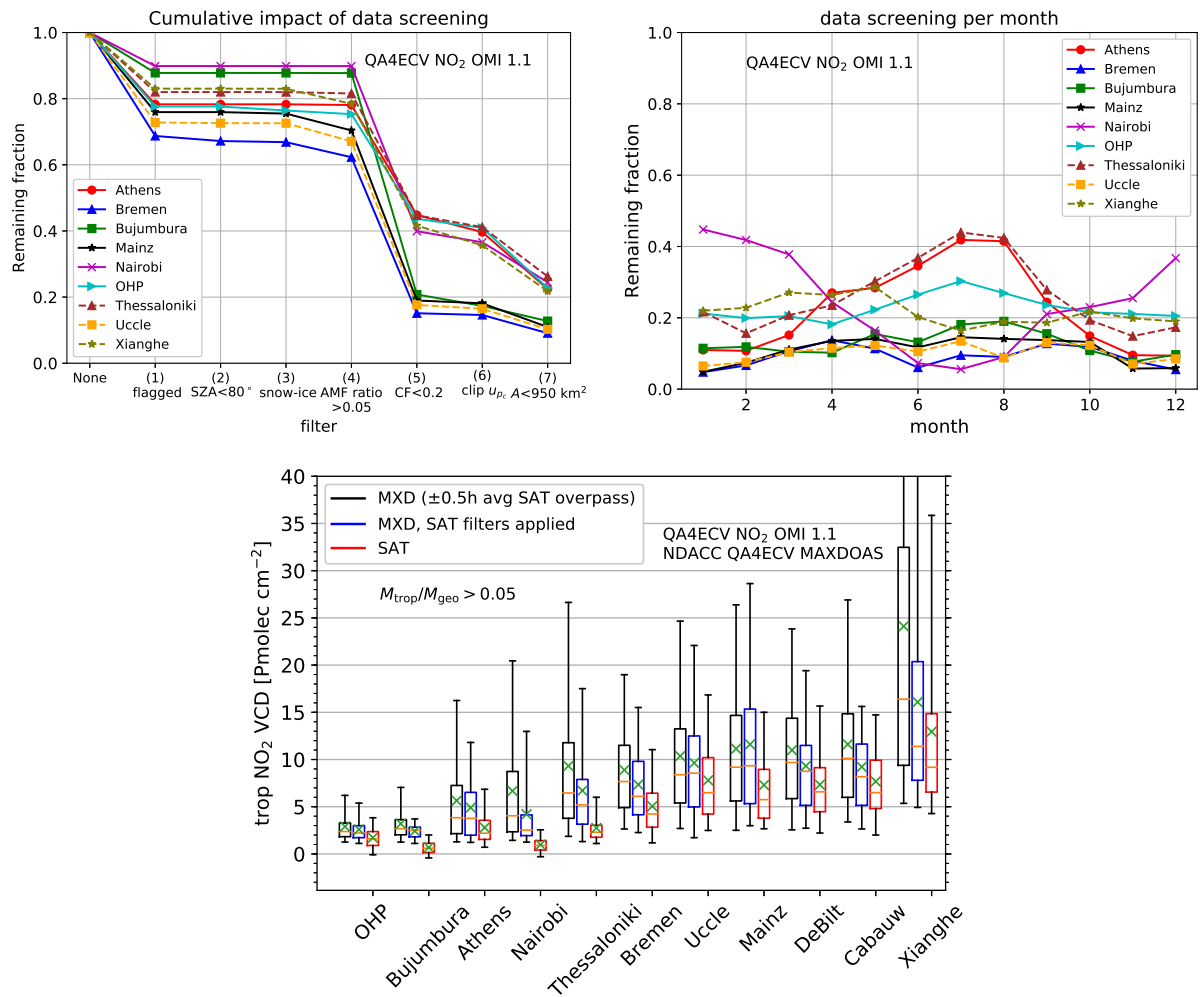


Figure S2. Same as Fig. 3, but with a less restrictive lower bound on $\frac{M_{\text{trop}}}{M_{\text{geo}}}$ of 0.05.

baseline filtering, and ~5% with the modified filtering). The sampling bias at Bremen and De Bilt is reduced with the alternative AMF ratio filter, while it is removed at Mainz.

S3 Horizontal sampling difference error: details of estimation

The RMS of horizontal sampling difference error, $\text{RMS}_{\Delta r_{\text{SAT,GB}}}$, can in principle be estimated by (i) taking the RMS of $N_{v,\text{trop,SAT}_2} - N_{v,\text{trop,SAT}_1}$, (ii) subtracting from this in quadrature the standard deviation due to uncorrelated random noise in the satellite measurement, and (iii) finally, assuming that $\text{RMS}_{\Delta r_{\text{SAT,GB}}}$ can be approximated as $\text{RMS}_{\Delta r_{\text{SAT}_1,\text{SAT}_2}}$, given that $\Delta r_{\text{SAT,GB}} \approx \Delta r_{\text{SAT}_1,\text{SAT}_2}$ (see section 3.4.3)

$$\begin{aligned} [\text{RMS}(N_{v,\text{trop,SAT}_2} - N_{v,\text{trop,SAT}_1})]^2 &= \sigma_{\text{SAT}_1,\text{noise}}^2 + \sigma_{\text{SAT}_2,\text{noise}}^2 + (\text{RMS}_{\Delta r_{\text{SAT}_1,\text{SAT}_2}})^2 \\ &\approx u_{\text{SAT}_1,N_s}^2 + u_{\text{SAT}_2,N_s}^2 + (\text{RMS}_{\Delta r_{\text{SAT,GB}}})^2 \\ \Rightarrow (\text{RMS}_{\Delta r_{\text{SAT,GB}}})^2 &\approx ([\text{RMS}(N_{v,\text{trop,SAT}_2} - N_{v,\text{trop,SAT}_1})]^2 - (u_{\text{SAT}_1,N_s}^2 + u_{\text{SAT}_2,N_s}^2)) \end{aligned} \quad (\text{S1})$$

In Eq. (S1), the standard deviation due to uncorrelated random noise is approximated by the ex-ante uncertainty component due to SCD random error. This is justified further below.

Fig. S3 presents, per site, the mean squared difference between SAT_1 and SAT_2 , split in a squared bias and a variance component. The variance component is by far the dominant one. The bias reaches at most ~0.6 Pmolec cm⁻² (at Athens, Bremen and Mainz), and is therefore only a very minor contributor to $\text{RMS}(N_{v,\text{trop,SAT}_2} - N_{v,\text{trop,SAT}_1})$ and to the observed bias between OMI and MAX-DOAS (discussed in section 3.4.6).

The difference in tropospheric column between both neighbouring pixels can be ascribed to differences in total slant column, in stratospheric slant column and in tropospheric AMF (see Eq. (1)). The contribution to the dispersion due to slant column variation can be approximated as $\sigma((N_{s,\text{SAT}_2} - N_{s,\text{SAT}_1})/M_{\text{SAT}_1})$ and the dispersion due to tropospheric AMF variation as $\sigma(-N_{v,\text{trop,SAT}_1} \times (M_{\text{trop,SAT}_2} - M_{\text{trop,SAT}_1})/M_{\text{SAT}_1})$. This is also shown in Fig. S3. It can be concluded that variation in the total slant column explains the largest part of the tropospheric column dispersion. As stratospheric slant column and tropospheric AMF do not vary much between neighbouring pixels, they can also not be a large source of uncorrelated random error. This, in turn, means that u_{SAT,N_s} , the uncertainty due to random error in the slant column, can be used approximately as the uncertainty due to all uncorrelated random error, justifying the approximation in Eq. (S1).

For the sites Bujumbura, Nairobi and OHP the dispersion $\sigma(N_{v,\text{trop,SAT}_2} - N_{v,\text{trop,SAT}_1})$ is roughly equal to the ex-ante noise uncertainty $\sqrt{u_{\text{SAT}_1,N_s}^2 + u_{\text{SAT}_2,N_s}^2}$ (in the order of 1 Pmolec cm⁻²), implying that horizontal sampling difference error is not significant compared to the random noise from the satellite measurement. Specifically for Nairobi and OHP, one has even $\sigma(N_{v,\text{trop,SAT}_2} - N_{v,\text{trop,SAT}_1}) < \sqrt{u_{\text{SAT}_1,N_s}^2 + u_{\text{SAT}_2,N_s}^2}$, indicating that the uncertainty due to random noise is overestimated at these sites, and/or that there is some error correlation between neighbouring pixels.

For the other sites $\sigma(N_{v,\text{trop,SAT}_2} - N_{v,\text{trop,SAT}_1}) > \sqrt{2}u_{\text{SAT},N_s}$, i.e., there is a measurable contribution of horizontal sampling difference error. However, it is always much smaller than $\text{RMS}(N_{v,\text{trop,SAT}} - N_{v,\text{trop,REF}})$. E.g., at the site Xianghe, $\sigma(N_{v,\text{trop,SAT}_2} - N_{v,\text{trop,SAT}_1}) \approx 2.5 \text{ Pmolec cm}^{-2}$ and $\sqrt{u_{\text{SAT}_1,N_s}^2 + u_{\text{SAT}_2,N_s}^2} \approx 1 \text{ Pmolec cm}^{-2}$ (see Fig. S3), therefore $\sigma_{\Delta r_{\text{SAT,GB}}} \approx 2.2 \text{ Pmolec cm}^{-2}$. The RMS of the OMI vs. MAX-DOAS comparison at Xianghe, $\text{RMS}(N_{v,\text{trop,SAT}} - N_{v,\text{trop,REF}})$, is 7.9

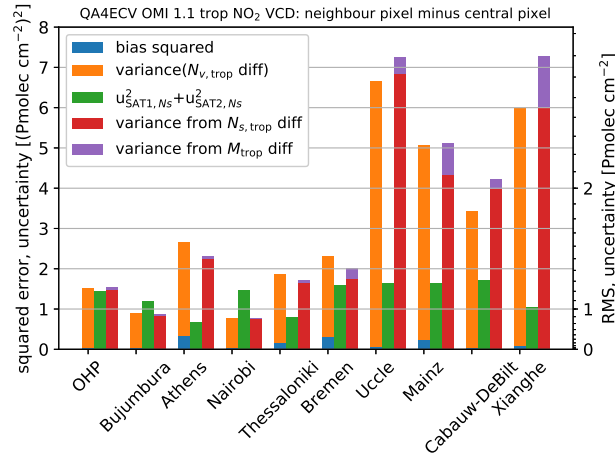


Figure S3. Per site three bar plots are provided. The left bar shows the mean squared difference of tropospheric VCD sets of QA4ECV OMI NO_2 pixels, where for set 1 the ground-pixel covers the MAX-DOAS site and for set 2 the pixel is next-nearest to the MAX-DOAS site. The mean squared difference is divided in two components: a bias component and a dispersion component. The middle bar shows the squared combined uncertainty due to slant column density random error. The right bar components give an estimate of the column variance between both pixels due to variation of the slant column (estimated to first order as $(N_{s,\text{SAT}_2} - N_{s,\text{SAT}_1})/M_{\text{SAT}_1}$) and due to variation of the tropospheric AMF (estimated to first order as $-N_{v,\text{trop},\text{SAT}_1} \times (M_{\text{trop},\text{SAT}_2} - M_{\text{trop},\text{SAT}_1})/M_{\text{SAT}_1}$). Note that the sum of variances due to SCD and tropospheric AMF difference can overshoot the variance of trop VCD difference (e.g., at Uccle), due to correlation and due to the first order approximation.

Pmolec cm^{-2} (see Fig. 12). Subtracting in quadrature $\sigma_{\Delta r_{\text{SAT},\text{GB}}}$ would reduce this to $7.6 \text{ Pmolec cm}^{-2}$. A similar reasoning for Uccle leads to a reduction of $\sigma_{\Delta r_{\text{SAT},\text{GB}}}$ from $4.9 \text{ Pmolec cm}^{-2}$ to $4.4 \text{ Pmolec cm}^{-2}$. For the other sites the contribution of horizontal sampling difference error is smaller. Horizontal sampling difference error is therefore a minor contributor to $N_{v,\text{trop},\text{SAT}_2} - N_{v,\text{trop},\text{SAT}_1}$.

5 S4 NO_2 monthly fields

For a selection of sites, spatial NO_2 fields were constructed for each month from the QA4ECV OMI 1.1 data, averaged over years 2004-2016. A variant of the temporal averaging approach of Wenig et al. (2008) is used. Per 0.02×0.02 grid cell the arithmetic average of covering satellite ground pixels is taken. Note that only ground pixels with area $< 950 \text{ km}^2$ are selected. Selection of months is based on minimal monthly bias (left) and maximal monthly bias (right) from Fig. 10.

- 10 The true resolution of these NO_2 fields is lower than the $0.02^\circ \times 0.02^\circ$ grid. The theoretical spatial smoothing window (taking into account the ground pixel size) is provided in Fig. S4. The NO_2 fields are shown in S5.

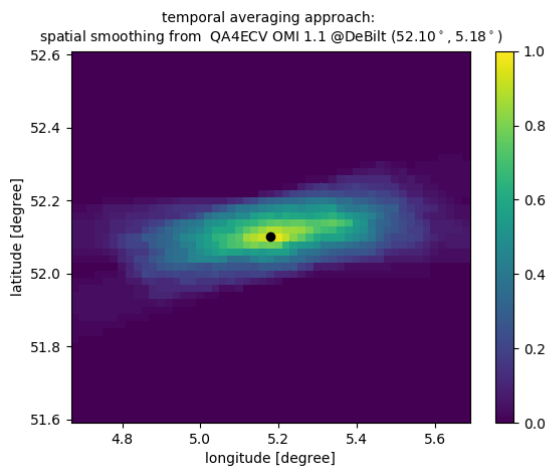


Figure S4. Spatial smoothing window of the NO₂ field constructed from QA4ECV OMI 1.1 data.

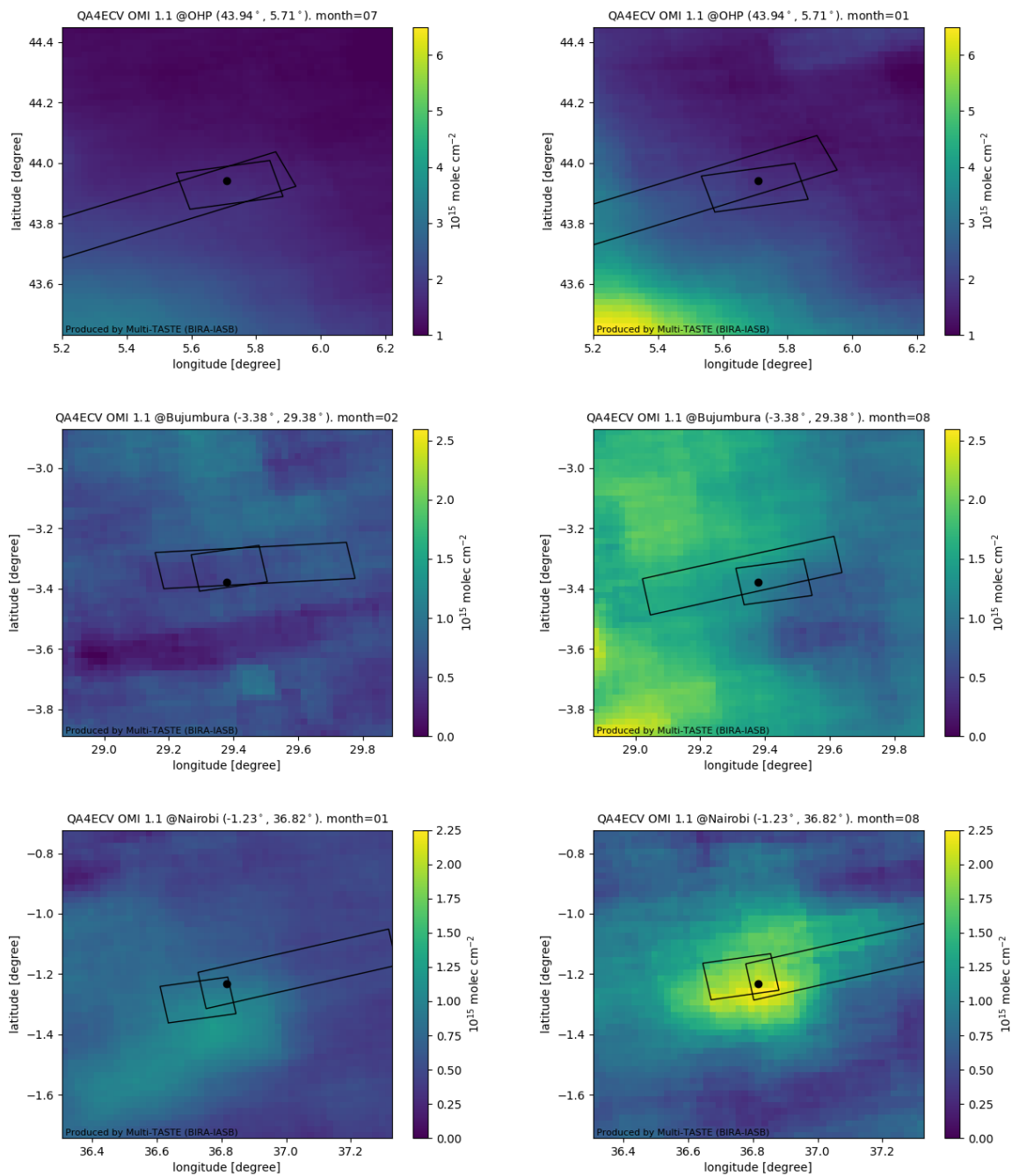


Figure S5. NO₂ monthly fields on a 0.02° × 0.02° grid, obtained from QA4ECV NO₂ OMI 1.1 by averaging over all years, for a selection of sites. Selection of months is based on minimal monthly bias (left) and maximal monthly bias (right) from Fig. 10.

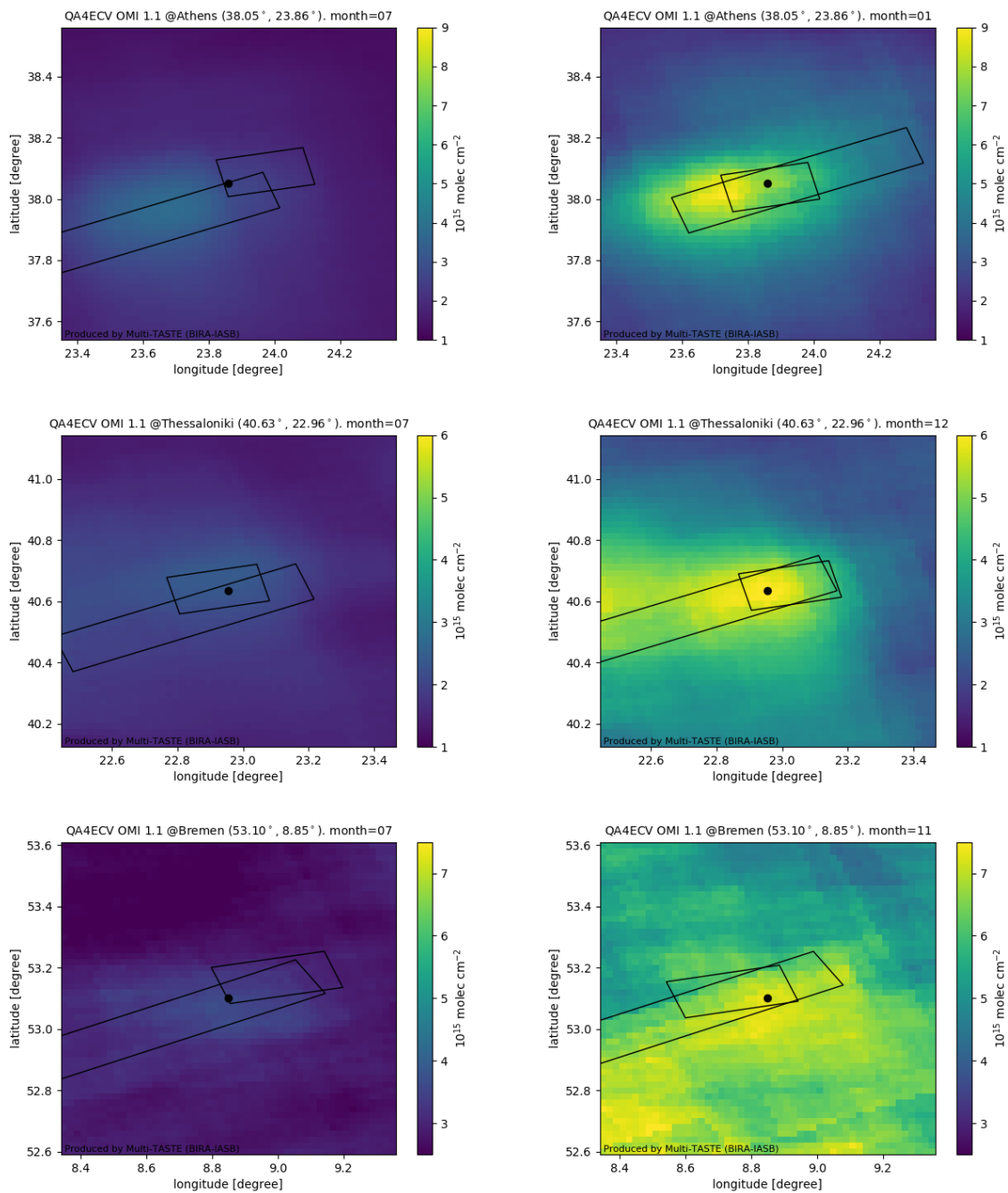


Figure S6. Continuation of Fig. S5.

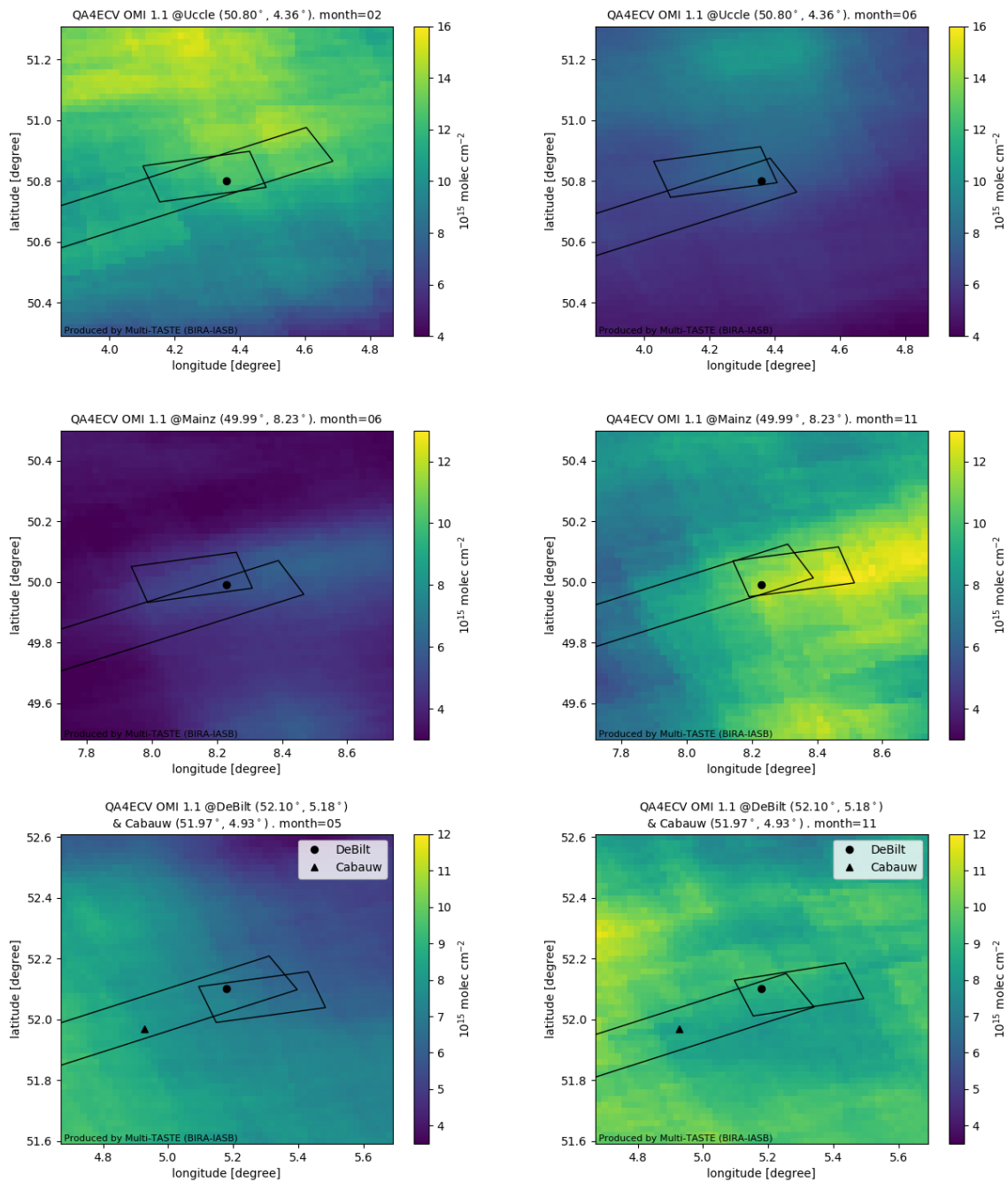


Figure S7. Continuation of Fig. S5.

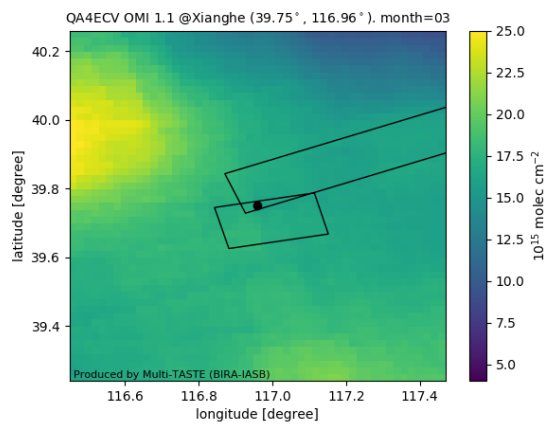
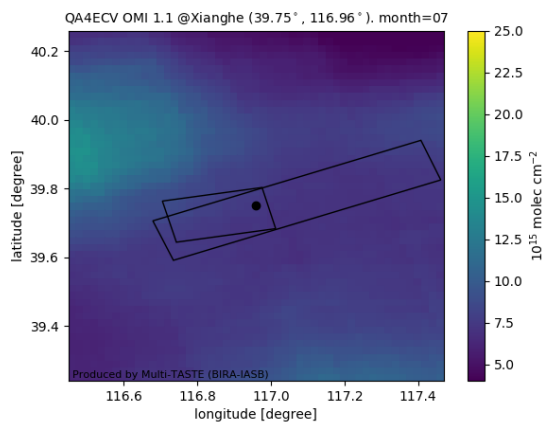


Figure S8. Continuation of Fig. S5.

S5 Dependence on screening criteria

Fig. S9 displays the dependence of mean difference between QA4ECV OMI tropospheric and MAX-DOAS (left column) and standard deviation of the difference (right column) on varying screening criteria. The impact of 4- σ clipping is also presented.

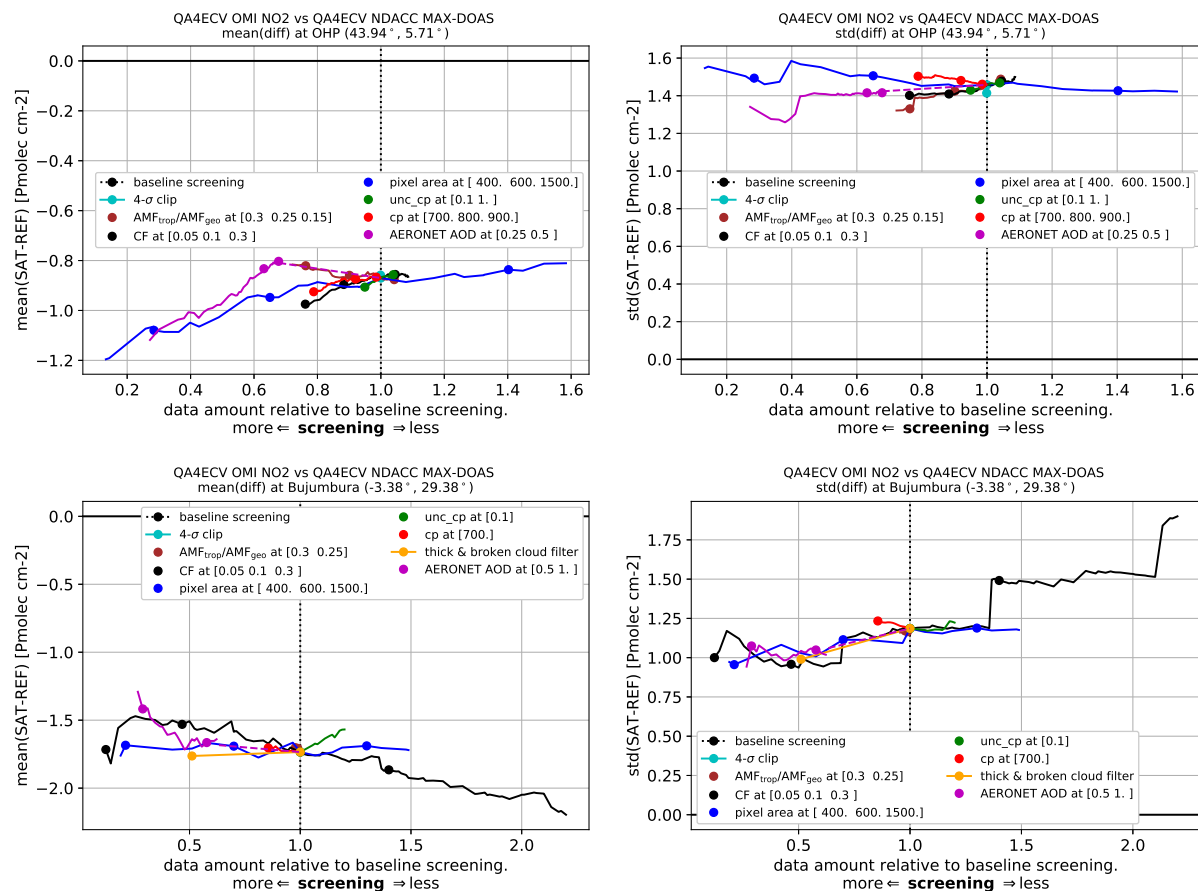


Figure S9. Mean difference (left) and standard deviation (right) in function of varying the screening criteria, for QA4ECV OMI NO₂ vs QA4ECV MAX-DOAS, for the sites OHP and Bujumbura. The x-axis shows the amount of selected (OMI, MAX-DOAS) pairs relative to the baseline screening (indicated with a vertical dashed line). Screening criteria varied here are minimum $\frac{AMF_{trop}}{AMF_{geo}}$, maximum ground pixel area, cloud fraction, uncertainty due to cloud pressure and AERONET AOD. Note that co-location with AERONET implies a subsetting of data, here indicated with a dashed line. Also provided are the impact of 4- σ clipping and, if available, the rejection of scenes flagged according to the MAX-DOAS data as 'broken cloud' or 'thick cloud'.

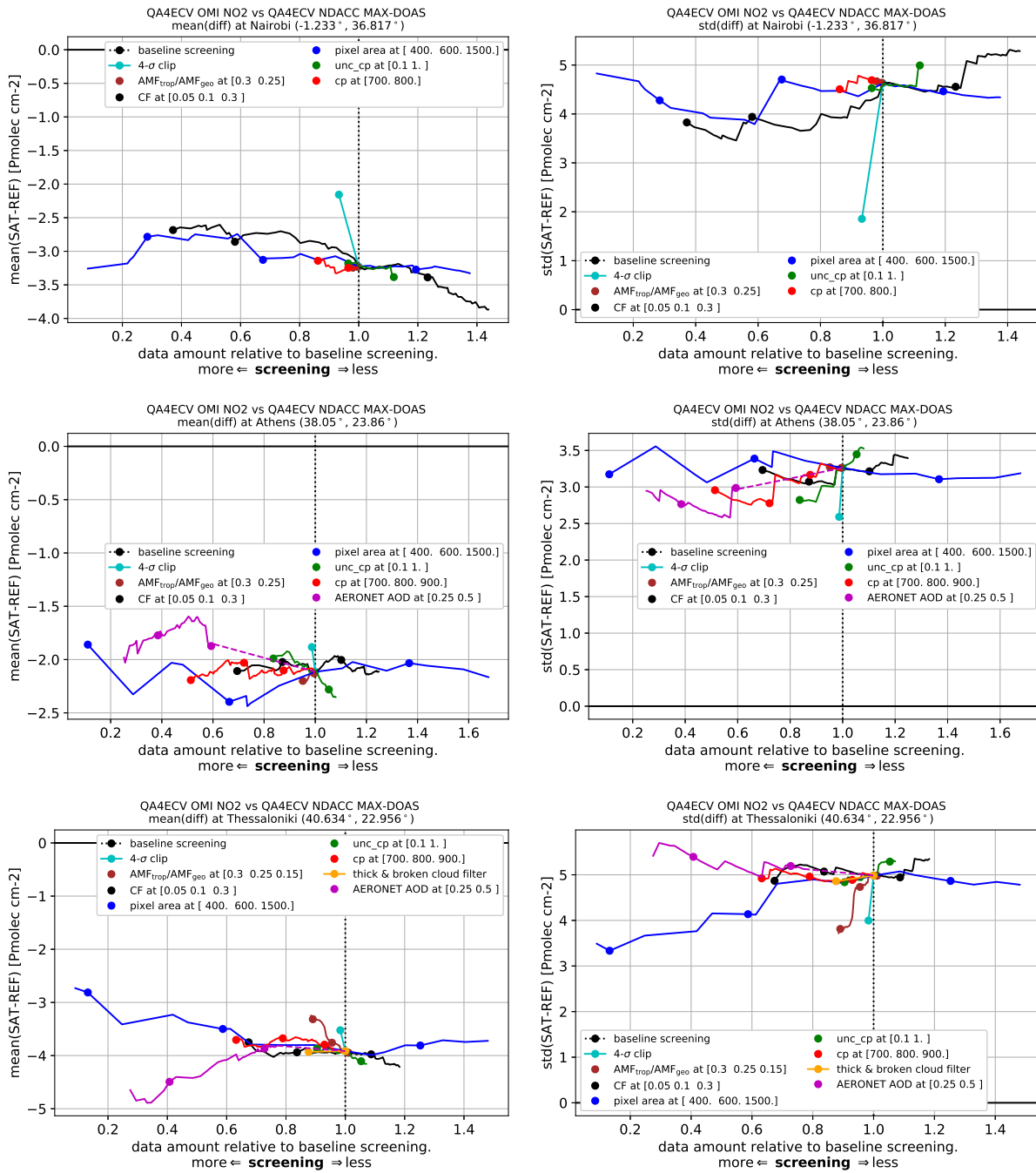


Figure S10. As Fig. S9, but for the sites Nairobi, Athens and Thessaloniki.

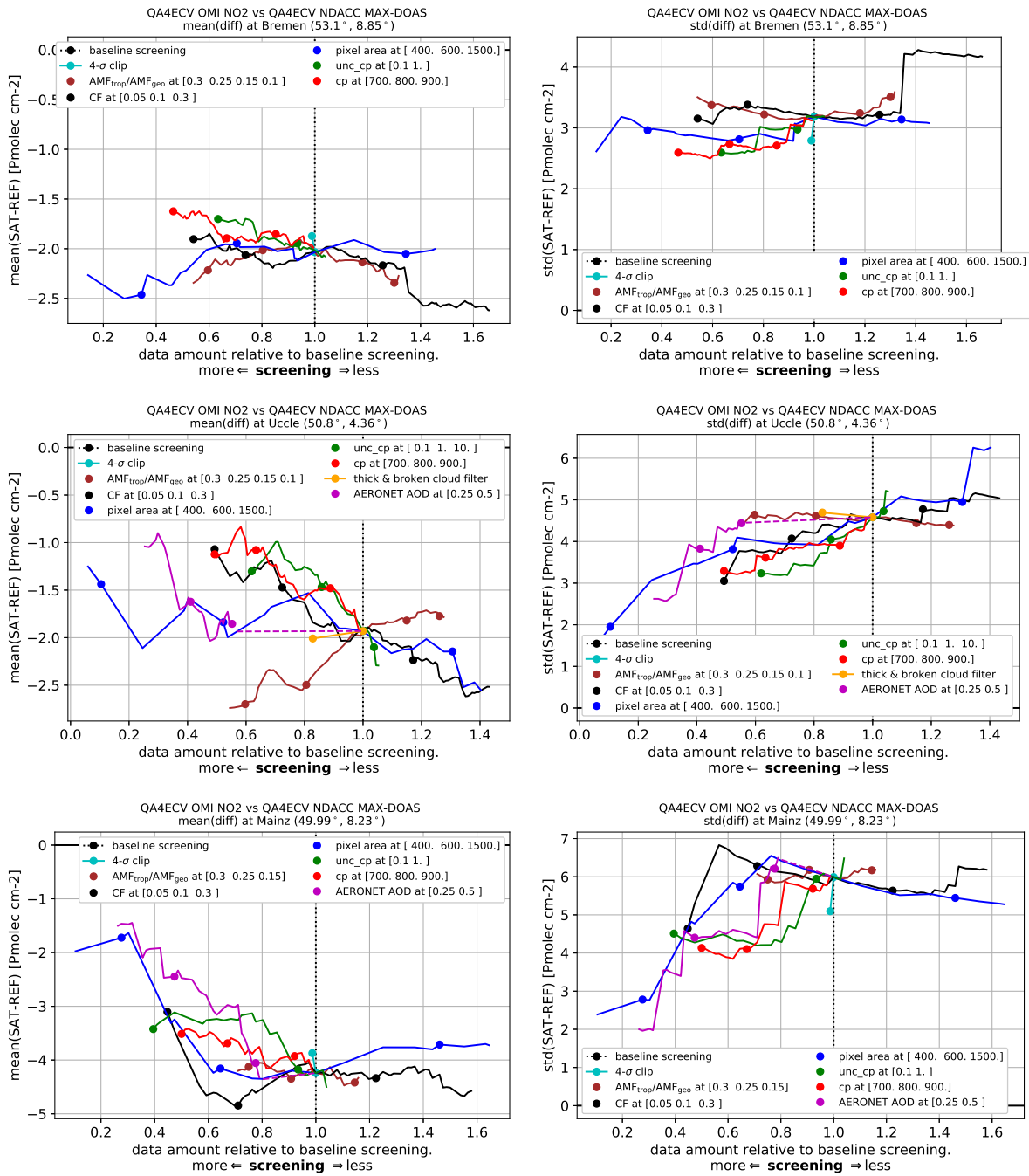


Figure S11. As Fig. S9, but for the sites Bremen, Uccle and Mainz.

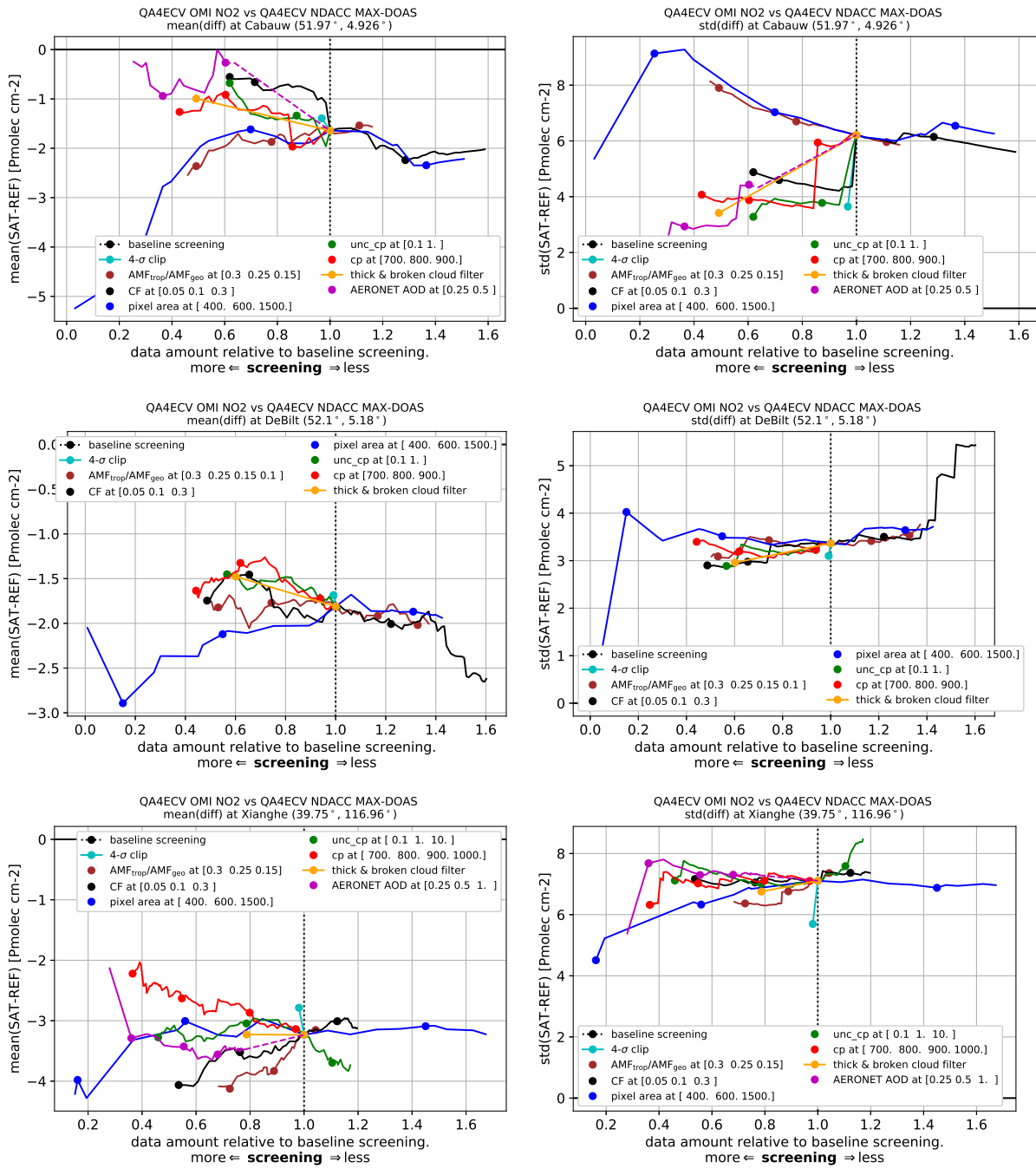


Figure S12. As Fig. S9, but for the sites Cabauw, De Bilt and Xianghe.

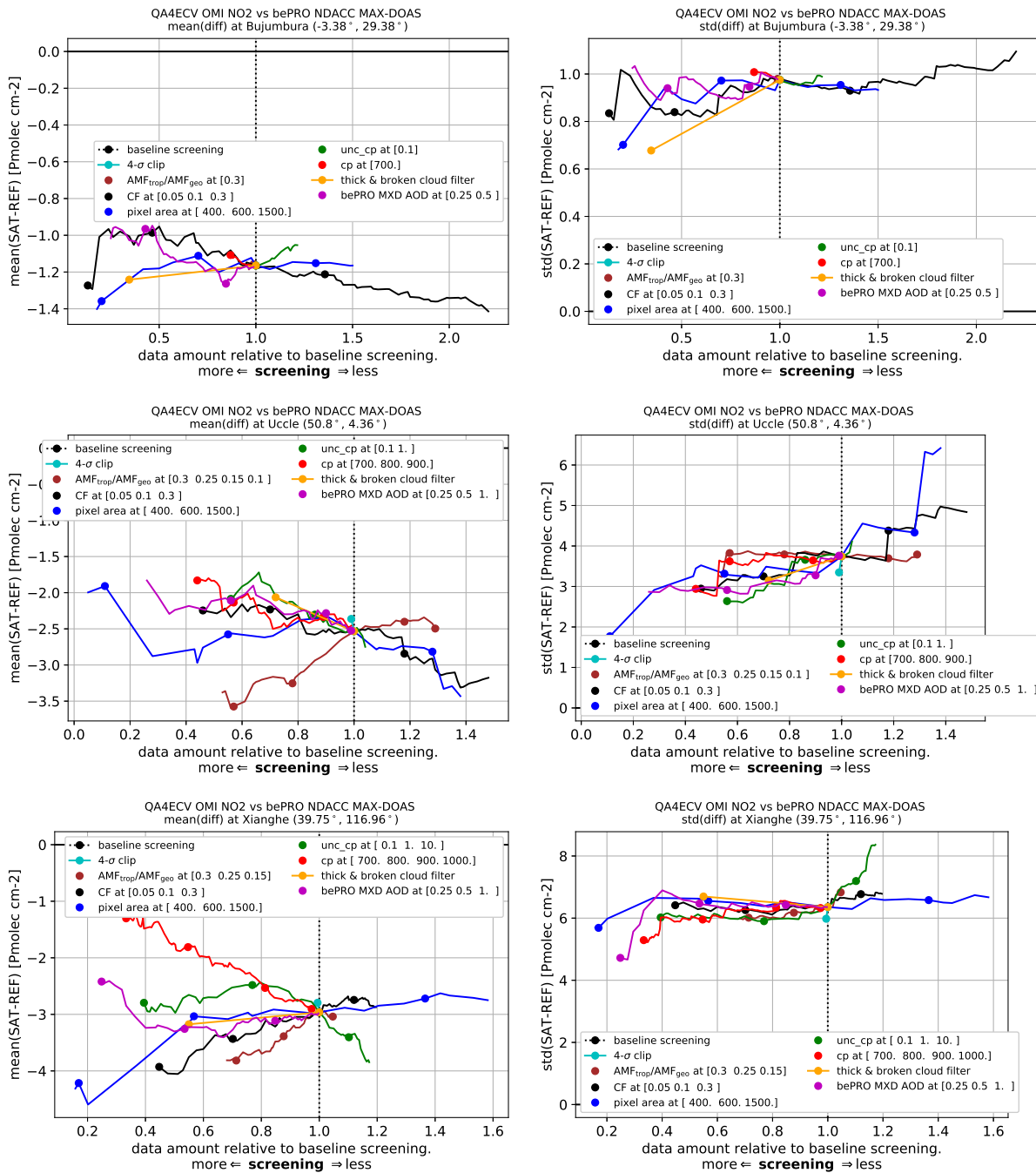


Figure S13. As Fig. S9, but for the bePRO MAX-DOAS processing of Bujumbura, Uccle and Xianghe. Note that for AOD, bePRO MAX-DOAS is used instead of AERONET.

S6 Vertical a priori profile harmonization and smoothing

Fig. 13 presents the mean squared deviation of QA4ECV OMI vs. bePRO MAX-DOAS at Uccle and Xianghe, using (i) the OMI satellite and MAX-DOAS data, (ii) direct smoothing of the MAX-DOAS retrieved profile using the satellite averaging kernel, (iii) replacement of the MAX-DOAS a priori profile shape with that of the satellite, (iv) a combination of first (iii), then

5 (ii).

In more detail:

– **(ii) Direct smoothing of the MAX-DOAS retrieved profile.** This is obtained as follows: the MAX-DOAS retrieved partial column density profile is shifted to the surface pressure level of the satellite (method of Zhou et al., 2009) and then mass-conserved regridded (Langerock et al., 2015) to the QA4ECV OMI pressure grid.

10 – **(iii) Replacement of the MAX-DOAS a priori profile shape with that of the satellite.** This is obtained as follows: the OMI a priori profile (from TM5) is shifted to the surface pressure of MAX-DOAS (method of Zhou et al., 2009), then regridded (Langerock et al., 2015) to the MAX-DOAS pressure grid, and rescaled to match the a priori VCD size of the original MAX-DOAS a priori. The resulting profile, defined on the MAX-DOAS grid, is then used to replace
15 the original MAX-DOAS a priori, using Eq. (10) of Rodgers and Connor (2003), thereby modifying the MAX-DOAS retrieved profile. With this procedure we have modified the shape of the MAX-DOAS a priori profile but not the a priori VCD size.

The motivation is as follows: the *column density size* of the MAX-DOAS a priori profile is obtained from a geometrical approximation MAX-DOAS measurement, therefore likely more correct than the TM5 modelling. The MAX-DOAS a priori *profile shape* however is modelled by a simple exponential, and therefore likely to be less correct than the TM5
20 modelling.

As the OMI retrieved column depends on the a priori profile shape but not on its size, and since the satellite a priori shape is unaltered in the above procedure, the OMI retrieved VCD is not modified.

– **(iv) Combination of first (iii), then (ii).** First all steps of (iii) are applied to obtain a harmonized MAX-DOAS retrieved profile. Then this profile is shifted (method of Zhou et al., 2009) and regridded (Langerock et al., 2015) to the OMI
25 pressure grid. Then Eq. (3) is applied to this profile using the OMI averaging kernel.